Parameter Optimization Of The Process Of AA6xxx and AA7xxx series Aluminium Extrusion

A THESIS PRESENTED IN FULFILMENT OF THE

REQUIREMENTS FOR THE DEGREE OF

DOCTOR OF PHILOSOPHY

IN

MECHANICAL ENGINEERING

AUCKLAND UNIVERSITY OF TECHNOLOGY,
AUCKLAND

NEW ZEALAND.

Padmanathan Kathirgamanathan

2013

Abstract

The mechanical properties and surface qualities of extruded aluminium products depend greatly on the micro-structural changes during the extrusion process. A clear understanding of the thermodynamics and tribology of the aluminium extrusion process with respect to the die design parameters and process parameters, namely temperature and extrusion speed are necessary to decide the optimum values of machine settings.

This research discusses the essential understanding of the process of aluminium extrusion, including the effects of die geometry and process parameters on flow patterns. It presents the development of a technique to find an optimal set of process and design parameter values for an isothermal process to extrude a product for a given shape and material properties with minimal defects. The inputs to this model are: the product geometry and its material data such as flow curve and microstructure during dynamic recrystallization. This is an inverse problem and the model is formulated as a non-linear least-squares minimization problem coupled with a finite element model for the extrusion process.

The minimization problem where the geometry of a profile is simple is done by constructing an iterative procedure using an optimization routine such as *MATLAB*'s *lsqnonlin* and at each iteration, the extrusion flow is solved using the finite element programme *ABAQUS*. However, the die design parameters for a complex geometry problem are different from a simple geometry problem. Further *ABAQUS* is not very efficient to handle adaptive meshing for a complex thin profile. The specialist finite element program DEFORM 3D for metal forming applications, which efficiently uses adaptive meshing controls to accommodate high

workpiece deformations, is used to overcome the problem. The optimal values of the die design and process parameters are estimated by improving the techniques available in the literature and compared with experimental results.

Acknowledgements

First of all, I would like to express my sincere gratitude to my supervisor, Professor Thomas Neitzert, for providing me an interesting industrial research problem to work on. Thomas has been an exceptional advisor, both academically and personally. His support, encouragement, suggestions, discussions and comments throughout my research were invaluable. I was fortunate to have had the opportunity to work with him.

I would also like to thank Professor Zhan Chen for his valuable comments on various parts of my thesis. My thanks also extend to my colleague Florian Kern for his continuous support and regular discussions.

My thanks also go to the Foundation for Research Science and Technology, School of Engineering, as well as School of Computing and Mathematical Sciences for financial supports.

List of publications from this project

(i) Kathirgamanathan P., and Neitzert T., Optimization method of extrusion dies with a thin and complex shape, Submitted to *Australian Journal of Mechanical Engineering*.

(ii) Kathirgamanathan P., and Neitzert T., Optimization of pocket design to produce a thin shape complex profile, *Production Engineering Research & Development*, 3-3, 231–241, 2009.

(iii) Kathirgamanathan P., and Neitzert T., Inverse Modelling for Estimation of Average Grain Size and Material Constants - An Optimization Approach, *Lecture Notes in Engineering and Computer Science*, 2, 850–854, 2008.

(iv) Kathirgamanathan P., and Neitzert T., Optimal process control parameters estimation in aluminium extrusion for given product characteristics, *Lecture Notes in Engineering and Computer Science*, 2, 1436–1441, 2008.

(v) Kathirgamanathan P., and Neitzert T., Modelling of metal extrusion using ABAQUS, *The Proceedings of 3rd NZ Metals Industry Conference 2006*.

Contents

List of Symbols

Q	activation energy $[Jmol^{-1}K^{-1}]$
d_{avg}	average recrystallized grain size [m]
b	bearing length $[m]$
Γ	boundary
k	conductivity $[Sm^{-1}]$
ϵ_c	critical strain
A	cross sectional area $[m^2]$
ρ	density of the metal $[kgm^{-3}]$
d	depth of pocket $[m]$
θ	die semi-cone angle $[degrees]$
r_p	distance between pocket axis and die axis $[m]$
x, y, z	distances measured in the X, Y and Z directions respectively $[m]$
Ω	domain
$\dot{\bar{\epsilon}}$	effective strain-rate $[s^{-1}]$
$\bar{\sigma}$	effective stress $[Pa]$
P_e	extrusion pressure
V	extrusion speed $[ms^{-1}]$
σ	flow stress $[Pa]$
μ	friction factor
R	gas constant $[Jmol^{-1}K^{-1}]$
q_n	heat flux $[Wm^{-2}]$
$\dot{q}$	heat generation term $[Ws^{-1}]$
$d0_{avg}$	initial grain size [m]
m, n	material constants
$\dot{\bar{\epsilon}}_{ave}$	mean strain-rate of the deformation zone $[s^{-1}]$
$\dot{\epsilon}_i$	normal strain-rate in the i direction $[s^{-1}]$
σ_i	normal stress in the i direction $[Pa]$
$\epsilon_{0.5}$	plastic strain for 50% recrystallization
R_0	radius of the billet $[m]$
R_e	radius of the extrudate or the die radius $[m]$
C_p	specific heat capacity $[Jkg^{-1}K^{-1}]$
ϵ	strain
t	time $[s]$
v_i	velocity components in the i direction $[ms^{-1}]$
χ	volume fraction recrystallized
w, w_1, w_2	width of pockets $[m]$

Chapter 1

Introduction

1.1 Overview of Numerical Simulations of Aluminium Extrusion

Aluminium extrusion is a common forming process worldwide. Extrusion produces a long profile of fixed cross-sectional area by pressing a hot billet through a hole with a certain shape. Both mechanical properties and surface quality of the extruded product depend mainly on initial billet temperature, extrusion speed and die geometry. If the speed is high, the temperature goes up due to faster plastic deformation and increased surface friction. This leads to surface defects on the product. Homogeneity of flow also influences the product quality. The flow velocity of every material particle in the cross-section across the die exit should be uniform for achieving products with minimal defects. The geometry of the die opening makes up an important feature of die design. It determines the homogeneity of flow and the amount of redundant work done during the deformation process. A profile, which minimizes the redundant work, will minimize the extrusion power. The knowledge of the temperature distribution, velocity distribution inside the forming zone and extrusion load is also very important for the determination of the

right extrusion process conditions.

The aim of any manufacturing process is the production of a steady quality product at a minimal cost. Generally effective goals include shortening the lead time in the design cycle, reducing tooling cost and machine downtime at the production stage, and developing a stable process with a minimal reject rate. In practice, die designers usually meeting their objective through trial and error methods. These methods are time consuming and expensive. Sometimes dies have to be discarded if it is difficult to rectify mistakes. This design process does not suit a modern industrial environment.

By using numerical simulation for an extrusion process and predicting material flow, the information of the material deformation, stress, strain, strain rate and temperature distribution inside the extrusion die can be obtained. This method will allow us to determine

1. whether a part can be formed without defects,

2. equipment forces and die stresses,

3. ways to reduce costly trials of proposed die designs,

4. ways to improve die designs to reduce production and material costs,

5. ways to minimize lead-time in bringing a new product to market.

This is an ongoing trend of modern manufacturing in the current industrial environment. As a simulation tool finite element modelling is a well-established numerical technique for manufacturing processes and has been gaining wider acceptance over the last several years.

1.2 The Problem Statement

1.2.1 Background

The current theoretical understanding of the extrusion process, its impact on the tooling technology, extruded product and overall yield are somewhat limited. This constraint not only restricts progress of making the existing production set-ups more reliable and running at an optimum level but also doesn't allow major advances of new processes as well as product developments.

The lack of the ability to reliably simulate the extrusion process leads to sub-optimum tooling designs and longer than necessary trial periods until a new tool runs to satisfaction. Product designs are restricted by the standard of current tool-design. Improved machine control strategies cannot be developed because the relationships between process and material conditions aren't well understood.

1.2.2 The Main Project Goal

The novel concept of this research is to

1. Determine the optimal process (ram speed, initial billet and die temperature) and design (die shape) parameter values to get a
   - (i) High quality product in terms of
     - (a) homogeneity,
     - (b) uniform flow,
     - (c) material properties(average grain size),
   - (ii) With minimal defects such as
     - (a) surface defects (eg. flow lines),
     - (b) internal cracks (eg. central bursts also known as chevrons in extrusion).

2. Identify the process parameters which are more sensitive to product defects.

3. Improve the theoretical understanding of the process of aluminium extrusion through a simulation of the forming process and the related changes in material structure.

Tool design and process control in the metal extrusion industry are still treated to some extent by a trial and error approach, which will be overcome by this project with the associated gains in reduced set-up time, improved process performance and efficiency of operation.

The numerical simulation of extrusion using the finite element method is the most promising option to replace the traditional trial and error as well as other analytical methods. A finite element model, which is capable of describing the behavior of metal flow during extrusion, requires several input data such as die geometry, material behavior laws, friction laws and operating conditions. In reality, material behavior can be obtained, but the die geometry, process conditions and appropriate friction values to achieve a profile with given material properties are often unknown.

1.2.3 Technical Target

The project will improve knowledge of the extrusion process and will lead to better tool designs, increase of die life before failure and increase of surface quality of the extruded product. The optimized die designs are also leading to reduced die costs. The time spent on designing new tools will be reduced significantly. The outcome of new product shapes which could not be attempted before and quality is difficult to quantify, but will certainly strengthen the competitive situation of commercial entities.

1.3 The Scope of the Problem

This research has relevance to the following:

(i) Improvement of the physical properties of the extruded material;

   (a) products with high quality in terms of homogeneity, uniform flow and given material properties.

   (b) products with minimal defects such as surface defects, internal cracks and central bursts.

(ii) Optimization of the cost of metal extrusion;

   (a) maximize die life,

   (b) minimize usage of energy,

   (c) minimize time of die trials.

1.4 Overview of the Research

The aim of this research is to present a numerical model capable of predicting an optimal set of conditions to extrude a product for a given shape and material properties with minimal defects. The presentation of this report is organized into 8 chapters including the present.

Chapter 2 consists of the main literature review. It contains background material for the numerical simulation of metal extrusion in general. An overview of the extrusion process, modelling of the metal extrusion process, and numerical techniques are described in the first three sections. Common forms of defects in extrusion processes are also explained. The last two sections of the chapter consider related problems and the work to be done to improve the extrusion process in general.

In Chapter 3 the simulation of the extrusion process using finite element modelling is introduced. This chapter starts with a brief description of finite element softwares Abaqus and DEFORM 3D which are used for the investigation. In the second half of the chapter, a small scale extrusion model is simulated using ABAQUS and it is demonstrated how temperature, stress, strains and velocity changes during the extrusion and how these quantities are related to die angle, die land length, friction, material properties, initial billet temperature and extrusion speed. In addition ways to increase the efficiency in terms of using different solution schemes, adaptive meshing, element type and different contact algorithms are described. The aim of this chapter is to understand the extrusion process in general and ways to solve extrusion problems more efficiently.

Chapter 4 investigates a numerical technique to estimate the optimal die profile and the process parameters such as extrusion speed and initial temperatures simultaneously. This chapter provides a detailed description of an inverse model capable of simultaneously estimating die design and process parameters. In addition, a series of examples are considered to describe how optimal values of design and process parameters can be determined and how changes in these values will influence optimization criteria.

The objective of Chapter 5 is to describe an inverse model capable of concurrently estimating the average grain size, activation energy and other material constants appearing in the model. The chapter starts with the description of the forward problem, difficulties with the forward problem and the data requirements for the inverse problem. Then the methodology of the inverse problem for estimating parameter values by using simulated strain and temperature values at a single node is presented.

Chapter 6 investigates the influence of shape, depth, and widths of a pocket to regulate the metal flow through a more complex thin die with varying thickness.

The chapter starts with the simulation of extrusion through a complex die which is currently in commercial use and analyzes the reasons for insufficient surface quality of the extruded product. Next, the methodology to improve the surface quality of the extruded product is presented, which includes the analysis of pocket design parameters and algorithms. Finally some numerical simulation results are presented to compare the newly designed die with the original die.

In Chapter 7, experimental data using the newly designed die and the original die are presented. This chapter describes the equipment, trial procedure and sample preparation as well as evaluation.

Chapter 8 presents the summary, conclusion and possible extension of this project.

This thesis includes information already published in [33], [34], [35] and [36].

Chapter 2

Metal Extrusion and Simulation

2.1 Introduction

Extrusion is a plastic deformation process in which a block of metal (billet) is compressed through a die opening of a smaller cross sectional area than that of the original billet as shown in Figure (2.1). During the process, heat is generated by both the frictional work and deformation work. This heat is transported with the extruded material while conduction, convection and radiation take place simultaneously. In broad terms some of the generated heat remains in the extruded material, some is transmitted to the container and die and some increases the temperature of the part of the billet that is not yet extruded.

It is a thermo-mechanical process and it involves interaction between the process parameters, tooling and deformed material. The whole process is composed of two distinctly different stages, namely the transient state at the beginning and steady state of the rest of the cycle. Further the wear process on the die bearing is dependent on the thermodynamics of extrusion which is very much influenced by the effects of extrusion variables. The tribology in metal extrusion has a direct influence on the accuracy of the shape and the surface finish of the workpiece.

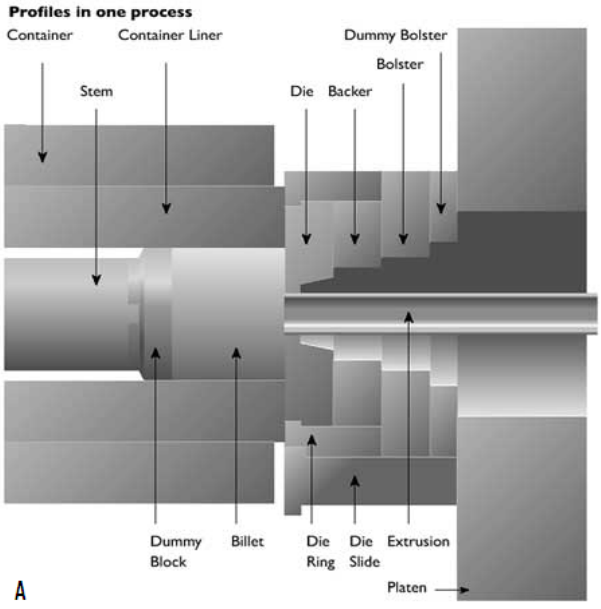

Figure 2.1: Machinery set up at the factory [[73]]

There are five main types of extrusion[65]:

1. Direct extrusion: A press pushes the ram on one end and the extrudate is forced through the die on the other end.

2. Indirect extrusion (or backwards extrusion): It involves a stationary billet with a moving die.

3. Hydrostatic extrusion: It is using a fluid to hydrostatically pressurize the material out of the container.

4. Impact extrusion: This is a high speed process for creating hollow shapes like soda cans.

5. Extrusion with active friction: In this process the extrusion die remains stationary while the ram and container move in the direction of flow. The benefits are improved homogeneity of metal flow, higher speeds and no metal flow interface at the container bottom[39].

In the extrusion process, the large deformations are mainly plastic or viscoplastic. The elastic component is very small and neglected. neglected. Therefore the theory of plasticity is used in metal forming processes to investigate and study the mechanics of extrusion. This will allow us

1. to analyse and predict the flow pattern, temperature, heat transfer, variation of local material strength, stresses, forming load, pressure and energy, and

2. to study how the metal flow during extrusion depends on material properties and initial billet temperature, ram speed, friction between billet and die surface and extrusion ratio.

2.2 Theoritical Aspects of Extrusion

To study the extrusion process in detail, the strain, strain rate, material flow stress, and friction between the interfaces are important. These can be defined as follows

1. The strain [ε]: It is a measure of deformation. There are two types. They are defined by

$$\text{Engineering strain} = \frac{\text{Change in length}}{\text{Original length}} \tag{2.1}$$

$$\text{True strain} = \ln\left(1 + \frac{\text{Change in length}}{\text{Original length}}\right) \tag{2.2}$$

2. The stress [σ]: It is a measure of force applied to a unit area of material, $\sigma = \frac{F}{A}$.

3. The strain rate [$\dot{\varepsilon}$]: It is a measure of the instantaneous rate of deformation a region of material is experiencing. The general definition would be $\dot{\varepsilon} = \frac{d\varepsilon}{dt}$. The mean strain rate may be computed from

$$\dot{\varepsilon_m} = \varepsilon \frac{6vD_0^2 \tan\theta}{D_0^3 - D_1^3}, \tag{2.3}$$

where v is ram velocity, θ is the semi-cone angle of the die entry, D_0 is the initial diameter of billet and D_1 is the final diameter of extruded product.

4. Material Flow Stress: It is a true stress-strain curve and is commonly called flow curve. It gives the stress required to cause the metal to flow plastically at any given strain. Different methods of mathematically defining the relationship are given in the literature. Some of them are

   Method 1

   $$\bar{\sigma} = c\bar{\epsilon}^{n}\dot{\bar{\epsilon}}^{m} + y \tag{2.4}$$

   where $\bar{\sigma}$ is the flow stress, $\bar{\epsilon}$ is the effective plastic strain, $\dot{\bar{\epsilon}}$ is the effective strain rate, c is a material constant, n is the strain hardening exponent, m is the strain rate exponent and y is an initial yield value.

   Method 2

   $$\dot{\bar{\epsilon}} = \gamma \left(\sinh\left(\alpha\bar{\sigma}\right)\right)^{n1} \exp\left(-\frac{Q}{RT}\right) \tag{2.5}$$

   where γ, α are constants, $n1$ is the strain rate exponent, Q is the activation energy, R is the gas constant, and T is the absolute temperature, $\bar{\sigma}$ is the flow stress, and $\dot{\bar{\epsilon}}$ is the effective strain rate.

   Method 3

   $$\dot{\bar{\epsilon}} = \gamma\bar{\sigma}^{n} \exp\left(-\frac{Q}{RT}\right) \tag{2.6}$$

   where γ is a constant, and n is the strain rate exponent.

5. Friction: It is the resistance to relative motion that is experienced whenever two surfaces are in contact with one another. The friction components for the direct extrusion process are

   (i) Billet-Container interface

   (ii) Dead-metal zone metal interface

(iii) Die-material interface

The friction models being used for the extrusion process can be divided into three different categories. They are classic friction models, the empirical friction models and the physically based friction models. The Coulomb friction model and Shear friction model are the two classic friction models. The frictional force in the constant shear model is defined by

$$f_s = \mu k \tag{2.7}$$

where f_s is the frictional stress, k is the shear yield stress and μ is the friction factor. Coulomb friction is used when contact occurs between two elastically/plastically deforming objects or an elastic object and a rigid object. The frictional force in the Coulomb law model is defined by

$$f_s = \mu p \tag{2.8}$$

where f_s is the frictional stress, p is the interface pressure between two bodies and μ is the friction factor.

The friction stress calculated using the Coulomb friction model may be higher than the shear flow stress of the workpiece material due to the high contact pressure at the workpiece-die interface. To avoid the overestimation of friction stress, the shear friction model may be an answer. But it is not easy to estimate the value of friction experimentally and therefore the selection of friction values can be guesswork. The empirical friction models are mainly based on experimental observations and the model parameters are normally related to extrusion speed and billet temperature. In physically based friction models, the friction force is considered as a summation of ploughing forces

generated from joined contact patches.

A comparative study of friction models for hot aluminium extrusion processes has been conducted by Wang and Yang [79] and have shown that the full sticking friction appeared to represent the interfacial contact between the hot aluminium and the die the best. Therefore, in FE simulations of hot aluminium extrusion, the classic friction models, with m or μ at or close to unity could be assigned as friction boundary condition at the workpiece/die interface. This is not only for saving computing time, but also for avoiding convergence problems.

6. The redundant work: Due to inhomogeneity of flow through the die, extra work is needed to deform the material to the final shape. The redundant work is approximately proportional to the strain ε and the extrusion pressure P_e and is approximately equal to [65]

$$P_e = \bar{\sigma}\,(0.8 + 1.2\varepsilon) \tag{2.9}$$

2.3 Microstructure Models

In extrusion as in any other manufacturing processes, product quality is an important cost factor. The product properties are closely related to the uniformity of the microstructure. There are various microstructure models [[9], [10], [11], [53]] available, which are based on laboratory observations. One example is the relationship between microstructural parameters (the average recrystallized grain size d, volume fraction recrystallized (χ) and process parameters ($\dot{\varepsilon}$, T, and ε)) developed

by Malas [53], which are given by

$$\chi = 1 - \exp\left(\log(2)\left(\frac{\varepsilon - \varepsilon_c}{\varepsilon_{0.5}}\right)^2\right), \tag{2.10}$$

$$\varepsilon_c = 4.76 \times 10^{-4} \exp(\frac{8000}{T}), \tag{2.11}$$

$$\varepsilon_{0.5} = 1.144 \times 10^{-3} d_0^{0.28} \dot{\varepsilon}^{0.05} \exp\left(\frac{6420}{T}\right), \tag{2.12}$$

$$d = 22600 \dot{\varepsilon}^{-0.27} \exp\left(-0.27 \frac{Q}{RT}\right), \tag{2.13}$$

where ε_c = critical strain, $\varepsilon_{0.5}$ = plastic strain for 50% recrystallization, d_0 = initial grain size, activation energy $Q = 310\ kJ/mol$ and gas constant $R = 8.314 \times 10^{-3}\ kJ/mol - K$.

2.4 Forward Problem of Extrusion Process

Extrusion is a thermo-mechanical deformation process in which a block of metal (billet) is forced through the die opening of a smaller cross sectional area than that of the original billet. In this process, the large deformations are mainly plastic or viscoplastic, allowing the elastic part to be neglected. Therefore a rigid-viscoplastic formulation can be adopted. Strain is a measure of deformation and at high strain rates metal flow is analogous to fluid flow[5]. Therefore the material behavior can be described as that of fluid flow as in [5], [12], [38], [59], [70]

(i) Conservation of mass: The law states that the rate of change of mass in a fixed region is zero.

$$\dot{\rho} + \rho D_{ij} = 0 \tag{2.14}$$

where ρ is the density of the material and

$$D_{ij} = \frac{1}{2}\left(\frac{\partial v_i}{\partial x_j} + \frac{\partial v_j}{\partial x_i}\right) \quad \text{in} \quad \Omega \tag{2.15}$$

is the deformation tensor. If the material is incompressible, density is unchanged and the Equation (2.14) is simplified to

$$D_{ij} = 0. \tag{2.16}$$

(ii) Conservation of momentum: It says that the rate of change of momentum is equal to the sum of external forces acting on the region.

$$\rho \dot{v_i} = \rho f_i + \sigma_{ij,j} \quad \text{in} \quad \Omega \tag{2.17}$$

where $\mathbf{f}$ is the body force per unit mass, and σ is the Cauchy stress tensor. It has been assumed that $\rho \dot{v_i} \approx 0$. Boundary conditions are

$$\sigma_{ij} n_j = \bar{t_i} \quad \text{on} \quad \Gamma_t \tag{2.18}$$

$$v_i = \bar{v_i} \quad \text{on} \quad \Gamma_v \tag{2.19}$$

Here, the domain Ω and its associated boundary Γ represent the current configuration of the body. Γ_t and Γ_v represent respectively, the part of the boundary Γ where traction and velocities are prescribed. n is the outward normal vector at the interfacial surface. Indices i, j, k are used to denote the components of the tensor and an apostrophe denotes the spatial derivatives with respect to the current configuration. The constitutive equation is

$$\sigma'_{ij} = 2\gamma D_{ij} \tag{2.20}$$

where $\gamma = \dfrac{\bar{\sigma}}{3\dot{\bar{\varepsilon}}}$, σ' is the deviatoric stress tensor, $\bar{\sigma}$ is the effective stress and $\dot{\bar{\varepsilon}}$ is the effective strain rate.

The Yield criterion is:

$$\bar{\sigma}(\bar{\varepsilon}, \dot{\bar{\varepsilon}}, T) = \sqrt{\frac{3}{2}\sigma'_{ij}\sigma'_{ij}}, \tag{2.21}$$

$$\dot{\bar{\varepsilon}} = \sqrt{\frac{2}{3}\dot{\varepsilon_{ij}}\dot{\varepsilon_{ij}}}. \tag{2.22}$$

(iii) Conservation of energy: It says that the rate of change of the total energy is equal to the sum of the rate of work done by applied forces and the change of heat content per unit time.

$$\rho C_p \left(\frac{\partial T}{\partial t} + v_r \frac{\partial T}{\partial r} + v_z \frac{\partial T}{\partial z} \right) = \frac{1}{r} \frac{\partial}{\partial r} \left(rk \frac{\partial T}{\partial r} \right) + \frac{\partial}{\partial z} \left(k \frac{\partial T}{\partial z} \right) + \dot{q} \tag{2.23}$$

and the boundary conditions are

$$T = \bar{T} \quad \text{on} \quad \Gamma_T \tag{2.24}$$

$$\left(k \frac{\partial T}{\partial r} - \rho C_p v_r T \right) n_r + \left(k \frac{\partial T}{\partial z} - \rho C_p v_z T \right) n_z = q_n \quad \text{on} \quad \Gamma_q \tag{2.25}$$

Initial Condition is

$$T\,(r, z, 0) = T_0(r, z) \tag{2.26}$$

where $\dot{q}$, q_n, T, k, ρ, and C_p are the heat rate generation term, heat flux normal to the boundary surface, temperature, conductivity, density, and specific heat of the material in that order. Γ_T and Γ_q represent respectively the temperature prescribed surface and the surface where heat transfer occurs.

The exact mathematical analysis of the extrusion process is quite complex and has not been fully resolved. Therefore in recent years, many numerical methods using finite element techniques have been reported in the literature[[8], [26], [28], [38], [50]].

2.5 Finite Element Analysis

2.5.1 Introduction

When a problem is impossible to solve using analytical techniques, numerical techniques can be used to obtain a solution. One of the popular numerical techniques is finite element analysis (FEA). It is a very common method for metal forming processes including extrusion and a suitable method for any problem with arbitrary geometry. The finite element formulation of a problem results in a system of simultaneous algebraic equations.

There are three different types of finite element formulations used in modeling metal forming processes. They are Lagrangian, Eulerian and arbitrary Lagrangian Eulerian (ALE) formulations. The selection of type is based on the problem to be solved and to some extent the computer resources available.

In Lagrangian formulation, the mesh moves with the material and deforms with the flow of material. In Eulerian formulation nodes and elements are fixed in space and the material flows through the mesh. The major advantage of this formulation is that problems related to mesh distortion are avoided. In this formulation a problem with large deformations can be modeled with very low computational cost. The ALE methods are arbitrary combinations of the Lagrangian and Eulerian formulations and were developed in an attempt to bring the advantages of both Lagrangian and Eulerian formulation together. In an ALE formulation the displacements of material and mesh are decoupled and the mesh can move independently of the material.

The solution methods of finite element analysis can generally be grouped as either implicit or explicit. The choice of solution methods depends on the model, computational resources and nonlinearity of the system. It is typically solved incrementally.

In the implicit approach the state of a finite element model is updated from time t to $t + \Delta t$. The state at $t + \Delta t$ is determined based on information at time $t + \Delta t$. There are several solution procedures used in the implicit finite element technique. The Newton-Raphson technique is the most common in this procedure. The solution procedure is iterative and a successful solution depends on the satisfaction of a convergence criterion at each step.

The explicit method solves for $t + \Delta t$ based on information at time t. This method was originally developed, and is mainly used, to solve dynamic problems involving deformable bodies. The major advantage of using this method is that a matrix inversion is not required. Therefore this method requires less memory and provides greater computing efficiency. However the time step for the solution process is subject to limitations since its time step is very small.

There are several steps in every finite element technique. The major steps are [60]:

1. Defining the system mathematically using a set of differential equations, boundary conditions and initial conditions.

2. Convertion of differential equations into integral form of equation (i.e weak form of equation). It can be done using (a) direct approach, (b) variational approach or (c) the method of weighted residual approach.

3. Discretize and chose the element type: The geometry of the problem is first broken down into smaller parts called elements. The process of breaking down into smaller elements is called discretisation. The elements can be of many different types including one dimensional beam elements, two-dimensional triangles and quadrilaterals, three-dimensional brick elements etc.

4. Choosing a displacement function: The function is defined within the element using the nodal values of the element. These are expressed in terms of nodal

unknowns (eg. $\phi(x) = \sum_i N_i(x)\phi_i$ where ϕ_i are the nodal values of the field variable and N_i is the interpolation function)

5. Evaluate the integral form over each element.

$$[K]^e\{\phi\}^e = \{f\}^e$$

where K is an $m \times n$ matrix, ϕ, f are a column vector with n entries.

6. Assembling the element equations to obtain global equations.

$$[K]\{\phi\} = \{F\}$$

7. Solve the modified global equations to find primary unknowns at nodes.

$$\{\phi\} = [K]^{-1}\{F\}$$

8. Post–computation of solution and quantities of interests.

2.5.2 Finite Element Formulation

The finite element formulation is derived from the minimization of the principle of virtual work [12]. The variational form of the principle of virtual power can be written as

$$\delta\pi = \int_\Omega \sigma'_{ij}\delta D_{ij}dV - \int_{\Gamma_t} t_i\delta v_i dS - \int_\Omega \rho f_i\delta v_i dV - \int_\Omega p\delta D_{ij}dV - \int_\Omega D_{ij}\delta p dV = 0, \tag{2.27}$$

where p is the hydrostatic pressure.

The flow formulation using the weighted residual method can be written as

$$\int_{\Omega}[(\sigma_{ij}^{'}-p\delta_{ij})+\rho f_i]W_i dV = 0 \tag{2.28}$$

$$\int_{\Omega} D_{ii}W_i dV = 0 \tag{2.29}$$

$$\int_{\Gamma_t}[(\sigma_{ij}^{'}-p\delta_{ij})n_j-\bar{t}_i]W_i dS = 0, \tag{2.30}$$

where W_i's are weighting functions. By using integral by parts and the Gauss theorem it can be shown that the Equations (2.28-2.30) are equivalent to Equation (2.27). Let

$$[D] = \begin{bmatrix} D_{rr} \\ D_{zz} \\ D_{\theta\theta} \\ 2D_{rz} \end{bmatrix} = \begin{bmatrix} \frac{\partial v_r}{\partial r} \\ \frac{\partial v_z}{\partial z} \\ \frac{v_r}{r} \\ \left(\frac{\partial v_r}{\partial z}+\frac{\partial v_z}{\partial r}\right) \end{bmatrix}.$$

and

$$[\sigma'] = \begin{bmatrix} \sigma'_{rr} \\ \sigma'_{zz} \\ \sigma'_{\theta\theta} \\ \sigma'_{rz} \end{bmatrix}$$

$$= \begin{bmatrix} 2\mu & 0 & 0 & 0 \\ 0 & 2\mu & 0 & 0 \\ 0 & 0 & 2\mu & 0 \\ 0 & 0 & 0 & \mu \end{bmatrix} \begin{bmatrix} D_{rr} \\ D_{zz} \\ D_{\theta\theta} \\ 2D_{rz} \end{bmatrix}$$

$$= [\mu]\,[D]$$

where

$$[\gamma] = \begin{bmatrix} 2\gamma & 0 & 0 & 0 \\ 0 & 2\gamma & 0 & 0 \\ 0 & 0 & 2\gamma & 0 \\ 0 & 0 & 0 & \gamma \end{bmatrix}$$

Now considering

$$\begin{aligned} \sigma'_{ij}\delta D_{ij} &= \sigma'_{rr}\delta D_{rr} + \sigma'_{zz}\delta D_{zz} + \sigma'_{\theta\theta}\delta D_{\theta\theta} + \sigma'_{rz}\delta D_{rz} + \sigma'_{zr}\delta D_{zr} \\ &= [\delta D]^T [\sigma'] \\ &= [\delta D]^T [\mu\gamma] [\mathbf{D}] \end{aligned}$$

Now considering a triangular element with three nodes and assume

$$[\bar{v}] = \begin{bmatrix} v_r(r,z) \\ v_z(r,z) \end{bmatrix} = [\mathbf{N}] [\mathbf{V}],$$

$$[D] = [\mathbf{N}'] [\mathbf{V}],$$

where

$$[\mathbf{N}] = \begin{bmatrix} N_1 & 0 & N_2 & 0 & N_3 & 0 \\ 0 & N_1 & 0 & N_2 & 0 & N_3 \end{bmatrix}, [\mathbf{V}] = \begin{bmatrix} v_{r1} \\ v_{z1} \\ v_{r2} \\ v_{z2} \\ v_{r3} \\ v_{z3} \end{bmatrix}$$

and

$$[\mathbf{N}'] = \begin{bmatrix} N_{1,r} & 0 & N_{2,r} & 0 & N_{3,r} & 0 \\ 0 & N_{1,z} & 0 & N_{2,z} & 0 & N_{3,z} \\ \frac{N_1}{r} & 0 & \frac{N_2}{r} & 0 & \frac{N_3}{r} & 0 \\ N_{1,z} & N_{1,r} & N_{2,z} & N_{2,r} & N_{3,z} & N_{3,r} \end{bmatrix},$$

where N_i's are interpolation functions. Let the matrix for traction on Γ_t be

$$[\bar{t}] = \begin{bmatrix} t_r \\ t_z \end{bmatrix}.$$

The virtual velocity and corresponding rate of deformation are defined as

$$[\delta\bar{v}] = \begin{bmatrix} \delta v_r \\ \delta v_z \end{bmatrix} = [\mathbf{N}]\,[\delta\mathbf{V}]$$

$$[\delta D] = [\mathbf{N}']\,[\delta\mathbf{V}]$$

$$\begin{aligned} D_{ii} &= \begin{bmatrix} 1 & 1 & 1 & 0 \end{bmatrix} \begin{bmatrix} D_{rr} \\ D_{zz} \\ D_{\theta\theta} \\ 2\varepsilon_{rz} \end{bmatrix} \\ &= [h]^T\,[D] \end{aligned}$$

where $[h] = [1 \quad 1 \quad 1 \quad 0]^T$. If $[\mathbf{p}] = [p_1 \quad p_2 \quad p_3]^T$ is a nodal pressure matrix and the shape function matrix $[N_p] = [N_{p1} \quad N_{p2} \quad N_{p3}]$, then

$$p = [N_p]\,[\mathbf{p}]\,.$$

For all elements Equation (2.27) can be written as

$$\delta\pi = \sum_e \delta\pi^e.$$

Now considering

$$\begin{aligned}
\delta\pi^e &= \int_{\Omega_e} [\delta V]^T [N'] [\mu\gamma] [N'] [V] \, dV - \int_{\partial\Omega_e \cap \Gamma_t} [\delta V]^T [N]^T [\bar{t}] \, dS \\
&\quad - \int_{\Omega_e} [\delta V]^T [N]^T \left[\bar{f}\right] \rho dV - \int_{\Omega_e} [\delta V]^T [N']^T [h] [N_P] \, dV \\
&\quad - \int_{\Omega_e} [\delta p]^T [N_P]^T [h]^T [N'] [V] \, dV \\
&= [\delta V]^T \left([K^e] [V] - [g^e]^T [p] - [F_d^e] - [F_b^e] \right) - [\delta p]^T [g^e] [V]
\end{aligned}$$

where

$$\begin{aligned}
[K^e] &= \int_{\Omega_e} [N']^T [\mu\gamma] [N'] \, dV \\
[g^e] &= \alpha \int_{\Omega_e} [N']^T [h] [N'] \, dV \\
[F_d^e] &= \int_{\partial\Omega_e \cap \Gamma_t} [N]^T [\bar{t}] \, dS \\
[F_b^e] &= \int_{\Omega_e} \rho [N]^T \left[\bar{f}\right] dV
\end{aligned} \tag{2.31}$$

The total virtual power is

$$\begin{aligned}
\delta\pi &= \sum_e \delta\pi^e = 0 \\
&= [\delta V]^T \{ [K] [V] - [g]^T [p] - [F] \} - [\delta P]^T [G] [V] \\
&= 0
\end{aligned}$$

where

$$[F^e] = [F_d^e] + [F_b^e]$$

Therefore the global matrix equation is

$$\begin{bmatrix} [K] & [g]^T \\ [g] & [0] \end{bmatrix} \begin{bmatrix} [V] \\ -[p] \end{bmatrix} = \begin{bmatrix} [F] \\ [0] \end{bmatrix} \tag{2.32}$$

Now, by using weighted residual and the Equations (2.23-2.26), the formulation can be written as

$$\begin{aligned} \int_\Omega \left[\frac{1}{r}\frac{\partial}{\partial r}\left(rk\frac{\partial T}{\partial r}\right) + \frac{\partial}{\partial z}\left(k\frac{\partial T}{\partial z}\right) + \dot{q} - \rho C_P \left(\frac{\partial T}{\partial t} + v_r\frac{\partial T}{\partial r} + v_z\frac{\partial T}{\partial z}\right)\right] W_i dV \\ - \int_{\Gamma_q} \left[\left(k\frac{\partial T}{\partial r} - \rho C_P v_r T\right) n_r + \left(k\frac{\partial T}{\partial z} - \rho C_P v_z T\right) n_z - q_n\right] W_i dS = 0 \end{aligned} \tag{2.33}$$

with $W_i = 0$ on Γ_t. By using the divergence theorem and simplification

$$\begin{aligned} \int_\Omega \left[\left(k\frac{\partial T}{\partial r}\frac{\partial W_i}{\partial r} + k\frac{\partial T}{\partial z}\frac{\partial W_i}{\partial z}\right) + \rho C_p \left(\frac{\partial T}{\partial t} + v_r\frac{\partial T}{\partial r} + v_z\frac{\partial T}{\partial z}\right) W_i\right] dV \\ = \int_\Omega \dot{q} W_i dV + \int_{\Gamma_q} \left[\rho C_P \left(v_r n_r + v_z n_z\right) T + q_n\right] W_i dS \end{aligned} \tag{2.34}$$

Let $W_i = N_i^e$ for an element e and node number i and replace surface integrals and volume integrals with summations of the integral over each element. Therefore Equation(2.34) can be written as

$$\begin{aligned} \sum_e \int_{\Gamma_e} \left[\left(k\frac{\partial T^e}{\partial r}\frac{\partial N_i^e}{\partial r} + k\frac{\partial T^e}{\partial z}\frac{\partial N_i^e}{\partial z}\right) + \rho C_p \left(\frac{\partial T^e}{\partial t} + v_r\frac{\partial T^e}{\partial r} + v_z\frac{\partial T^e}{\partial z}\right) N_i^e\right] dV \\ = \sum_e \int_{\Omega_e} \dot{q} N_i^e dV + \sum_e \int_{\Gamma_q \cap \Omega_e} \left[\rho C_P \left(v_r n_r + v_z n_z\right) T^e + q_n\right] N_i^e dS \end{aligned} \tag{2.35}$$

Let $T^e = [N^e]\,[T^e(t)] = N_j^e T_j^e(t)$ and

$$
\begin{aligned}
K^e_{C_{ij}} &= \int_{\Omega_e} \left[\left(k_r \frac{\partial N_i^e}{\partial r}\frac{\partial N_j^e}{\partial r} + k_z \frac{\partial N_i^j}{\partial z}\frac{\partial N_j^e}{\partial z} \right) \right] dV \Rightarrow [K_c]^e = \int_{\Omega_e} [N']^T\,[\mathbf{k}]\,[N']\,dV \\
K_{V_{ij}} &= \int_{\Omega} \rho C_P N_i^e \left[v_r \frac{\partial N_j^e}{\partial r} + v_z \frac{\partial N_j^e}{\partial z} \right] dV \qquad \Rightarrow [K_V]^e = \int_{\Omega_e} [N]^T\,\rho C_P\,[\mathbf{v}]\,[N']\,dV \\
K_{S_{ij}} &= \int_{\Gamma_q} \left[\rho C_P \left(v_r n_r + v_z n_z\right)\right] N_i^e N_j^e dS \qquad \Rightarrow [K_S]^e = \int_{\Gamma_q} \rho C_P\,[\mathbf{v}]^T\,[\mathbf{n}]\,[N]^T\,[N]\,dS \\
B^e_{ij} &= \int_{\Omega_e} \rho C_P N_i^e N_j^e dV \Rightarrow [B]^e = \int_{\Omega_e} \rho C_P\,[N]^T\,[N]\,dV \\
F^e_{\dot{q}i} &= \int \dot{q} N_i^e dV \qquad \Rightarrow [F_{\dot{q}}] = \int_{\Omega_e} \dot{q}\,[N]^T\,dV \\
F^e_{q_n i} &= \int_{S_q} q_n N_i^e dS \qquad \Rightarrow [F_S] = \int_{\Gamma_q} q_n\,[N]\,dS \\
[K]^e &= [K_c]^e + [K_V]^e - [K_S]^e \\
[K]^e &= [F_{\dot{q}}]^e + [F_s]^e
\end{aligned}
$$

where

$$
[\mathbf{k}] = \begin{bmatrix} k_r & 0 \\ 0 & k_z \end{bmatrix}, \quad [\mathbf{v}] = \begin{bmatrix} v_r \\ v_z \end{bmatrix}, \quad [\mathbf{n}] = \begin{bmatrix} n_r \\ n_z \end{bmatrix}
$$

Therefore Equation (2.35) can be written as

$$
[B]\left[\dot{T}\right] + [K]\,[T] = [F] \tag{2.36}
$$

By using the Crank-Nicholson implicit method it can be written

$$
[T]_{t+\frac{\Delta t}{2}} = \frac{1}{2}\{[T]_t + [T]_{t+\Delta t}\} \quad \text{and}
$$

$$
\left[\dot{T}\right]_{t+\frac{\Delta t}{2}} = \frac{1}{\Delta t}\{[T]_{t+\Delta t} - [T]_t\}
$$

Equation (2.36) can be simplified as

$$[2\,[B] + [K]\,\Delta t]\,[T]_{T+\Delta t} = [2\,[B] - [K]\,\Delta t]\,[t]_t + 2\Delta t\,[F]_{t+\frac{\Delta t}{2}} \tag{2.37}$$

In this approach the deformation and heat transfer analysis are solved as follows.

1 Equation (2.32) is solved to find the nodal velocity

2 Plastic deformation and frictional energy terms for the step are calculated.

3 Heat generation term $\dot{q}$ of equation (2.23) is calculated using step 2.

4 The nodal temperatures are calculated from Equation (2.37).

5 Time and current billet geometry are updated.

6 Stop if the time is reached otherwise go to step 7.

7 Equation (2.37) is updated using the temperature values obtained from step 4 and go to step 1.

There are several commercial finite element software products available to solve above process. In this project ABAQUS and DEFORM 3D have been used to implement the finite element modelling. Figure 2.2 shows the process steps in these software products.

2.6 Extrusion Defects

The goal of extrusion is to produce parts that not only conform to dimensions but also have minimum defects and the correct metallurgical specifications. In general defects are a consequence of non homogeneous deformation. These defects can be categorized as (some are shown in Figure 2.3):

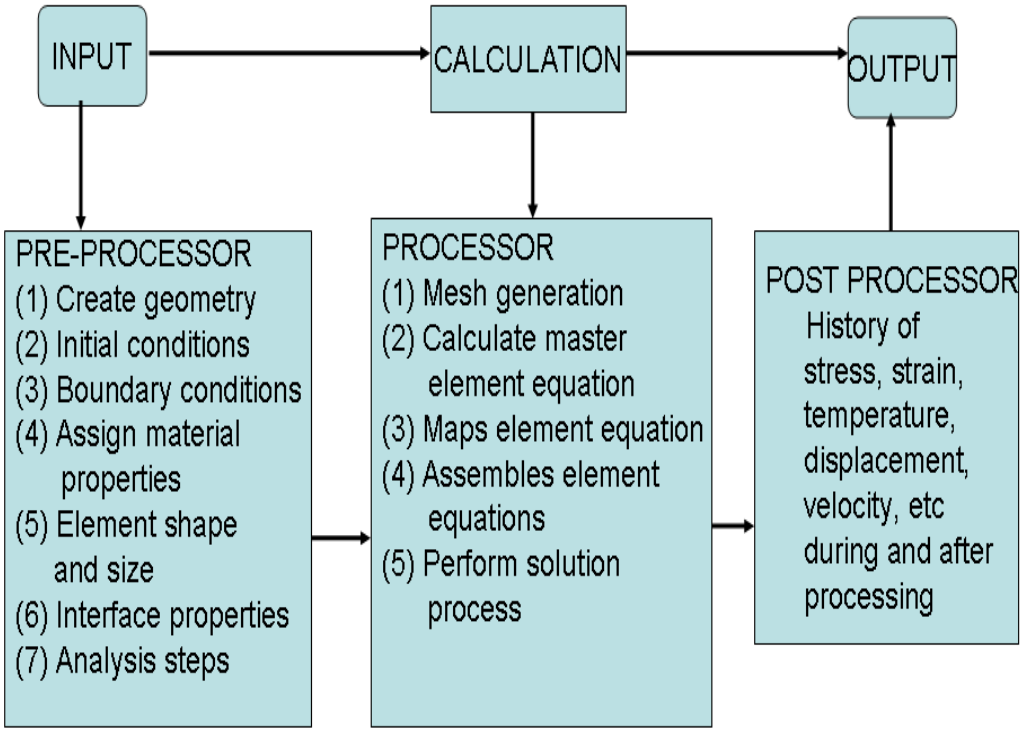

Figure 2.2: Steps in FEM.

(i) Bending: Velocity in one region is faster than in an other region

(ii) Chevron cracking (central burst): It is a one kind of internal defect occuring during the extrusion process and causes serious problems to the quality of the product. It is not possible to identify the defects by means of a simple surface examination of the workpiece. Therefore it is important to identify the conditions that may lead to the defects. By using suitable simulation methods it may be possible to choose appropriate parameter values and to modify the forming processes to minimize central burst. The die design and process parameters are the most important factors in preventing central bursts.

The chances of chevron cracking (or central burst) to occur increase with increasing axial stress inside the forming zone. This is mainly due to the inadequate values of friction, speed and temperature.

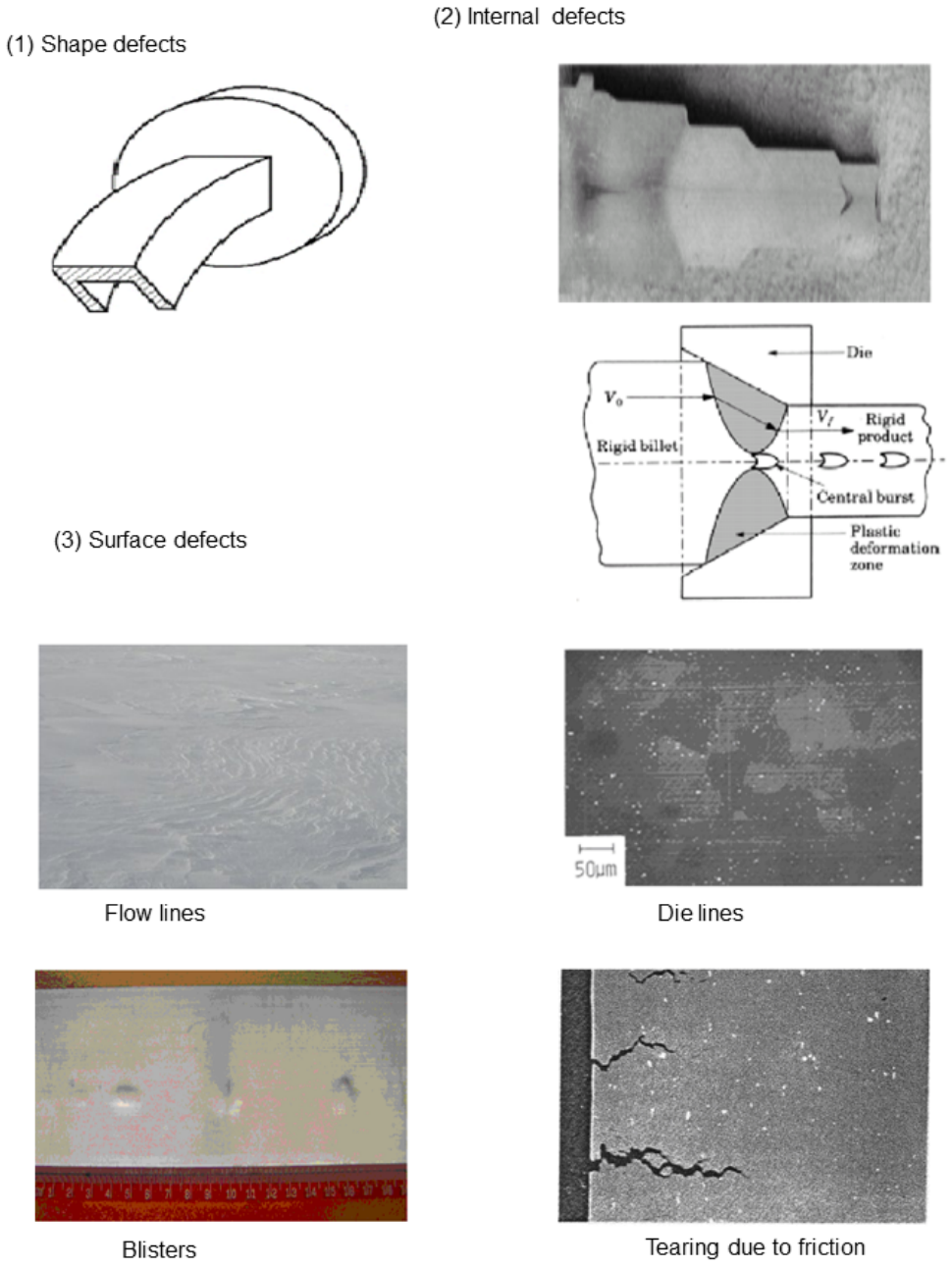

Figure 2.3: Defects in extrusion [58], [65].

(iii) Surface defects: It is a common problem among all extruders. This can be classified into

(a) Cracking: It can be seen from the literature[68] that three factors can influence the forming of cracks in the surface of extruded materials: They are

   (a) the history of the stress and strain of the billet during the extrusion process;

   (b) the tensile stresses in the surface layers of the material near to the die exit;

   (c) stick-slip.

(b) Lines on the surface

   - Flow lines: They are very irregular in size, shape and position. According to the available literature[55] it is a region of highest shear stress. They are caused by poor mixing inside the forming zone.

   - Die lines: They appear in the machine direction. There is generally no pattern to the line(s). These lines are caused by

     (a) a build-up of additives on or near the top of the die gap,

     (b) a piece of burnt metal or a contaminate lodged in the die below the die lips.

     These defects can be eliminated by cleaning the die before and/or during a production run. These lines will create a weakened section, which may tear easily.

   - Port lines: These lines usually range from 1 cm to 2 cm wide and are evenly spaced across the machine direction. These lines are formed when the temperature of the material is not consistent as it enters the die. This visual effect can be eliminated by keeping the material at an appropriate temperature for the particular type being extruded, as well as a consistent temperature throughout the

die.

- Weld lines: It is a continuous line in the product. It appears when the die surface contacting the material has a nick or defect. This may result in a weak area in the product that is prone to tearing.

(c) Die pickup: It is a tear-drop shaped spot aligned in the direction of extrusion. It can be caused by accumulated aluminum and aluminium oxide on the die-bearing surface or by inadequate homogenization of the billet before extrusion.

Some of these surface defects might not be seen on the final product because of protective coatings provided that the defects are within a tolerance level.

2.7 Previous Work

It is only during the last 35 years that mathematical modelling and simulation of aluminium extrusion have been reported in literature even though the extrusion industry is more than 100 years old. This is because of large computational demands that are associated with this kind of simulations. Early work was mainly concerned with 2-D extrusion problems or simple 3-D geometries with low extrusion ratios. With the increase of computer power more complex extrusion problems have been modelled.

Over the years several modelling techniques have been used for the analysis of extrusion processes. Table 2.1 shows a detailed summary of available approaches. This research aims at finding the right process and design variables to achieve a product with desired characteristics with minimal defects are considered. Literature closely related to these problems are being referred.

The thermodynamic and tribological relationships during extrusion of aluminium were analysed by Saha [64] in 1998. He investigated the frictional be-

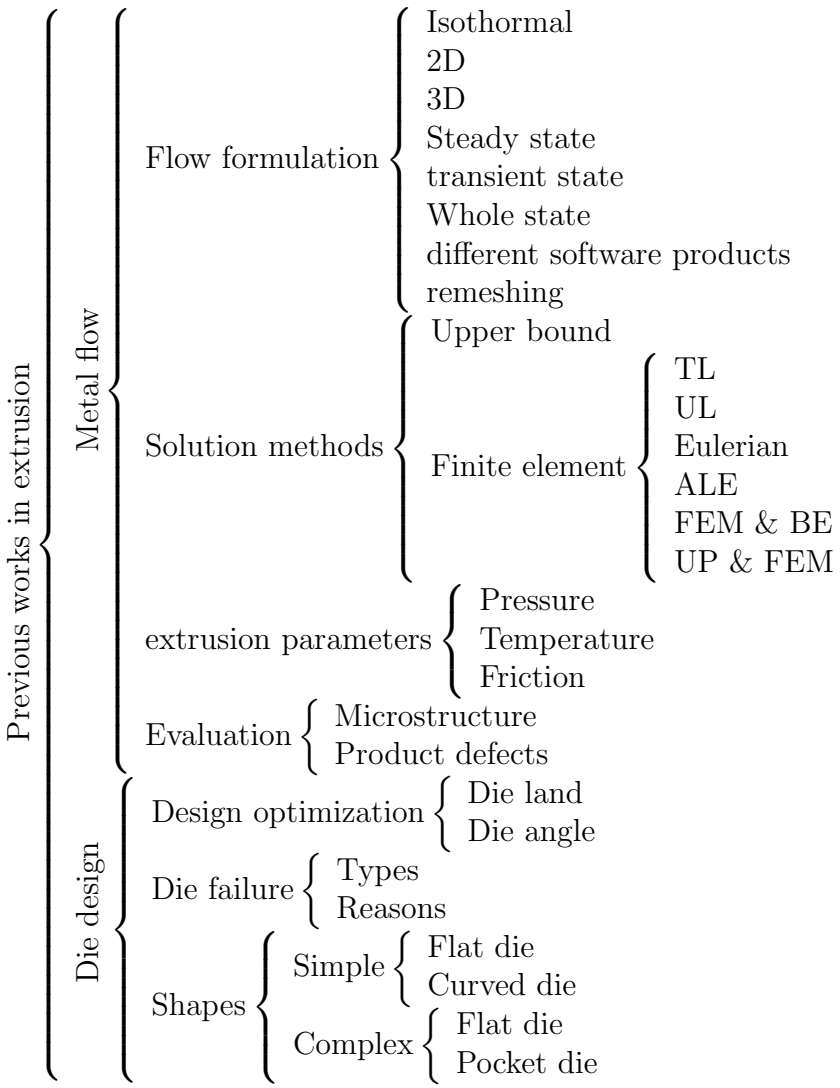

Table 2.1: Summary of previous works

haviours at billet–container, dead metal zone–flowing material and die bearing–material interfaces during aluminium extrusion processes and found that

(i) accuracy of shape and the surface finish during extrusion depend on the friction and wear in the extrusion process,

(ii) when the material is flowing through the die opening friction between die and material interface varied in a complicated manner,

(iii) the wear process in the die bearing is dependent on the thermodynamics of the extrusion process, which are very much influenced by the effects of extrusion variables.

Wifi *et al*[78], used the incremental slab technique and Bezier-curve technique to find the optimum curved die profile that minimizes the extrusion load for a hot extrusion process.

In 1999, Ulysse [74] addressed an important topic of extrusion die design. In this work he designed the bearing for a two-hole square die. The finite element method combined with techniques of mathematical programming is used in this work to determine the optimal bearing length. The optimal bearing length is found by minimizing the exit velocity variations at the exit of the bearings. He adapted a two dimensional die design geometry because optimisation simulations for realistic shapes are computationally intensive.

In the same year, the zero bearing (actually having a very small bearing length) die has been proposed by Rodriguez *et al* [62], [63]. With this kind of die, the design of the pocket is the only means to regulate the flow velocity at the die exit. The type of die is called single-bearing die, offering advantages in permissible extrusion speed and good surface quality. However, when a wide thin-walled profile is geometrically complex, zero bearing length variation technology may not be very helpful to control metal flow.

Then in 2000, efforts are made by Chanda *et al* [8] to determine the state of stress, strain and the temperature of a commercial aluminium alloy (AA6061) during the extrusion process using a three dimensional finite element simulation method. In this work they considered extrusion through square and round dies at reduction rations of 20:1 and 60:1 and found that

(i) when the reduction ratio is 20 : 1 the round extrudate has a higher maximum temperature than the square extrudate in the steady state of the extrusion

process,

(ii) when the reduction ratio is 60 : 1 the square extrudate has a higher maximum temperature at the initial stage of the process. This shows that the hot shortness is more likely to occur at an early stage of the process when the reduction ratio is high.

(iii) In the square extrudate, the temperature distribution is inhomogeneous and the corners tend to have a high temperature, especially when the reduction ratio is low.

(iv) The square extrudate has much stronger tendency toward tearing especially at a higher reduction ratio since the tensile component of stress at the surface of the square extrudate is three times as high as that at the surface of the round extrudate.

(v) The distributions of strain in front of the round die and square die are different.

(vi) The strain at the entrance of the square die is more confined and the strain gradient is larger.

(vii) The maximum strain in the square extrudate is smaller than that in the round extrudate due to the flow retardation by the square die.

Lee *et al*[37] used the finite element method combined with a semi-empirical mathematical microstructure evolution model to produce a uniform microstructure. They used Bezier-curves to generate all possible die profiles and and found that

(i) By maintaining uniform strain rate at the forming region it is possible to extrudate a product with uniform microstructure.

(ii) In the hot extrusion process, the change of die profile and process conditions influences the uniformity of the microstructure.

In 2000, Lof [50] reported a number of developments in the numerical simulation of extrusion. This includes the modelling of the bearing area and the development of a practical method for the simulation of the extrusion of complex profiles. He demonstrated that elastic effects have a dominant influence on the bearing channel. This was done by comparing simulations with a viscoplastic model and an elasto-viscoplastic model. He also investigated the effects of changes in bearing geometry.

Then in 2001 Chanda *et al*[7] tried to characterise the formation of the deformation zone and dead metal zone during the initial non-steady phase of the extrusion process in relation to process variables and die shape. They also used the same 3D finite element technique for the computer simulation, AA6061 aluminium alloy for the material and two different shapes of the die such as square and round. They carried out a number of simulations and demonstrated that

(i) The maximum strain rate is higher in front of a square die than in front of a round die.

(ii) The maximum strain rate appears at the square die corners where severe shear deformation occurs.

(iii) The size of the dead metal zone varies with the friction factor at the billet-container interface.

(iv) A change of die shape, while the reduction ratio is kept the same, does not change the size or shape of the dead metal zone.

In that same year Flitta *et al*[18] investigated the nature of friction in extrusion processes and its effect on material flow. This investigation focused on simulation of the extrusion process and in particular the effect of the initial billet temperature

on friction and its consequences on material flow. All the simulations are performed with the implicit finite element codes FORGE2 and FORGE3. It was found that

(i) The friction values are not constant for all extrusion temperatures and increases approximately linearly with increasing initial billet temperature.

(ii) For an accurate simulation of extrusion, the friction coefficient must be identified continuously during the process cycle.

(iii) The increase in friction results in an increase of the initial extrusion load.

In 2003, Zhou *et al*[86] performed 3D computer simulations on the extrusion of AA7075 aluminium billets with non-uniform temperature distributions in order to inhibit an excessive temperature rise that tends to occur during the conventional extrusion of an uniformly preheated billet. From this simulation study they have found that

(i) The continued temperature rise leading to hot shortness as occurring during the conventional extrusion of a AA7075 aluminium billet with uniform temperature could be lessened or even inhibited by imposing a temperature profile along the length of a preheated billet.

(ii) With the non-linear temperature distribution imposed on the billet, the maximum work piece temperature could be kept within a small range, although the temperature distribution in the billet remained non-stationary during extrusion.

(iii) Imposing a billet temperature profile could lead to a stable die face pressure, which would be of help in maintaining the consistency of the dimensions and shape of the extrudate.

(iv) The temperature distribution at the cross section of the extrudate varied while it flowed through the die. The extrudate temperature at the die exit

became more homogeneous than at the entrance. The highest temperature was found to be near the die entrance. Upon leaving the die, the extrudate had a higher temperature at the outer surfaces and legs than in the core.

(v) Tensile principal stress occurred near the corners of the die orifice and tearing would occur, if its value exceeded the fracture strength of the material.

Lin *et al*[49] proposed a method for the optimization of the die profile for improving die life of a hot extrusion process. This method provides an effective approach for optimum design of the die curve. It is based on a gradient method and a rigid viscoplastic finite element method. They expressed the die profile by a cubic spline curve and applied an updated sequential quadratic programming method as an optimization technique.

Zhou *et al*[86] presented a 3D finite element simulation model of the whole cycle of aluminium extrusion throughout the transient state and the steady state using the updated Lagrangian approach. In this study he said that

(i) The distribution of velocity, effective strain and temperature in the deforming billet are not stationary, even in the steady state

(ii) Following an initial steep increase, the maximum temperature of the workpiece increases progressively till the end, which represents the typical pattern of temperature development in the conventional aluminium extrusion.

(iii) The extrusion die is exposed to varying pressure and has varying, inhomogeneous temperature distributions.

Duan *et al*[13] introduced various metallurgical models for aluminium alloys under hot working conditions. They integrated physical models which are based on dislocation density, subgrain size, and misorientation into a commercial finite element modelling program simulating extrusion. From this study they found that

(i) Under constant ram speed, the temperature and subgrain size increases with increasing ram displacement. The distribution of microstructure along the section and the length is not uniform.

(ii) A uniform distribution of microstructure along the length can be performed by the use of both iso-subgrain size and isothermal extrusion process.

(iii) FEM is a very effective and efficient way to design the ram speed profile.

(iv) The die configuration has a very strong influence on the static recrystallisation behaviour. The volume fraction recrystallised can be substantially reduced by the adoption of an appropriate choked die configuration.

(v) Compared with the deformation using a flat faced die with 90^o corner, the deformation is more uniform when using an extrusion die with a die choke.

(vi) Changing container temperature helps to control the recrystallisation. The higher the container temperature, the lower the volume fraction of recrystallisation.

(vi) The selected criterion for the control of ram speed in either isothermal or iso-subgrain size extrusion directly determines the quality of the designed ram speed profile.

Venugopal *et al*[77] presented a method based on a dynamic material model and finite element simulation to identify the optimal processing conditions for 304L stainless steel material. It is a two stage approach. In the first stage, microstructural models developed by Yada[53] were used to obtain an optimal deformation path to achieve a grain size of 26 μm. Then in the second stage, a geometric mapping was used to identify extrusion parameters such that the strain rate profile during the process matches the optimal trajectory calculated in the first step.

Li *et al* investigated the capabilities of using pockets to control metal flow. They run a series of pocket design simulations using a finite element technique to investigate the influence of pocket angle (θ_1 or θ_2 in Figure 2.4) on the metal flow. It has been shown that there is an inverse linear relationship between pocket angle and flow velocity when $\sqrt{d^2 + w^2}$ is constant. That is, a smaller pocket angles result in large exit velocity and a larger pocket angle results in small exit velocity. They also found that the pocket volume does not significantly affect the flow velocity.

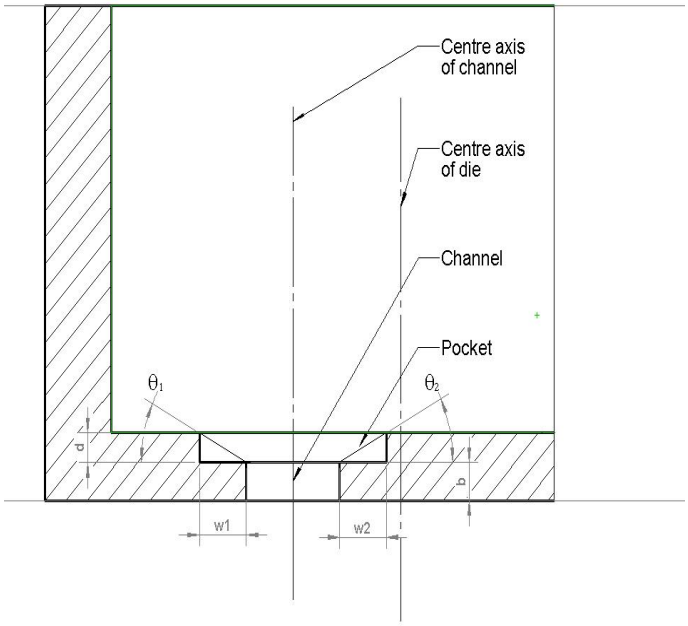

Figure 2.4: Pocket shape-side view

Peng and Sheppard demonstrated the effect of using a pocket to regulate the material flow and temperature distribution. They considered geometry similar to Figure (2.4) and run several simulations by moving the centre axis position of the pocket towards and away from the centre axis of the die. In this study first they clearly demonstrated the necessity to use a pocket and the sensitivity of the pocket

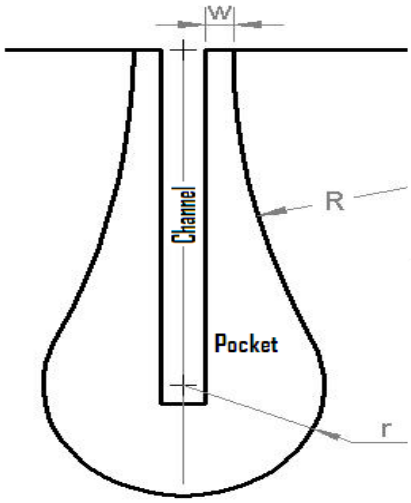

Figure 2.5: Pocket shape-Top view

axis location relative to the channel axis. That is the sensitivity of the difference $w_1 - w_2$. They have also demonstrated from this study that the thickness w_2 should be less than w_1 and would require more research to find the optimal difference between w_1 and w_2.

In 2006, Golovko and Grydin proposed a new method for flat pocket die design using a U-shaped profile. They have demonstrated the channel with significantly larger length resulted in variation of flow speeds along the channel exit and proposed to divide the channel into smaller elements with different bearing lengths.

Then in 2008 Fang *et al* presented a series of simulations using DEFORM 3D finite element software to produce a wide thin-walled aluminium profile. They predicted the velocity and temperature distribution and demonstrated that the geometrical parameters of the pocket can be used to balance the metal flow instead of changing the local die bearing length. They designed the pocket as in Figure 2.5 to balance the metal flow. In the figure an increase in parameter r leads to a significant increase in pocket cross sectional area and volume but it has very little impact on flow homogeneity. The changes in parameter R lead to a significant

impact on the metal flow. The pocket depth also considerably influences the flow speed.

In the same year of 2008 Yuan *et al.* proposed a design with a guiding angle to reduce surface defects. They demonstrated using a series of numerical simulations that the metal flow is more homogeneous and the tendency to generate a dead metal zone is minimized. They also demonstrated that the axial stress on the die exit is decreased and therefore surface cracks caused by additional stress are avoided.

In 2009, Fang *et al.* [16] presented a case study to demonstrate the usefulness of 3D computer simulation to achieve optimum product quality and maximum throughput, in the case of extruding the AA7075 alloy into a complex profile with varied wall thicknesses. The design of the extrusion die and the choice of process parameters were integrated by means of 3D computer simulation. In this research, three double-pocket dies with different bearing lengths were designed and the extrusion speed was varied to predict the optimal extrudate temperature, extrusion pressure requirement and surface quality. This was later validated experimentally.

In 2010 HE You-Feng *et al.* [31] demonstrated using two different multi-hole porthole dies with and without pockets. These pockets could be used to effectively adjust the metal flow and especially the maximum temperature at the die bearing and the peak extrusion load could be decreased. This indicates the possibility of increasing the extrusion speed and productivity.

In 2010, Valberg [75] published a book Applied Metal Forming: including FEM analysis. This book describes metal forming theory and explains how experimental techniques can be used to study the forming conditions of metal forming operations with great accuracy. In addition, it is shown for each of the main classes of metal forming operations including extrusion, how FEA can be applied precisely to characterize forming conditions, and ways to optimize processes. Examples are also provided to prove how theory, experiments, and FEA in combination can be

used to calculate and characterize the conditions of an extrusion process.

2.8 Unresolved Issues

To extrude a product with given shapes, good surface quality and homogenous structure the metal flow through the die should be as uniform as possible. This is not possible without knowing the right set of process and die design parameters and further these values will vary with product shapes. Therefore optimal values of process and design parameters for each product shape have to be determined before a die can designed.

An extrusion model, which is capable of describing the behaviour of material flow, requires material data, die design variables and process variables. In reality, material data can be measured using available measuring instruments, but values of die design variables and process variables are often unknown and have to be calculated. The calculation procedure should also include the microstructure of the work-piece material. Many mathematical models have been reported in the literature for predicting average grain size. The values of constants appearing in these models are based on experimental observations and therefore the uncertainties of constants are very high. Small changes in these values can cause large variations in the grain size estimation and eventually these errors will magnify in the estimation procedure of process and design parameters. Therefore discovering a new methodology to identify optimal values of those constants is an important part of modelling extrusion processes to increase the reliability of the numerical simulation.

Several methods and formulations can be used based on finite element modelling to predict the extrusion process. Some methods can capture the material flow in a very accurate way but are computationally expensive. Some methods are computationally faster but less accurate. The problem being considered here has a complex

geometry and thin profiles, which necessitates a large billet area reduction. A few sharp corners are also commonplace in the die structure and frequent remeshing will be inevitable during the simulation of the extrusion process. These matters pose considerable challenges to the numerical modeller. Therefore the computational efficiency in terms of (a) speed (b) optimization algorithms as well as (c) fast and accurate re-meshing techniques are very vital to deliver an accurate solution.

2.9 The Research Strategy and Methodology

The purpose of the investigation is to improve the surface quality of extruded products of 6XXX and 7XXX series aluminium alloys in terms of homogeneity of grain sizes. The research strategy and methodology is divided into several stages. Knowledge of aluminium extrusion processes and modelling techniques has been taken from previous literature.

In the first step, the numerical simulation of the extrusion process with a simple die is considered using finite element software and to identify in particular how

1. temperature, stress, strain and velocity changes during the extrusion process,
2. shape of the die and process parameters influence the properties of the extruded part and
3. the efficiency of the simulation process can be increased.

The computational tools used are: ABAQUS, DEFORM 3D and MATLAB.

The second step is related to the numerical analysis of the surface quality in terms of grain size and homogeneity of extruded products with various different die shapes and process conditions. The aim of this stage is to find optimal process and design parameters for an extrusion process to extrude a product with a simple geometry with given material properties. This is an inverse problem and the model

is formulated as a non-linear least minimization problem coupled with finite element techniques. Computational tools used to implement are MATLAB's lsqnonlin function for the optimization and ABAQUS for the finite element calculations. The PYTHON software is used to build an interface between MATLAB and ABAQUS.

The third stage involves the estimation of average grain size history during the extrusion process and other material constants by using simulated strain and temperature values during the extrusion process. The problem of finding the average grain size is based on linear and non-linear least squares coupled with microstructure control models. It is an ill posed inverse problem and therefore the solution is not stable. Tikhonov's regularization is used to stabilise the solution process. Least squares methods are implemented using MATLAB's inbuilt functions.

The fourth stage involves the simulation of 3D extrusion processes and the identification of design parameters to control the flow in three dimensions for a die with simple and complex geometry. The simulation process of the extrusion of complex geometry is different from the simulation of simple geometry in many ways. Firstly, a Bezier curve technique cannot only be used to optimize the metal flow for the complex geometry. Secondly, simulation of flow through complex, very thin parts is computationally very demanding because of severe element distortions. ABAQUS and DEFORM 3D are to be used to simulate these extrusion processes and analyse the way to simulate the extrusion process efficiently.

The last and fifth stage involves the simulation of 3D extrusion processes through a thin and complex shaped profile and studying in particular:

1. How the flow through the die can be adjusted by using a suitable pocket in front of the die entry,

2. Identification of design parameters to regulate the flow,

3. Investigate the influence of design parameters to regulate the exit speed,

4. Investigate the influence of design parameters on the homogeneity of flow in terms of velocity, temperature and shear stress,

5. Investigate the influence of process parameters on the homogeneity of flow in terms of velocity, temperature and shear stress.

The purpose of these investigations is the estimation of an optimal set of conditions to extrude a profile with minimal defects. Based on these observations and using simple optimization principles three algorithms are developed to design an optimum shape die and identify the right set of process conditions to extrude a product with minimal defects.

Chapter 3

FEA Modelling of Extrusion

3.1 Overview

FEA is a numerical technique for finding approximate solutions. A range of problems in the mechanical engineering discipline commonly use the finite element method for design and developments. It gained popularity due to its ability to model most physical problems by means of mathematical algorithms. Implementing this method usually involves large amounts of computations and can be more efficient if commercially available well developed software programs are used. The choice of the right software is an important factor in determining the quality and scope of simulation that can be performed.

ABAQUS is considered as a general purpose highly sophisticated finite element software program that can be used to solve a variety of problems. It is specially suited for nonlinear finite element analysis. Further it is widely used in industrial and academic environments. It allows modelling at a high level of detail and allows the user to set up a model to analyse complex problems. DEFORM 3D is another finite element software specially suited for metal forming applications. It uses adaptive meshing techniques more efficiently than ABAQUS to accommodate

large deformations that are very common in metal forming and especially in extrusion. Overall, both have their advantages and it was decided to use ABAQUS and DEFORM 3D as suitable software packages for our investigations.

ABAQUS and DEFORM 3D are used in this chapter to create a finite element model of an axisymmetric extrusion process. The main theme of this chapter is to simulate forward extrusion, to analyse the thermo-mechanical process of extrusion and to study the interaction between the process parameters, tooling and deformed material. Through the proper use of these software products, a large amount of information can be obtained which is not easily gained through experimental work.

At the end of this chapter the role played by FEM softwares in the simulation process of extrusion and the results of the simulation will be demonstrated.

3.2 DEFORM

DEFORM is specially designed for metal forming problems and is based on an implicit Lagrangian computational routine. Its graphical user interface provides easy data preparation and analysis. It has a fully automatic, optimized re-meshing system tailored specially for deformation problems. It consists of three major components:

1. Pre-processor: It can be used for creating, assembling, or modifying the data required for the simulation. It also generates the required database file for the simulation.

2. Simulation engine: It is used for performing the numerical calculations required to conduct a simulation, and writes results to the database file. It generates a new FEM mesh of the workpiece whenever necessary.

3. Post-processor: It can be used to display results graphically and for extracting

numerical data.

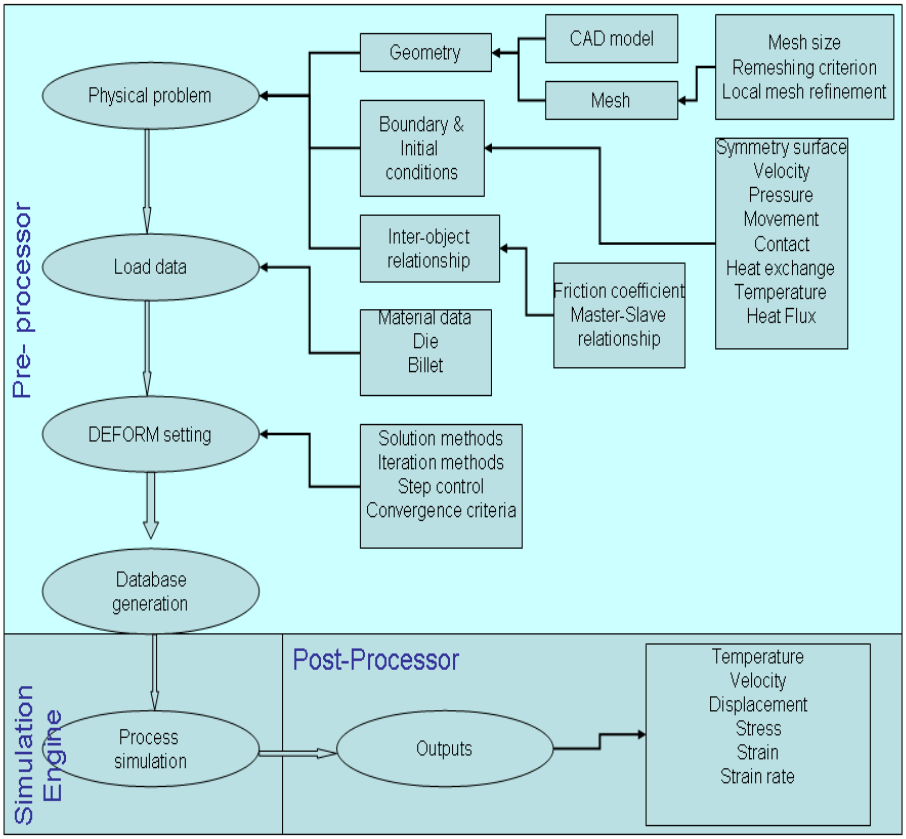

Figure 3.1: Modelling process in DEFORM

3.3 Modelling Process in DEFORM

This section details the sequence of steps used in DEFORM. These are shown in Figure 3.1. The recommended sequence for designing a simulation process is

1. Define the physical problem

   (a) Geometry:

i. Part properties: In an extrusion process, geometry contains the die, billet and ram. These can be modelled using any CAD program and imported to the DEFORM platform. The billet undergoes deformation and therefore it has to be modelled as elastic/plastic. Die and ram can be modelled either as elastic/plastic or rigid. In reality die and ram also undergo deformation but compared to the billet, the die's, and ram's deformation is negligible and therefore these are defined as rigid in this study.

ii. Mesh: DEFORM has several types of meshes which includes Eulerian, Lagrangian and a combination of arbitrary Lagrangian Eulerian and coupled Eulerian Lagrangian. Iterative solvers in DEFORM are more optimized for a Lagrangian mesh [19] and therefore the simulation can be done faster using Lagrangian meshes than other meshes. The other key advantage using a Lagrangian mesh is that it knows the entire time history of the key variables at every point during the simulation and therefore even if the simulation crashes a new simulation can be started where it was stopped [19].

(b) Boundary and initial conditions: There are several types of boundary conditions which have to be assigned separately. If the geometry is symmetrical then by defining a symmetrical boundary condition simulation time can be reduced. Other boundary conditions include deformation and thermal.

(c) Inter object relationship: The function of inter object relations defines how the die and billet in a simulation interact with each other. It is very important to define inter object relationships properly for a simulation to model an extrusion process correctly. The critical variables to be defined between die and billet are friction, interface heat transfer coefficient,

contact relation and separation criterion.

2. Load material data: DEFORM has a material library containing models of common materials and alloys currently in use. Required data can be obtained from the library. This includes flow stress curve, Young's modulus, Poisson's ratio, thermal expansion, thermal conductivity, emissivity, diffusion coefficient and hardness etc. It also has a capability to define a new material if the constitutive equation of the material is known.

3. Define settings: The proper set up of settings prior to the simulation is important to achieve an accurate solution.

   (a) Solution methods: For most problems, the default method should be acceptable.

   (b) Iteration methods: This is the manner in which the simulation solution is updated. There are two methods available within DEFORM.

      (i) Newton-Raphson: It is appropriate for most problems since it converges in fewer iterations than the direct method, but solutions are more likely to fail to converge than with the direct method.

      (ii) Direct: It requires more iterations to do the simulation.

   (c) Step controls: The steps are defined either as a specific time interval or a specific distance travelled by the ram.

   (d) Convergence criteria: It includes a 200 iteration limit for convergence, velocity and force error norms to determine, when convergence is reached.

4. Submit the data for simulation.

5. Review the results.

3.4 ABAQUS

ABAQUS is a general-purpose finite element program. It can be used to carry out the computational analysis of an extrusion process. ABAQUS offers two integration methods; implicit and explicit. ABAQUS Standard uses the implicit scheme and ABAQUS Explicit uses the explicit scheme. In extrusion the billet undergoes severe plastic deformation, which will require the adjustment of the mesh to prevent excessive element distortion. ABAQUS Explicit has adaptive meshing capabilities that automatically re-meshes throughout the analysis. ABAQUS Standard does not have this ability.

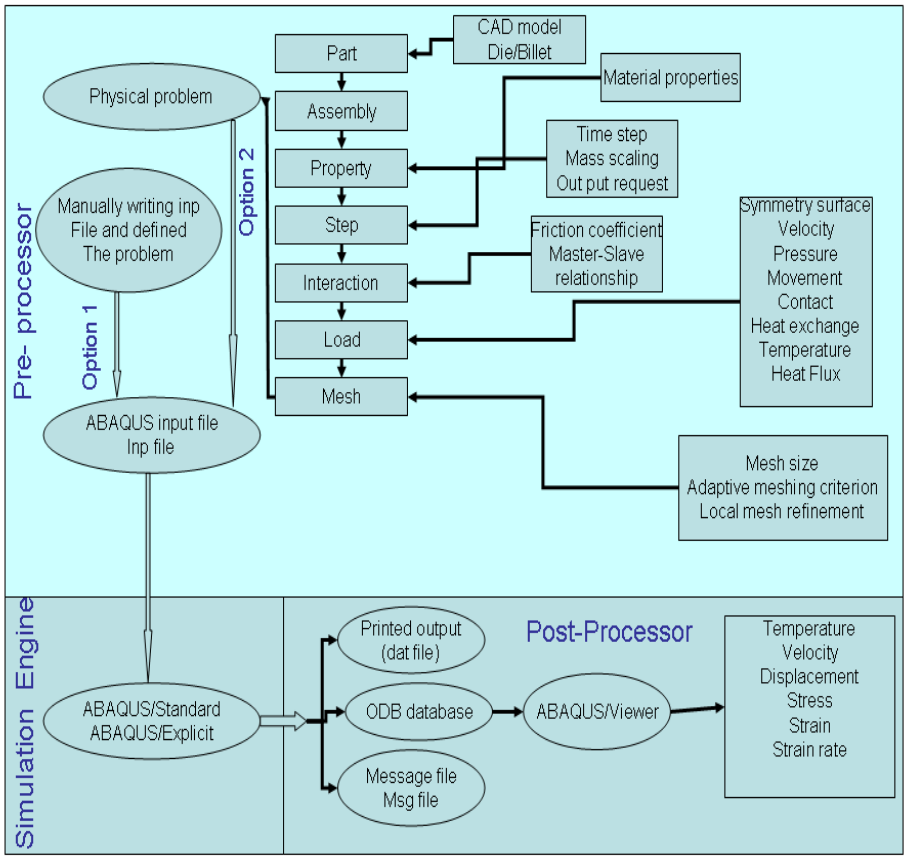

Figure 3.2: Modelling process in ABAQUS

Figure 3.2 shows the interrelationship between input, processing and output of *ABAQUS*. It works by reading and responding to a set of commands (called KEYWORDS) in an input file. The keywords contain the information to define the mesh, the properties of the material, the boundary conditions and to control output from the program. The input file can be created either manually by building a script or by using ABAQUS/CAE. Building input files by hand for large complex problems is difficult and time consuming. ABAQUS/CAE builds models very quickly and it has also the facility to import geometry of a model from any CAD software. It also has advanced meshing and visualization facilities and provides a better modelling environment for users. The results of an *ABAQUS* simulation can be viewed using ABAQUS/Viewer, which can be used to plot various quantities that may be of interest. Alternatively, the program can print results to a file, which can be looked at with a text editor.

3.5 Modelling Process in ABAQUS

Any *ABAQUS* model consists of several components, which describe the problem to be analyzed, and the results to be obtained. The modelling process can be mainly divided into six parts as (1) Building a model, (2) Define material properties, (3) Mesh, (4) Apply loads and boundary conditions, (5) Run analysis and (6) View results.

The input file for these steps can be set up using a text editor. Since this is too difficult for large or complex geometries ABAQUS/CAE can be used to set up these steps very quickly and easily.

1. Building a model: In ABACUS/CAE parts (die and billet) of the model are created or imported and then those parts are assembled using assembly module. Figure 3.3 shows the geometry of workpiece and tools. The work

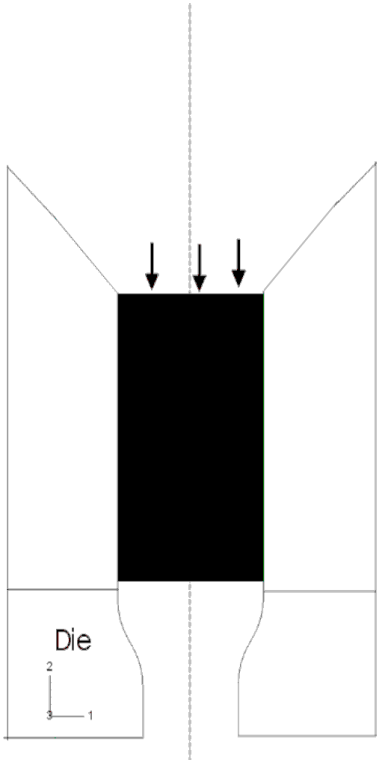

Figure 3.3: Geometry of workpiece and tools.

piece is pushed down by prescribing a velocity for the nodes along the top of the billet. As the billet is pushed down, material flows through the die opening to form the final shape.

2. Material properties: Material properties of die and billet can be assigned using the property module. The billet is a deformable body and the die can be modelled either as deformable or rigid. Rigid also means any heat transfer inside is neglected and only the temperature of the rigid body reference node is fixed and it is assumed that no heat is transmitted between the billet and the die. The billet is deformable and generation of heat due to plastic dissipation inside the billet and the frictional heat generation at the workpiece/die interface are considered.

3. Mesh: Next the mesh module to define the mesh is used. The finite element

mesh is used to specify the geometry of the work–piece. It is a set of nodes together with a set of elements, which is shown in figures 3.4 and 3.5.

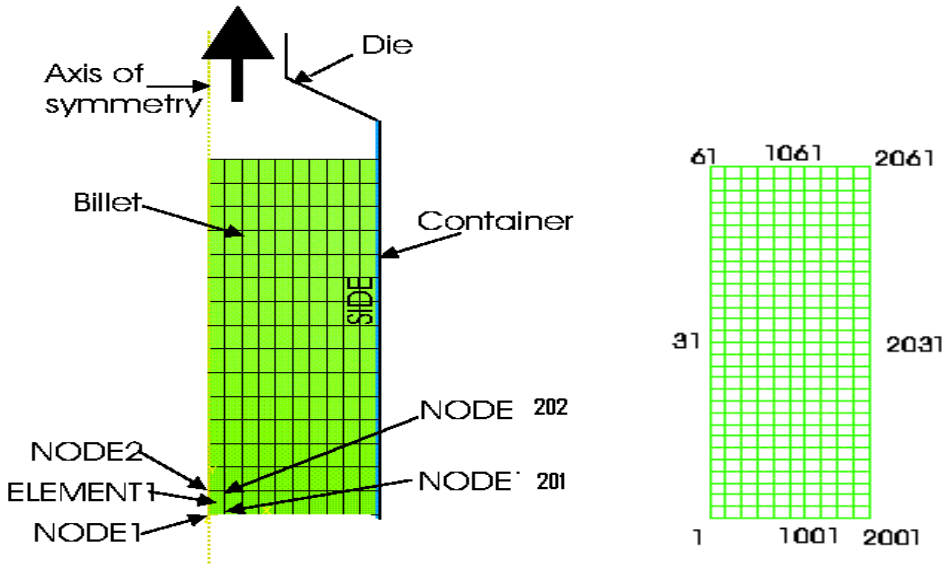

Figure 3.4: Mesh used for the simulation.

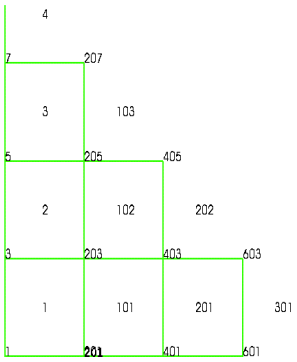

Figure 3.5: Node and element numbers.

The nodes are a set of points within the work–piece. Nodes have a node number, which is used to recognize the node. Elements are used to partition the solid into discrete regions and they have an element number. Every element is allocated an integer number, which is used to recognize the element.

There are many possible shapes for an element. A few of the more common element types are 3 node triangle, 6 node triangle, 4 node quadrilateral, 8 node quadrilateral, 4 node tetrahedron, 10 node tetrahedron, 8 node brick and 20 node brick.

Each element in the workpiece consists of solid material. The type of material within each element must be stated, jointly with values for the all-material properties such as density, Young's modulus, Poisson's ratio, stress-strain relation etc.

4. Contact definition, boundary conditions, initial conditions: Simulation of extrusion requires contact between die and billet. Modeling of the interface interactions must be defined clearly. Important general aspects should include

   (a) Contact algorithm: It determines how the bodies interact with each other. There are two types available: Penalty and kinematic. With the penalty algorithm contact–force time–histories are smoother and it allows small contact penetration. But on the other hand the kinematic algorithm is unconditionally stable. Both algorithms approximately require the same amount of computation time.

   (b) Friction: Coulomb friction is a general friction model most appropriate to describe the interaction of contacting sliding surfaces. The model describes the frictional behaviour between the contact surfaces using a coefficient of friction. However at appropriately high pressure it may fail to describe the actual friction conditions.

   (c) Over/under closure: Using the master-slave approach, slave nodes are not allowed to penetrate the master surface. For extrusion processes, the die is designated as the master surface and the billet as the slave

surface.

(d) Heat transfer: The heat transfer between contacting objects.

Whenever contact is modelled, it will be necessary to indicate pairs of surfaces that might come into contact and then define the way the two surfaces interact by specifying the coefficient of friction between them.

It is also necessary to specify the initial values for field variables such as displacement and temperature distribution.

5. Running analysis: There are two basic types of analysis.

   (a) ABAQUS/Standard: It uses the implicit method for integration of equations. It is possible to use all available elements in ABAQUS but computing takes longer than with the explicit method.

   (b) ABAQUS/Explicit: It uses the central difference method. Fewer element types can be used with the explicit method.

   Once the method of analysis is chosen, ABAQUS should be told to apply the load in a series of steps. Many different boundary conditions can be defined in each step. Unless it is specified otherwise, the loads (or displacements) will vary linearly from their values at the start of the step to their values at the end of the step. ABAQUS will try to go from the start of each step to the end of each step in a single time-step. The analysis may or may not converge. If it doesn't converge, ABAQUS will automatically decrease the time step size, and will instead apply the load in a series of smaller increments.

   For models requiring considerable computing time, mass scaling is frequently employed. The density can be increased by increasing the mass. For this situation, the model response must be monitored to ensure the ratio of kinetic energy to internal energy does not exceed 10 percent.

Adaptive meshing is a powerful tool available in ABAQUS/Explicit. It is performed using the arbitrary Lagrangian Eulerian method. It is available for all first order, reduced integration continuum elements. The billet will undergo severe deformation and any initial mesh, which distorts to a certain level, will prevent completion of a solution. The adaptive meshing technique will allow the mesh to be modified automatically as the analysis proceeds. It is an important tool and will also reduce the computational requirements to achieve accuracy.

6. Viewing results: Like other finite element softwares ABAQUS first calculates the displacements of each node in the mesh. The quantities such as velocity, acceleration field, strain components, principal strains, and strain invariants, elastic and plastic strains, strain rates, stress components, principal stresses, stress invariants, forces applied to nodes or boundaries, contact pressures yield stresses and material failure criteria can be calculated as functions of time at selected points in the mesh from the displacement field.

3.6 Simulation of Extrusion Process

3.6.1 Flow Simulation

The idea of this section is to demonstrate how temperature, stress, strains and velocity change during the extrusion process. This is applicable to many metal extrusion and not particularly to any specific alloy. For illustration purposes a billet of radius 28 mm and length 90 mm is considered. The billet is pushed down 19 mm by prescribing a constant velocity of 5 ms^{-1} for the nodes along the bottom of the billet. As the billet is pushed down, material flows through the die opening to form a solid rod with a 10 mm radius. The following data values were used in

the ABAQUS/Explicit simulations: Young's modulus $E = 3.8 \times 10^{10}\ Pa$, coefficient of expansion= $8.4 \times 10^{-5}\ {}^{o}C^{-1}$ at $T = 20\ {}^{o}C$, Poisson's ratio= 0.33, inelastic heat fraction = .9, specific heat = 880 $Jkg^{-1}K^{-1}$, initial temperature= $20^{o}C$, density= 2672 kgm^{-3}, conductivity = 204 $Wm^{-1}K^{-1}$ when $T = 0\ {}^{o}C$, = 225 $Wm^{-1}K^{-1}$ when $T = 300\ {}^{o}C$ and Figure 3.6 shows the plastic behaviour of the material. These values are chosen to reflect the response of a typical commercial purity aluminium alloy.

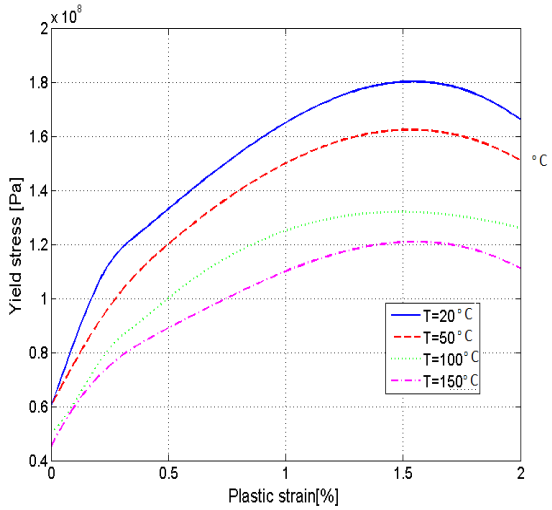

Figure 3.6: Material data

Here the heat transfer in the die is not modeled (i.e. isothermal rigid body) and cold–extrusion at room-temperature is considered. The temperature of the rigid body reference node is fixed and assumed that no heat is transmitted between the billet and the die. The generation of heat due to plastic dissipation inside the billet and the frictional heat generation at the workpiece/die interface are considered.

Figure 3.7 shows the deformed mesh when the simulation has been continued sufficiently for some parts of the billet to be extruded through the die. Figure 3.8 ((a), (b), (c) and (d)) depict the contour plot of temperature, circumferential plastic strain, circumferential stress and velocity respectively and Figure 3.9((a), (b),

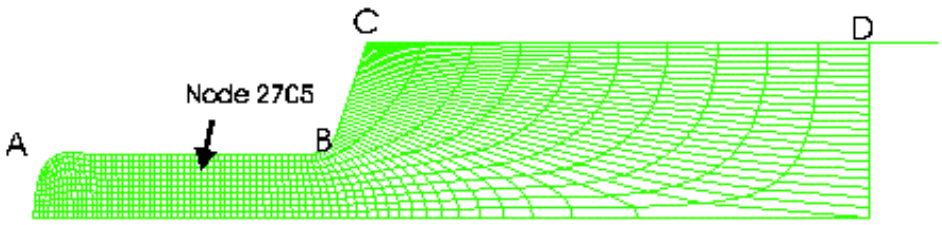

Figure 3.7: Deformed mesh

(c) and (d)) depict the temperature, circumferential plastic strain, circumferential stress and velocity at node 2705 (see Figure 3.7).

3.6.2 Die Design Parameters

Die geometry optimisation is necessary in order to reduce defects and improve parts properties and quality of the extruded product. The die optimisation problem is a function of design parameters namely die angle, die-land length and friction. This section demonstrates the relationship between the product quality and the die design parameter values.

(i) **Die angle:** Die angle θ is in general the angle between the central axis and surface of the die. It is also known as semi-cone angle. Here the angle between the die surface and the horizontal ($90 - \theta = \alpha$) is used as in Figure 3.10. There are a few factors influencing the die angle design in the direct extrusion processes. To investigate these factors numerical experiments are done with various die angles. Figure 3.11a, and 3.11b show respectively the comparison of velocity and temperature along the outside edge (ABCD) of the billet for angles $\alpha = 0^o$ and $\alpha = 45^o$. It can be seen that there is not much difference between the velocity profile, but the temperature at the corner B increases slightly when the angle α is small. Figure 3.12 shows the variation

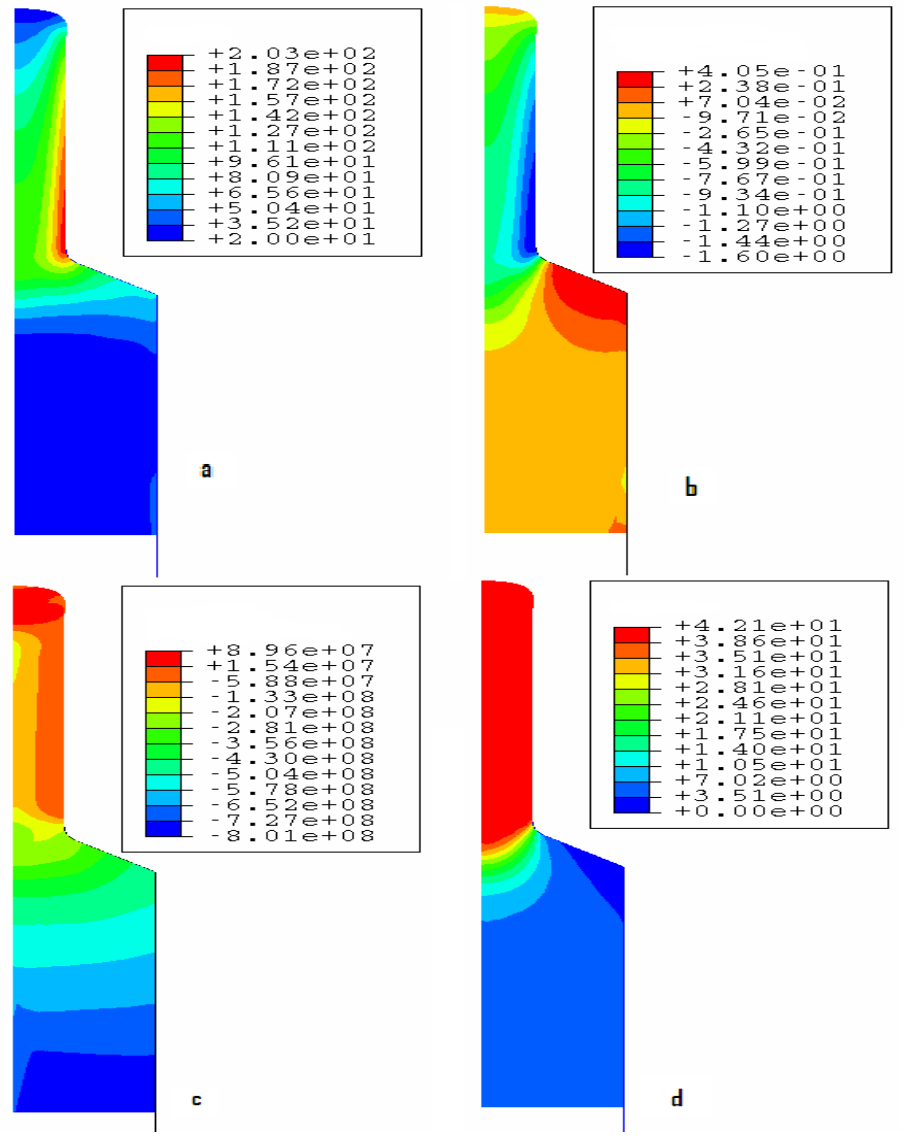

Figure 3.8: (a)Temperature (^oC), (b) Circumferential plastic strain,(c) Circumferential stress (Pa) and (d) Velocity at nodal points (ms^{-1})

of extrusion pressure with time for different die angles. From this figure it can be seen that the maximum extrusion pressure is initially high when the die angle is small. When the angle is large the contact surface area is large and this leads to larger friction at the die-billet interface. When the angle is small the surface area is small but more "turbulence" occurs and

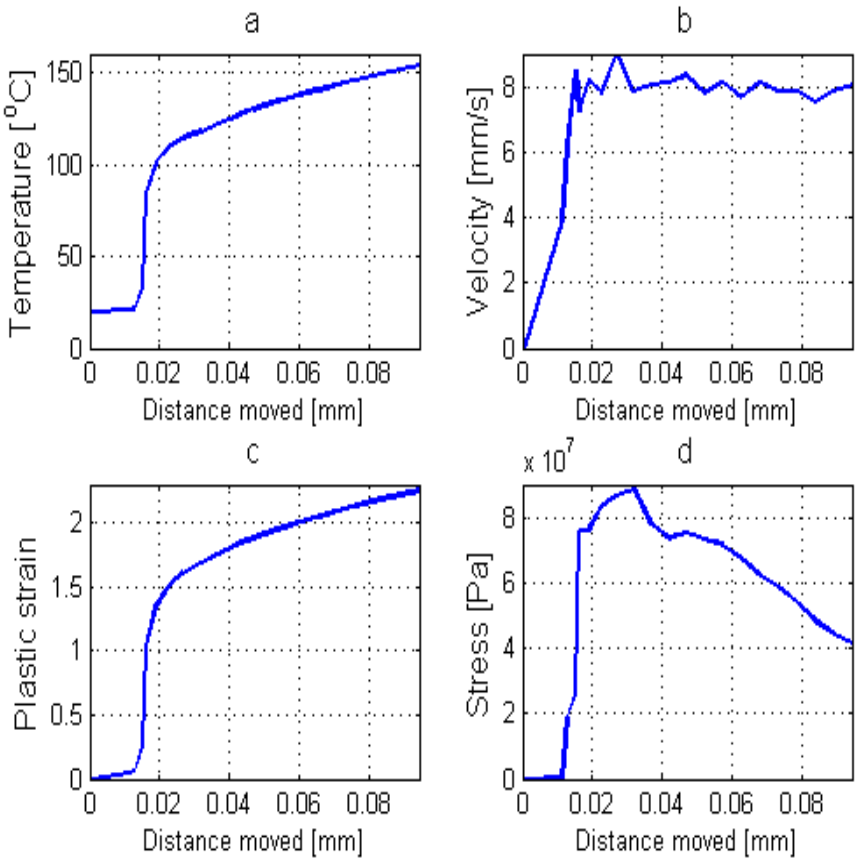

Figure 3.9: (a)Temperature (^oC), (b) Circumferential plastic strain, (c) Circumferential stress (Pa) and (d) Velocity at node 2705 (ms^{-1})

this increases the extrusion pressure required. There is an optimum angle for minimum extrusion pressure, which depends on material, temperature and friction condition such as lubrication.

(ii) **Die land length:** If the die is not designed optimally the extruded material's velocity at the die exit may not be uniform. A non-uniform velocity at the die exit may lead to a variation in the thickness across the width of the die[71]. The velocity of the extruded material and the difference in its maximum and minimum values across the die opening are plotted in Figure (3.13)a and (3.13)b for the die land lengths $l1 = 11\ mm$, $l2 = 13\ mm$, $l3 = 15\ mm$,

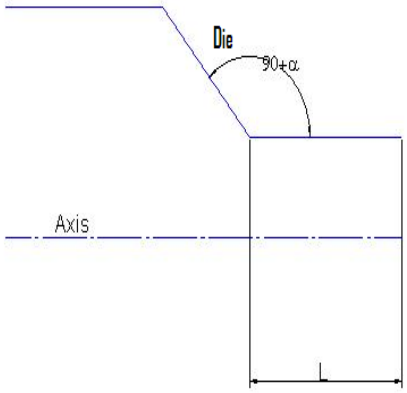

Figure 3.10: Die angle and die land length L

$l4 = 18\ mm$, $l5 = 120\ mm$, $l6 = 22\ mm$, and $l7 = 25\ mm$. These figures show that the uniformity of the velocity depends on the die land length. There is an optimal value for the die land length but it also depends on material, temperature and friction condition such as lubrication.

Figure 3.14 depicts the circumferential stress at die exit for three different die land lengths. It can be seen that the circumferential stress decreases with the increasing die land length. The review of literature [67] showed that the tensile circumferential stresses cause end cracking of the extruded material. From the simulation result in Figure 3.14 it can be concluded that the increasing die land length is a good way of reducing the circumferential tensile stress in the extruded material at the die exit. Therefore estimation of the optimal value of die land is very important to extrude high quality products.

(iii) **Friction:** Since the exact friction value is not known the friction value should be varied to study the effect. In order to investigate the effect of friction between the billet and die surface, the values of coefficient of friction were varied from 0.05 to 0.25 with the die entrance angle of 18^o. Figure 3.15 shows the contour plot of velocity distribution in the vertical direction, temperature dis-

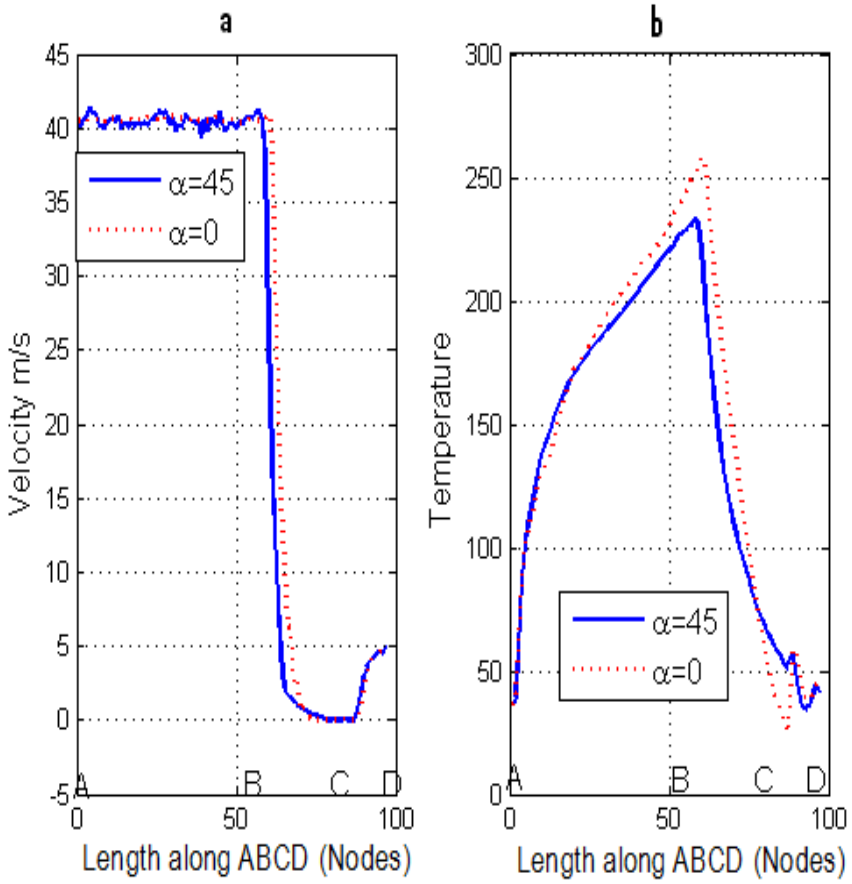

Figure 3.11: (a) Velocity of the nodes along outside edge of the billet (ABCD), (b)Temperature

tribution and circumferential stress distribution when the friction is 0.05 and 0.25. It can be seen that the velocity variation along the radius of the extruded billet at the die entrance increases sharply with the increasing friction factor. It can also be seen that the temperature and circumferential stress closer to the die exit increase with increasing friction factor.

3.6.3 Inaccuracy of Material Properties

Certain assumptions, owing to the lack of understanding of many real phenomena may establish unusual errors. Flow stress data should cover the whole process of ex-

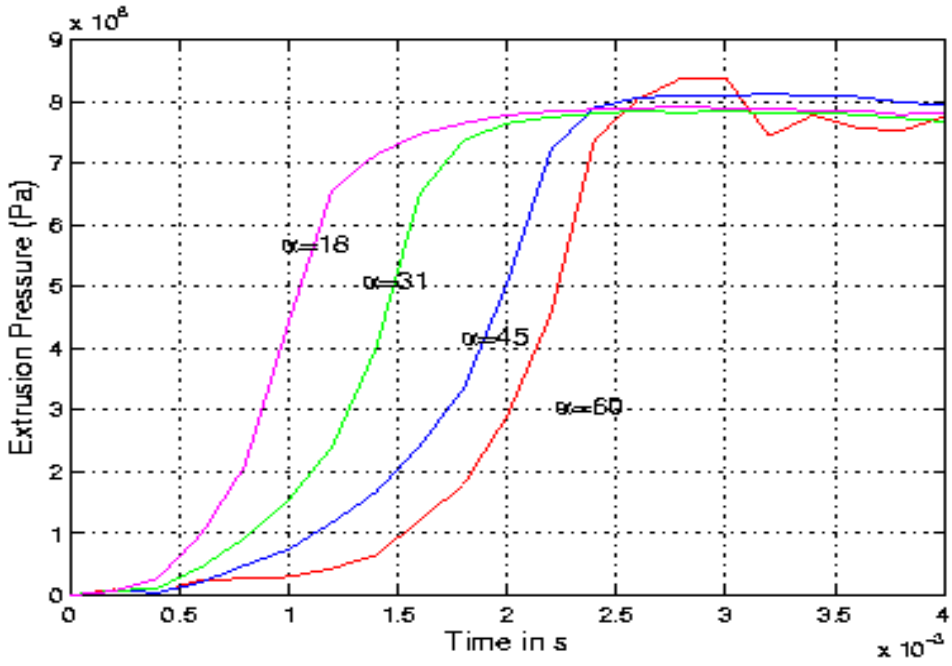

Figure 3.12: Effect of die angle

trusion including temperature, strain, strain rate and microstructure. Further the flow stress of metal at high temperature is strongly dependent on the microstructure, specifically the grain size [67]. If the flow curve data is provided for certain temperatures, a simulation program will use extrapolation to calculate other values. This will create errors since flow curve data depend on other parameters such as grain size, strain rate etc. Therefore the extrapolation of data might cause an unexpected wrong result as well.

Figure 3.16 depicts respectively the temperature along edge, pressure at the bottom, velocity at node 2705 and temperature changes at node 2705 for two different types of flow stress models. In these figures data1 and data2 is obtained using the flow stress at varying and fixed temperature respectively. Figure 3.17 shows the effects (relative change) ofn temperature, extruded velocity, circumferential stress and circumferential plastic strain histories at the node 2705 for the two types of

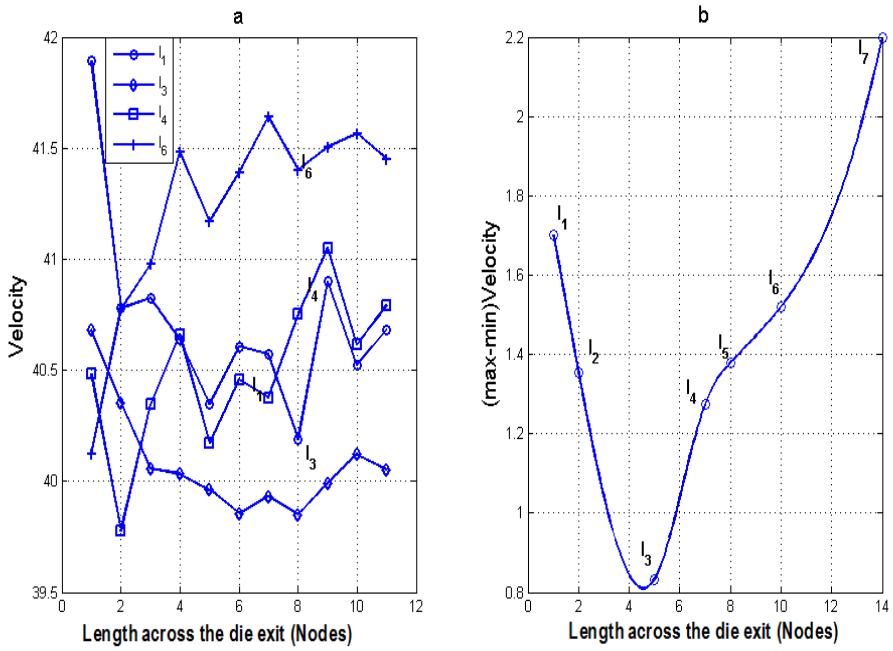

Figure 3.13: Effect of die land length:(a) Velocity across the die opening, (b) Difference between max and min velocity across the die opening.

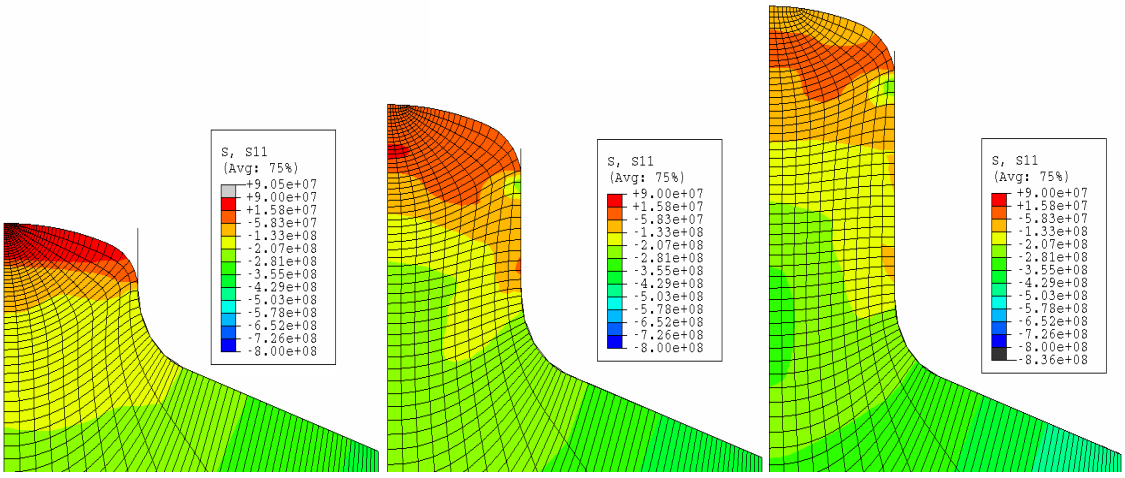

Figure 3.14: Circumferential stress at die exit:(a)Die land= 11 mm , (b) Die land= 14 mm,(c)Die land= 25 mm.

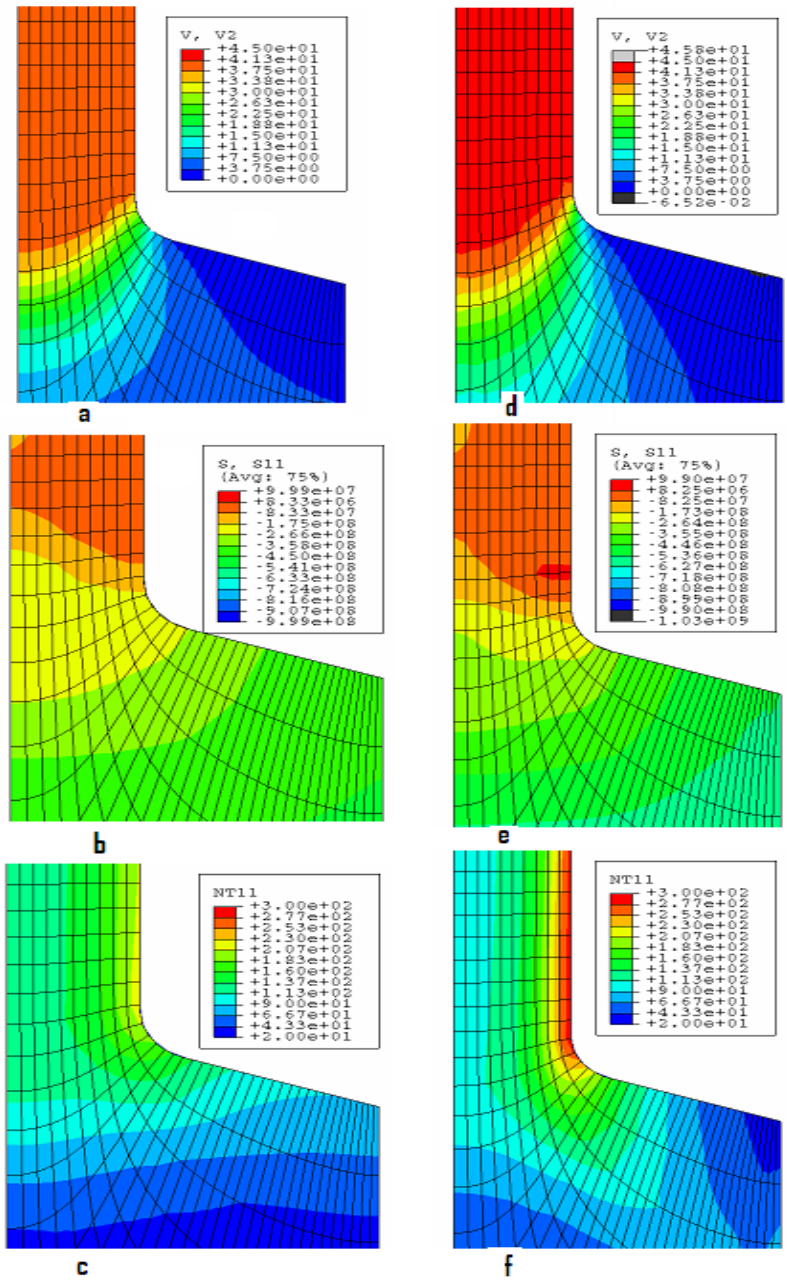

Figure 3.15: Comparison of contour plots with different friction condition:(a)velocity (in m/s) distribution in the vertical direction when friction=0.05 , (b)circumferential stress (in Pa) distribution when friction=0.05,(c) temperature(in ^oC) distribution when friction=0.05,(d)velocity (in m/s) distribution in the vertical direction when friction=0.25,(e)circumferential stress (in Pa) distribution when friction=0.25., (f) temperature distribution when friction=0.25

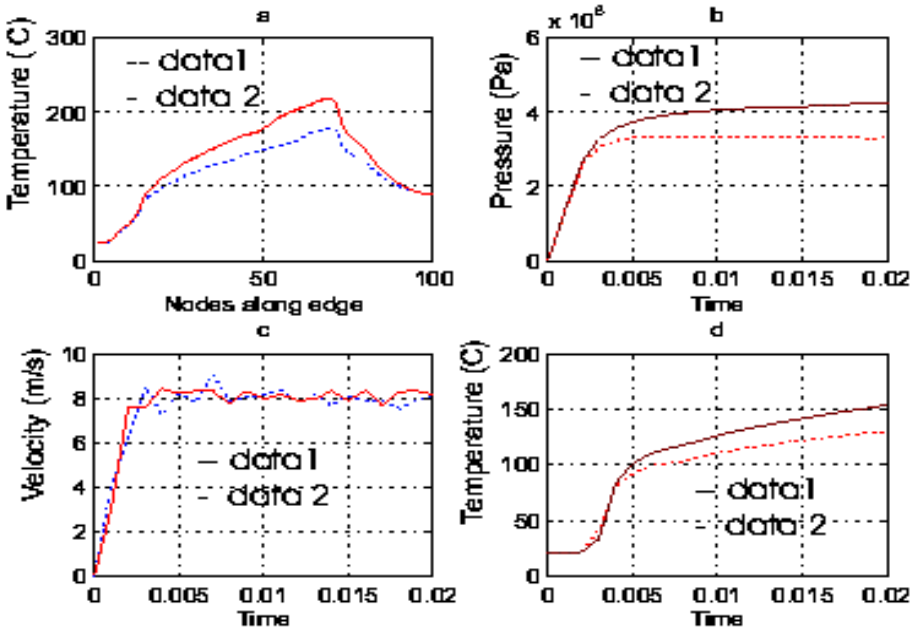

Figure 3.16: Material change (a)Temperature along edge, (b)pressure at the bottom,(c) Velocity at node 2705,(d)Temperature changes at node 2705

flow stress models. The idea here is to demonstrate the relative influence of error due to extrapolation of material data. One model only uses the stress-strain values when the temperature is 150^oC and the other model uses the stress-strain values when the temperature is interpolated $150C$, 100^oC, 50^oC and 20^oC temperature curves as in Figure 3.6. From these figures it can be seen that the simulation of material flow is dependent on the flow stress model.

3.6.4 Computational Issues

(i) **Implicit and explicit scheme:** Implicit and explicit schemes are the two numerical techniques available in ABAQUS. ABAQUS/Standard uses the implicit scheme and the direct integration method. ABAQUS/Explicit uses the central-difference explicit scheme. ABAQUS/Explicit provide fewer element choices than ABAQUS/Standard. The analysis time in the explicit method

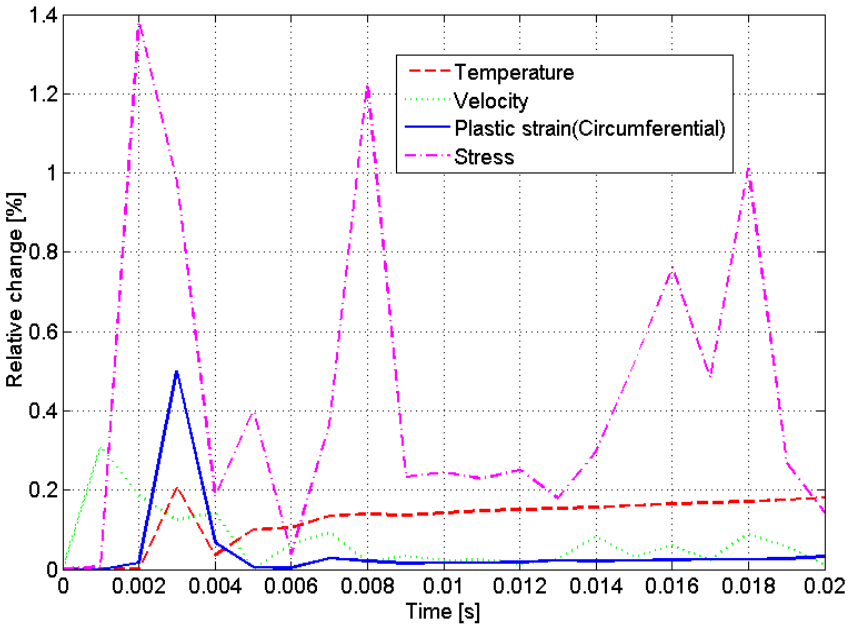

Figure 3.17: Relative changes

rises only linearly with problem size, whereas the time of solving the nonlinear problem associated with ABAQUS/Standard rises more exponentially with problem size. Further the explicit method has the characteristic of less memory requirement and greater computer efficiency since the need for the consistent stiffness matrix is prevented. Therefore, ABAQUS/Explicit is more attractive than ABAQUS/Standard for very large nonlinear problems like extrusion, because it converges faster to the correct result.

(ii) **Adaptive meshing:** The adaptive meshing scheme is important for finite element modelling involving large deformation to reduce element distortion. To investigate if the adaptive mesh is able to improve the simulation, problems with the same mesh densities are used with and without adaptive meshing. The results of the simulation using the explicit scheme are given in Figure 3.18. The CPU time for the adaptive meshing model is higher than the non-

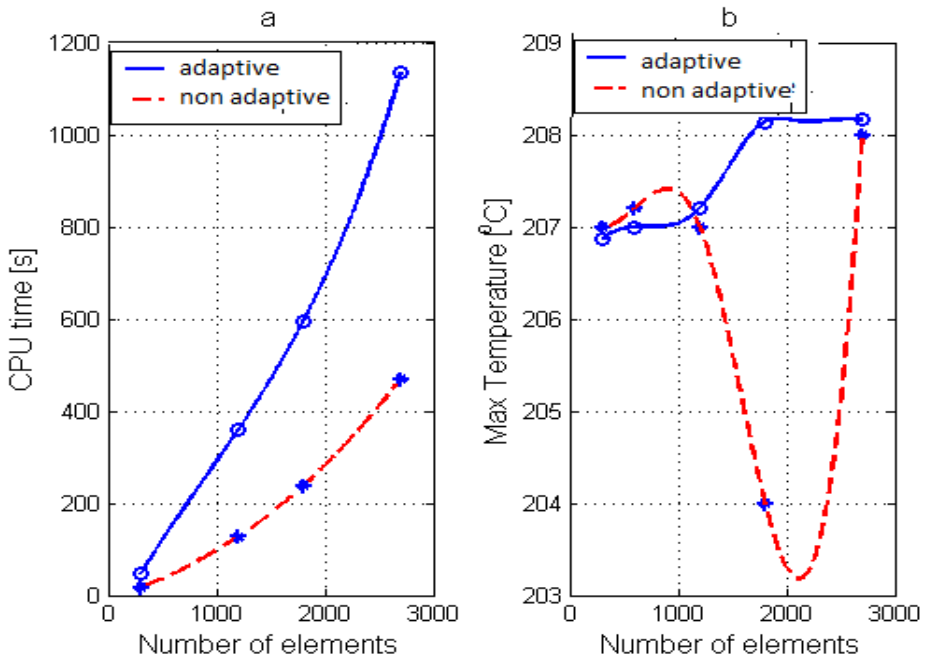

Figure 3.18: Comparison of adaptive and non-adaptive meshing:(a) CPU time, (b) maximum temperature

adaptive meshing model but on the other hand the accuracy of the solution for the adaptive mesh model increases and then converges to a certain value with increasing element numbers, but the non-adaptive meshing solution fluctuates with the element numbers. This might be a numerical error due to element distortion. From these it can be clearly seen that the adaptive meshing technique is an essential tool to obtain accurate numerical solutions and to reduce the computational effort needed to achieve accuracy ultimately.

(iii) **Element type and mesh density:** The billet is modelled with either ABAQUS CAX4T or CAX4RT elements with reduced integration. In the reduced integration scheme there is only one integration point in the center of the element used. This may result in numerical inaccuracy from the hourglass mode. But, in ABAQUS a small quantity of artificial hourglass stiffness

is introduced in the reduced integration element to control the spread of the hourglass mode. This stiffness is more effective at limiting the hourglass modes when more elements are used in the model. This means that reduced-integration elements can provide acceptable results as long as a reasonably fine mesh is used. The reduced-integration elements are very tolerant of distortion and therefore it is recommended to use a fine mesh of these elements for extrusion problems since the distortion levels are very high near the die surface.

Figure 3.19 illustrates the effects of different types and mesh densities using the implicit scheme. Figure 3.19a shows the highest temperature calculated at one particular point on the extruded bar with various mesh densities and two different element types. Figure 3.19b shows the time taken to complete the simulation with various element and mesh densities. When the mesh density is small there is a difference between the values obtained with the reduced and full the integration method. This difference decreases with increasing mesh density. It can also be seen that when the mesh density is small the simulation under-predicts the temperature with both types of elements.

(iv) **The contact algorithm:** ABAQUS uses either a penalty or a kinematic contact algorithm to interact between two surfaces. The penalty contact algorithm can model some types of contact that the kinematic contact algorithm cannot (e.g contact between two rigid surfaces). For extrusion problems only one surface can be dealt with as rigid and therefore the contact between the die and the billet can be enforced by either kinematic or penalty contact algorithm. For surface-to-surface contact problems like extrusion, ABAQUS uses a kinematic contact algorithm by default. Figure 3.20 depicts the comparison of temperature, velocity and circumferential stress at the node 2705 obtained using both algorithms. This figure shows the results obtained using these two

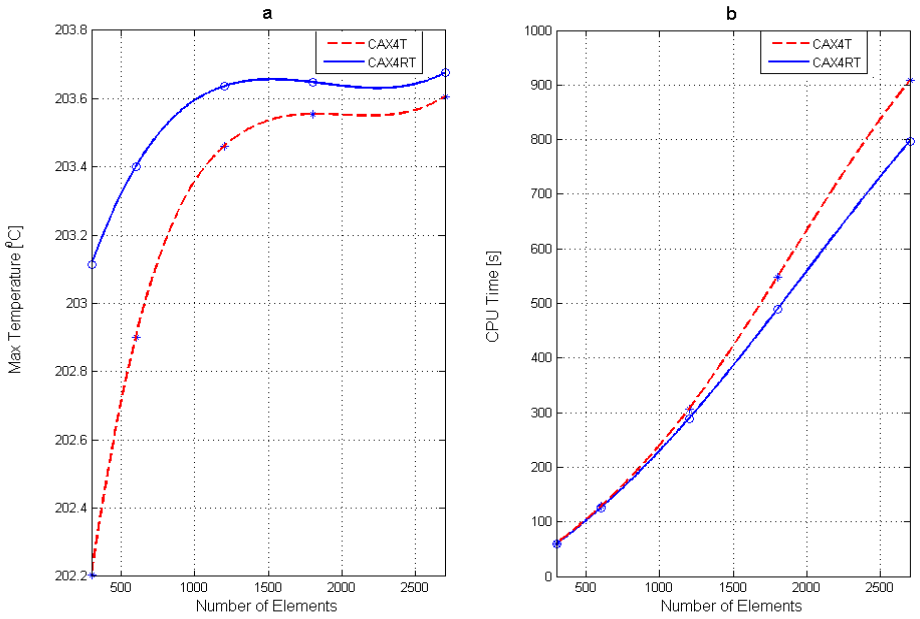

Figure 3.19: Comparison of temperature estimation, CPU time with different mesh

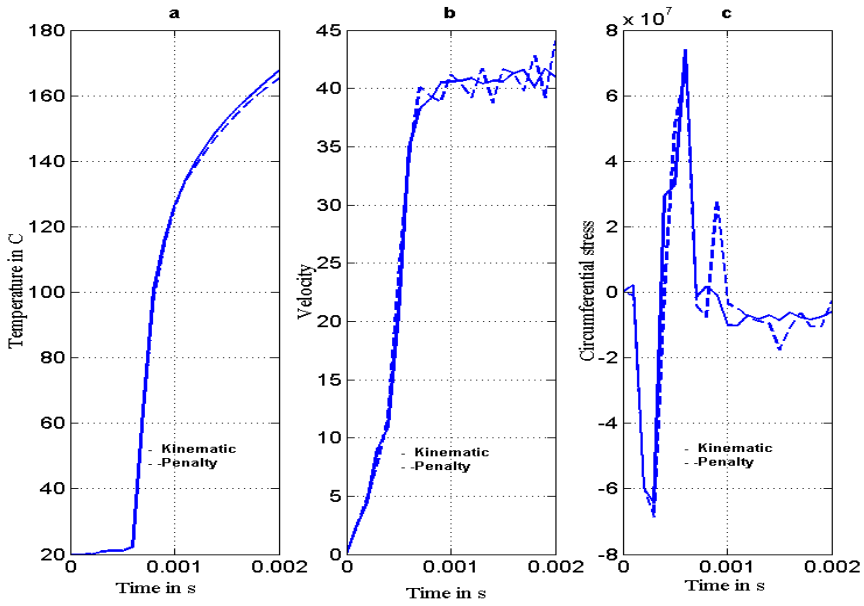

Figure 3.20: Comparison of:(a) Temperature, (b) extruded velocity, (c) circumferential stress at the node 2705 obtained using kinematic and penalty contact algorithms

algorithms are nearly same in this example. One oscillates more than other and it may affect convergence. The choice of right algorithm depends on user experience. In this section kinematic algorithm is chosen since it converges faster than other.

3.7 Discussion

The finite element simulation using Abaqus presented in this chapter forms the start of a research project of finding optimal sets of process and design parameters to extrude a product with minimal defects. It has been demonstrated that finite element analysis is an efficient tool to predict the deformation behaviour and the following has been established:

1. A small scale simulation is capable of providing limited qualitative information of the extrusion process such as material flow pattern, temperature variation and velocity profile.

2. Heat generation due to deformation is significant in the extrusion. The increase in temperature largely occurs at the early stages of extrusion and reaches a steady state. The largest temperature increase occurs at the die-billet interface.

3. Ram speed can influence the flow pattern significantly.

4. The interfacial friction between the billet and the die wall also adds to non-uniform deformation patterns during the extrusion process.

5. The accuracy of the material model is important.

6. The extruded part's properties vary dramatically with die angle, die land length, friction and material properties.

7. Ways to increase the efficiency of the simulation in terms of using different solution schemes, adaptive meshing, element types and different contact algorithms are discussed.

Chapter 4

Optimal Process and Design Parameters Estimation for a Simple Die

4.1 Introduction

The metal flow during extrusion through a die is complex and not uniform, which causes cross-cracking, bending, distortion and twisting of the extruded product. To improve the quality of the workpiece, the die cross-section layout and operating conditions must be taken into account in the design of a new product.

Computer simulation of extrusion using the finite element method is a popular option to replace the traditional trial and error method during process design. The finite element model, which is capable of describing the behavior of metal flow during extrusion, requires several input data such as die geometry, material behavior laws, friction laws and operating conditions.

In reality, material data can be obtained using available experimental data, but optimal values of die geometry and operating conditions are often not accurately

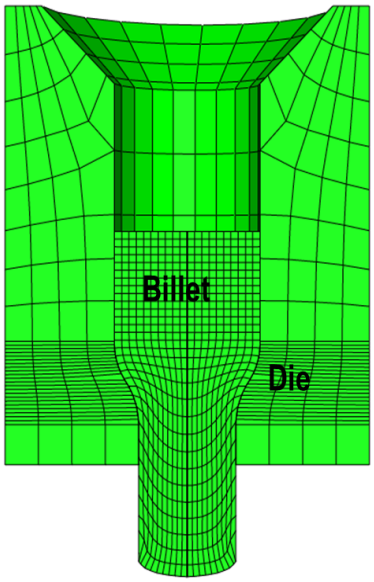

Figure 4.1: Extrusion process

known and therefore guessed. Methods to determine die geometry and operation conditions are an important part of designing an extrusion process.

The novel concept of this chapter is to determine the optimal conditions of isothermal extrusion with regards to billet temperature, container temperature, extrusion speed and microstructure for a non-adiabatic die profile basing it on techniques available in the literature.

4.2 Forward Problem

It is assumed that a block of metal (billet) is placed inside the container and pushed through the die opening of a smaller cross sectional area than that of the original billet as shown in Figure 4.1. At high strain rates metal flow is analogous to fluid flow and therefore the material behavior can be described using Equations 2.14-2.26. The analytical solution of these equations is not possible. But finite element techniques deliver approximate numerical solutions of it. It is implemented this

with The ABAQUS finite element program.

4.3 Inverse Problem

The goal here is to determine the input data (parameters) of the forward problem which leads to a given result. In this problem, the die design parameters and process parameters are unknown, but the shape and properties of the final product are known. It has been assumed here that the desired grain size of the material is known, but the exact die geometry, initial billet temperature and ram speed are unknown. Our aim is to estimate the exact die geometry and the process parameters. This problem is known mathematically as an inverse problem and can be seen as an optimization problem whereby the objective function to minimize is the gap between the expected result and finite element simulation results.

First of all, a mathematical definition of the gap between the expected and simulation results is required as an objective function. The aim of optimization is to find the best set of parameters that minimizes an objective function by improving the performance in the direction of optima. The aim of the approach is to find the global minimum on a given search space by maximizing or minimizing the objective function subjected to the given constraints. In the case of a minimization problem, the mathematical formulation of the problem can be stated as follows

$$\begin{aligned} \text{Minimize} \quad & f(\mathbf{p}) \\ \text{subject to} \quad & g_j(\mathbf{p}) \geq 0 \quad j = 1, \ldots, n1 \\ & h_k(\mathbf{p}) = 0 \quad k = 1, \ldots, n2 \end{aligned} \tag{4.1}$$

where $f(\mathbf{p})$ is the objective function, $g_j(\mathbf{p})$, $h_k(\mathbf{p})$ are constraints function and $\mathbf{p}$ is a vector of design and process variables.

4.3.1 Design Variables

In order to determine the optimal die profile, it is essential to describe an arbitrary die profile by a mathematical expression and obtain the design variables from the expression. The design variables will then be optimized to get a desired result. In this study Bezier curves with five control points are used to obtain the arbitrary die profile. The Bezier curve which has the control points $(x_i, y_i),\ i = 1, \ldots, 5$ is given by [54]

$$\begin{aligned} x(t) &= \sum_{i=0}^{N} x_{i+1} B_{i,N}(t), \text{ and} \\ y(t) &= \sum_{i=0}^{N} y_{i+1} B_{i,N}(t), \end{aligned} \tag{4.2}$$

where $N = 4$, $t \in [0, 1]$, and

$$B_{i,N}(t) = \frac{N!}{i!(N-1)!} t^i (1-t)^{N-i}$$

Using these control points, infinitely as many die surfaces can be created. Some of these possible die surfaces are shown in Figure 4.2B. These are Bezier curves obtained using its control points P_1, P_2, P_3, P_4 and P_5. All these possible die profiles are constructed by moving the control points P_2, P_3, P_4 and P_5 to all possible positions. If point P_2 coincides with P_1 and P_4 coincides with P_5 then the die profile becomes conical.

4.3.2 Process Variables

Theoretically, the process variables which can influence the extrusion process are the ram speed V_R, initial temperature of the billet T_{B0}, initial die temperature T_{D0} and the friction conditions m at the billet/tool interface.

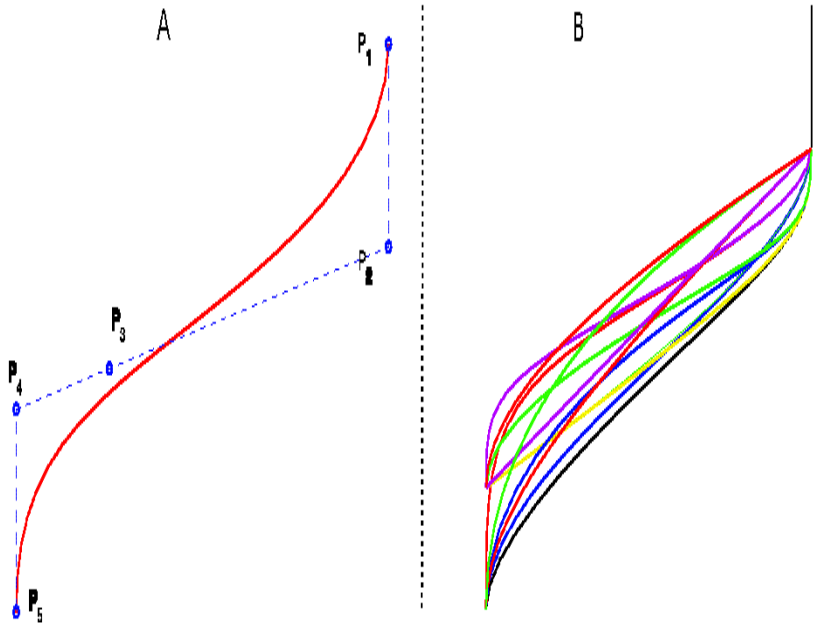

Figure 4.2: Bezier curves and their control points.

4.4 Important Factors in the Product Optimization

4.4.1 Die Life

It is obvious that high extrusion loads will lead to an intolerable amount of wear in a die. Therefore it is important to minimize the extrusion load. In addition, the life time of a die can be affected by wear and this wear is closely related to the load on the surface of a die cavity. By distributing the load on the die surface wear can be distributed along the surface and it leads to increases in die life. Therefore the optimization constraint for increases in die life has to be in the form ($\sigma_{VAR} =$)

$$\min_{\mathbf{Y}} \sum_{i} \left[(\sigma_{i+1} - \sigma_i)^2 + (\tau_{i+1} - \tau_i)^2 \right]^{\frac{1}{2}} + \lambda \mathbf{p} \tag{4.3}$$

where σ_i is the axial stress in the $i-$th node, τ_i is the friction stress in the $i-$th node, $\mathbf{p}$ is the extrusion load, λ is a penalty parameter and $\mathbf{Y}$, is a vector of design and process parameters. Figure 4.3 and Figure 4.4 respectively give the extrusion pressures and die pressure variations on the die surface with different die geometries. Here the term die geometry number refers to the number of different die shapes under consideration. The order of die geometry number depends on how the control points of die geometry are arranged in a sequence. Figure 4.5 gives the extrusion pressure and load distribution on the die surface. These graphs clearly show the importance of the above optimization criteria and demonstrate how the extrusion pressure and load on the die surface vary with the different die geometry. These results further indicate that there is no die geometry which gives both lowest extrusion pressures, die pressure and load variation on the die surface. Therefore a trade off between these variables is necessary to find the optimum die geometry.

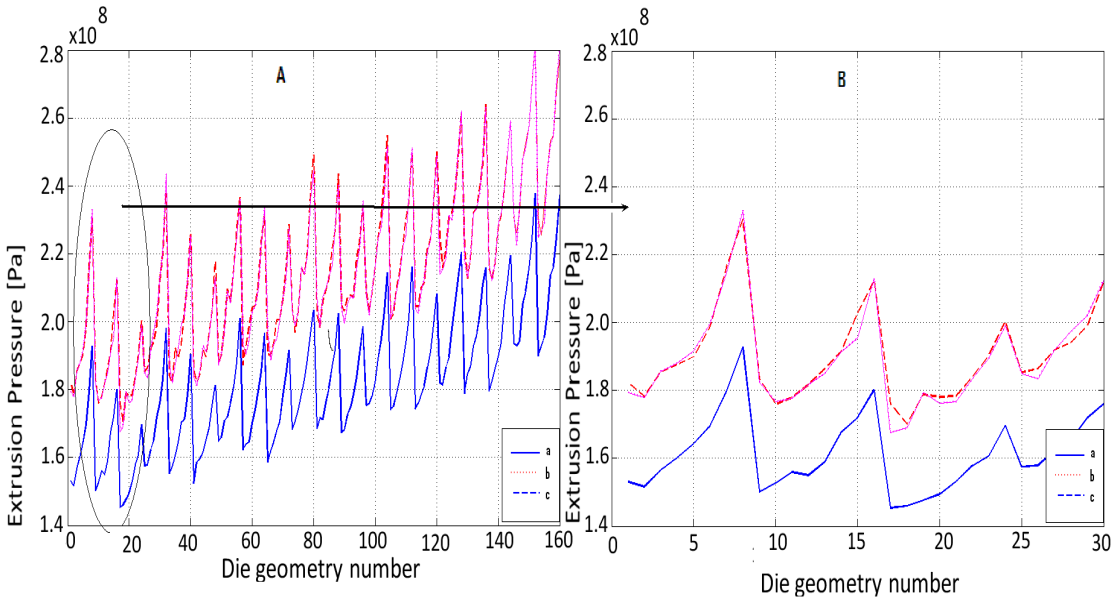

Figure 4.3: (A) Extrusion pressure variation [**a**: $V_0 = 6.3\ mm/s$, $TD_0 = 450^oC$, $TB_0 = 500^oC$, **b**: $V_0 = 25\ mm/s$, $TD_0 = 450^oC$, $TB_0 = 500^oC$, **c**: $V_0 = 25\ mm/s$, $TD_0 = 400^oC$, $TB_0 = 450^oC$.]

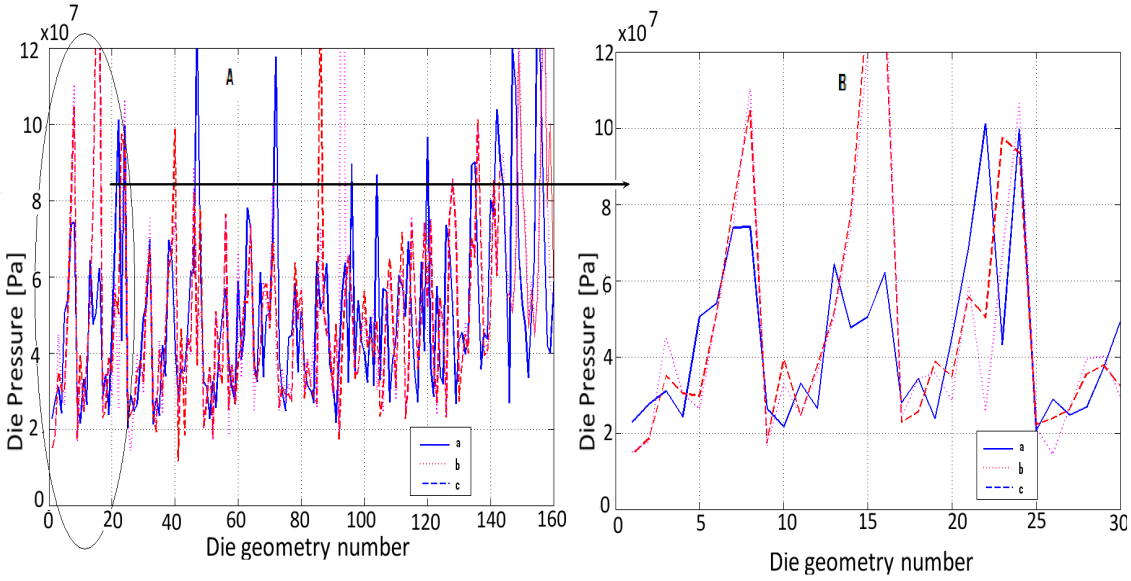

Figure 4.4: Die pressure variation with die geometry [**a**: $V_0 = 6.3\ mm/s$, $TD_0 = 450^oC$, $TB_0 = 500^oC$, **b**: $V_0 = 25\ mm/s$, $TD_0 = 450^oC$, $TB_0 = 500^oC$, **c**: $V_0 = 25\ mm/s$, $TD_0 = 400^oC$, $TB_0 = 450^oC$.]

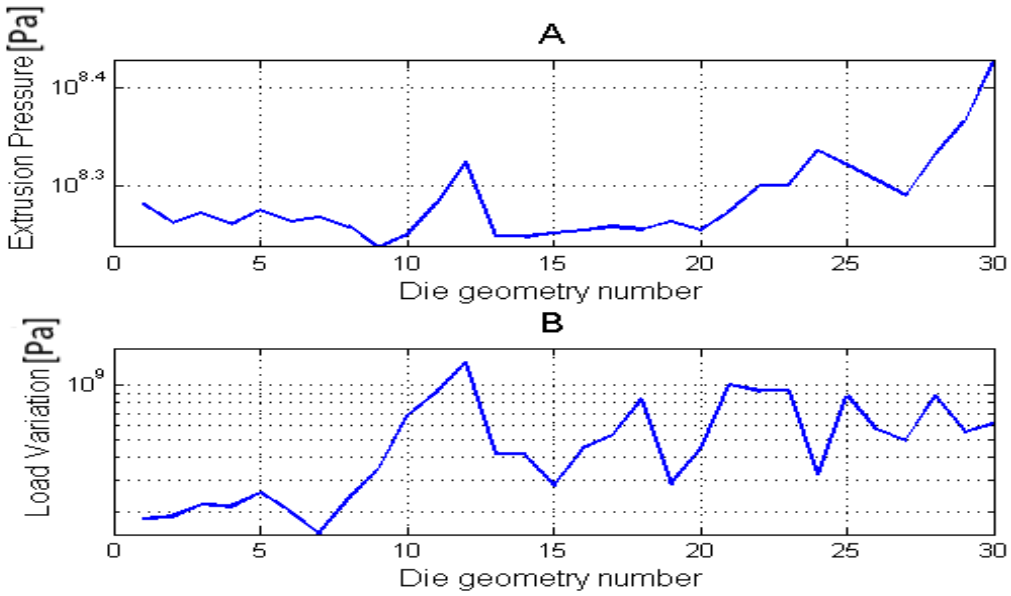

Figure 4.5: Comparison of extrusion pressure and Load variation on die surface with die geometry [**a**: $V_R = 6.3\ mm/s$, $TD_0 = 450^oC$, $TB_0 = 500^oC$]

4.4.2 Isothermal Extrusion

Isothermal extrusion is a process of maintaining a constant temperature during the extrusion process inside the deformation zone. Achieving this condition is very important for the production of uniform, high-quality products. Isothermal conditions can be achieved mechanically by adjusting the speed of the ram, initial temperature of billets and die and by carefully designing the die for each product. Several techniques can be used to achieve an isothermal extrusion process. These can be divided mainly into three types: (1) Setting up a longitudinal thermal gradient in the billet (tapered billet) before starting extrusion i.e the temperature decreases faster in the front part of the billet than in the rear. (2) Maintaining the extrudate exit temperature by varying the ram speed. (3) Maintaining the extrudate exit temperature by varying the die shape. Although there are many advantages that could be achieved, there are also some problems with regard to isothermal extrusion. If the velocity gradient varies it could trigger a part to bend or twist [57], thereby creating stresses and this is also applicable for variations in temperature. Therefore it is important to adjust the material flows through the die by changing the die shape. Based on these considerations the optimization constraint to achieve isothermal extrusion can be written as follows.

$$\min_{\mathbf{Y}} \int_0^{t_f} \left(T(x, y, t) - T_d\right) dt, \tag{4.4}$$

where $T(x, y, t)$ is the temperature inside the deformation zone as a function of space and time, T_d is the average temperature or desired temperature inside the deformation zone and t_f is the time to complete the particular extrusion process.

The shape of the deformation zone and four points A, B, C and D inside the zone are shown in Figure 4.6. The average temperature variation T_{VAR} inside the

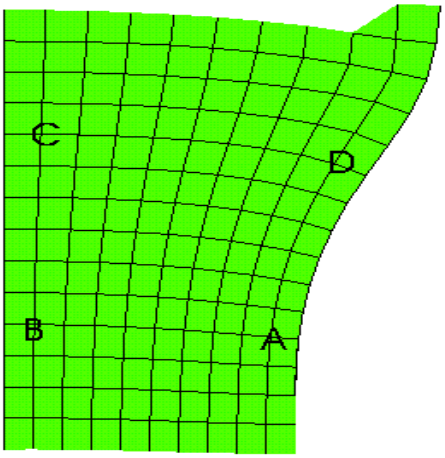

Figure 4.6: Deformation zone.

forming zone is defined as

$$T_{VAR} = \left(\frac{(t_A - \bar{t})^2 + (t_B - \bar{t})^2 + (t_C - \bar{t})^2 + (t_D - \bar{t})^2}{4} \right)^{\frac{1}{2}},$$

where t_A, t_B, t_C, t_D are the temperatures at the points A, B, C, D respectively as shown in the figure above and $\bar{t}$ is the average temperature.

Figures 4.7A, 4.7B depict respectively the temperature variation across the die exit and T_{VAR} against different die geometries for two different ram speeds and initial die and billet temperatures. These figures indicate that the variations in temperature inside the forming zone and exit temperature are more influenced by ram speed than initial billet temperature and die geometry. They also demonstrate some ideas for choosing an optimization criterion for achieving isothermal condition.

4.4.3 Flow Balance

An evenness of exit flow is an important part in die design to avoid part distortion and to be able to yield an extruded part within specified tolerances. The uniform

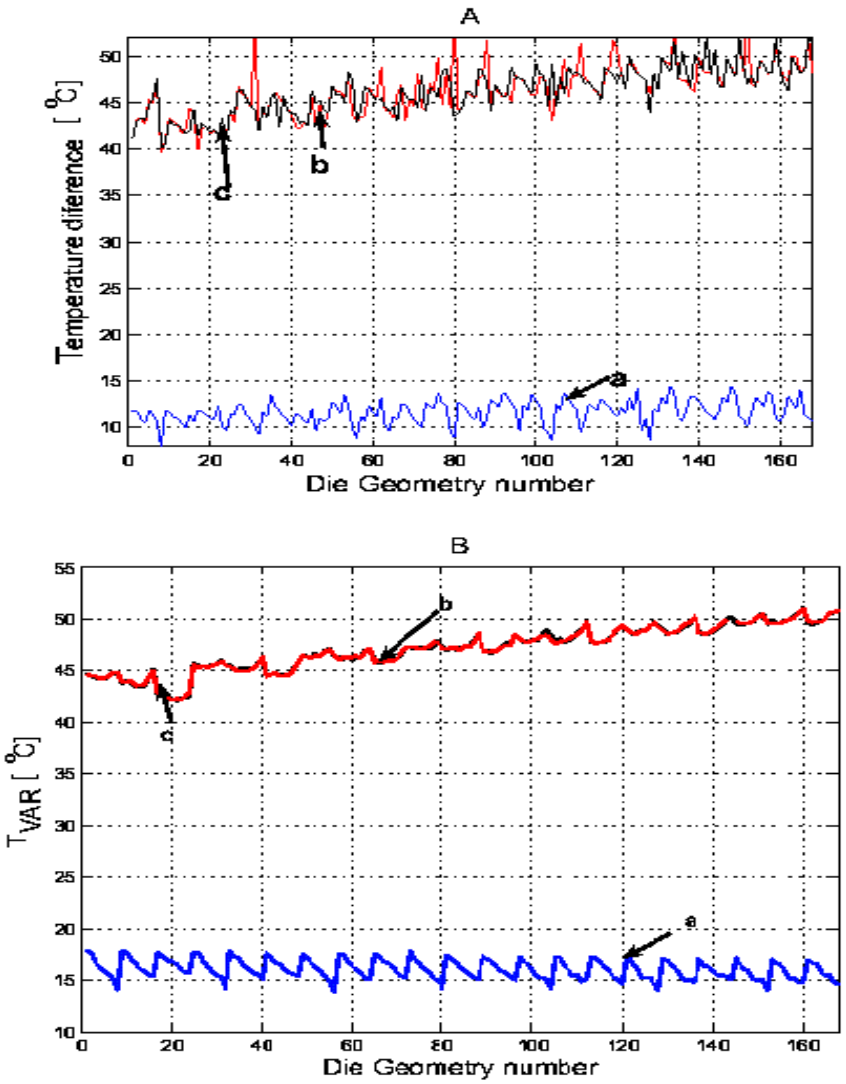

Figure 4.7: Comparison of (A) maximum temperature difference at the die exit and (B) T_{VAR} with different die geometries, ram speeds and initial temperatures [**a**:$v = 6.3\ mm/s$, $TD_0 = 450^oC$, $TB_0 = 500^oC$, **b**: $v = 25\ mm/s$, $TD_0 = 450^oC$, $TB_0 = 500^oC$, **c**: $v = 25\ mm/s$, $TD_0 = 400^oC$, $TB_0 = 450^oC$.]

die exit velocity can be obtained by adjusting the die land length. The optimization constraint to increase the evenness of exit flow is therefore

$$\min_{\mathbf{Y}} \left[\sum_{1}^{N} (V_i - \bar{V})^2 \right], \tag{4.5}$$

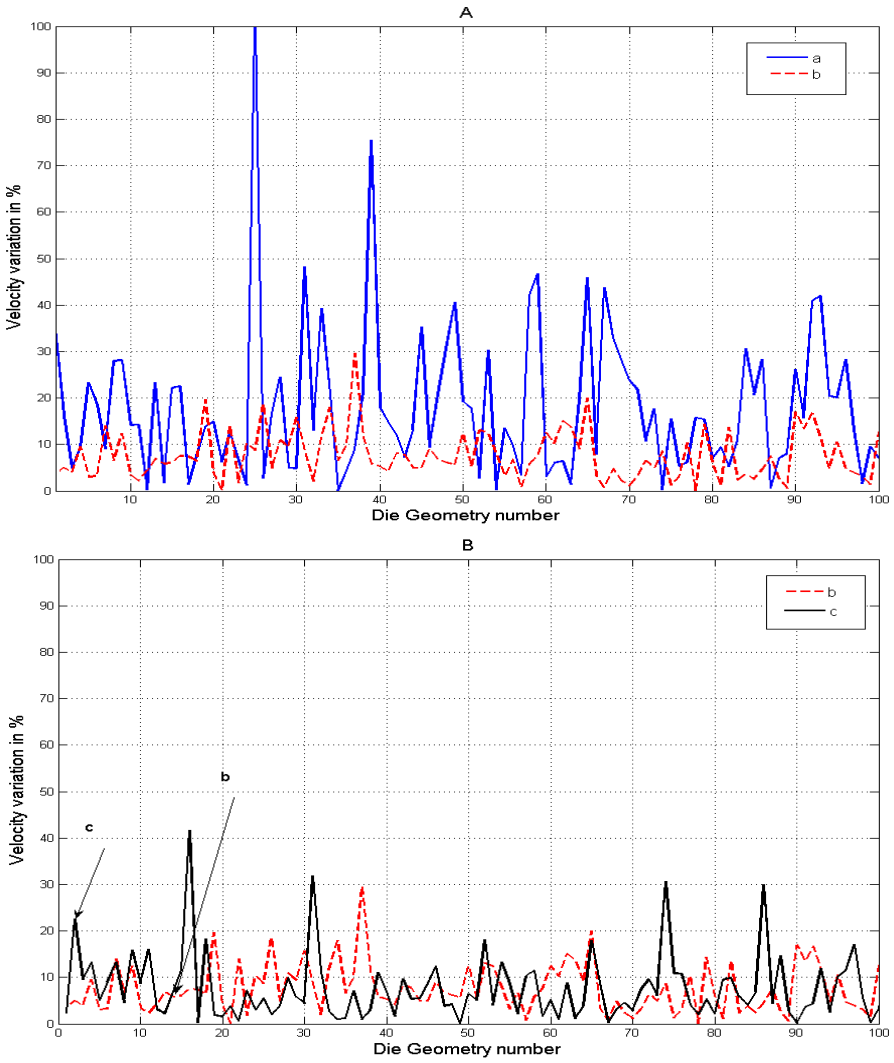

Figure 4.8: Flow balance: (A) Comparison with two different ram speeds, (B) Comparison with two different initial temperatures [**a**:$v = 6.3\ mm/s$, $TD_0 = 450^oC$, $TB_0 = 500^oC$, **b**: $v = 25\ mm/s$, $TD_0 = 450^oC$, $TB_0 = 500^oC$, **c**: $v = 25\ mm/s$, $TD_0 = 400^oC$, $TB_0 = 450^oC$.]

where V_i is the nodal velocity of the $i-$th node, N is the number of nodes along the die exit and $\bar{V}$ is the average nodal velocity along the die exit. Figure 4.8 depicts the exit velocity variation across the die exit against different die geometries for different ram speeds and initial die billet temperatures. These figures indicate that the variations in flow velocity across die exit are influenced by both ram speed,

initial billet temperature and die geometry. Further the velocity variations are more sensitive to the die geometry than initial billet temperature and ram speed. These results demonstrate that the problem of minimizing flow variation can be achieved by altering die design parameters, ram speed and initial billet temperature.

4.4.4 Distortion

The success of an extrusion process depends mainly on reducing the distortion and minimizing the redundant strain in the extruded product as well as controlling the strain rate inside the deformation zone. Literature [37] in the field of metal forming processes suggests that redundant strain and distortion are related to each other. Based on the theory and available literature the following three criteria can be used to minimize distortion.

(i) Distortion variation:

$$\min_{\mathbf{Y}} \left[\sum_{1}^{N} (U_i - \bar{U})^2) \right] \tag{4.6}$$

where U_i is the displacement of the node i and $\bar{U}$ are the average displacements of transverse nodes at the die exit.

(ii) Average effective strain:

$$\min_{\mathbf{Y}} \left[\sum_{1}^{N} (\varepsilon_i - \bar{\varepsilon}_{Ideal})^2) \right] \tag{4.7}$$

where $\bar{\varepsilon}_{Ideal}$ is the ideal effective strain and is defined by

$$\bar{\varepsilon}_{Ideal} = 2 \ln \frac{R_0}{R_f} \tag{4.8}$$

for axisymmetric extrusion.

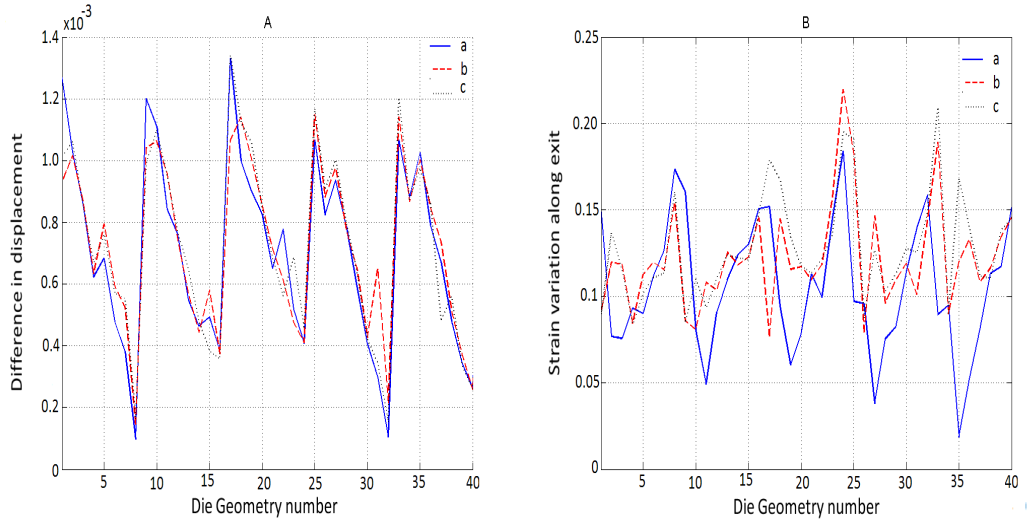

Figure 4.9: Comparison of (A)Displacement variation, (B) Strain variation at the die exit with different die geometries, ram speeds and initial temperatures[**a:** $v = 6.3\ mm/s$, $TD_0 = 450$, $TB_0 = 500$, **b:** $v = 25\ mm/s$, $TD_0 = 450^oC$, $TB_0 = 500^oC$, **c:** $v = 25\ mm/s$, $TD_0 = 400^oC$, $TB_0 = 450^oC$].

(iii) Strain rate deviation:

$$\min_{\mathbf{Y}} \left[\sum_{1}^{N} (\dot{\varepsilon}_i - \bar{\dot{\varepsilon}})^2) \right] \tag{4.9}$$

Figure 4.9 depicts the average displacement variation and strain variation of the transverse nodes across the die exit against different die geometries for different ram speeds and initial die billet temperatures. Figure 4.10B and Figure 4.10C depict the relative displacement of the nodes along the transverse lines with respect to its original position and the strain values respectively. It can be seen clearly that the strain increases from the centre line to the outer surface and is approximately proportional to the displacement of the transverse nodes. If the strain values along the transverse line are equal to the ideal effective strain (Equation 4.8) then there would be no distortion at all.

Figure 4.11A depicts the comparison of average strain rate variation along the transverse line at the die exit for different dies at two different ram speeds. Figure

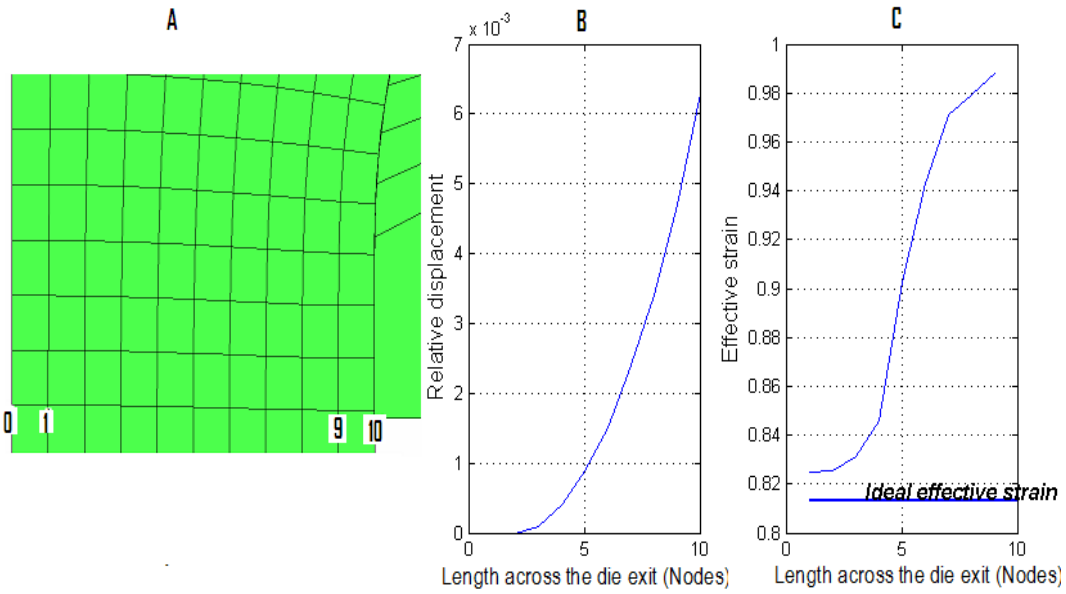

Figure 4.10: (A) Nodes along transverse line, (B) Relative distortion, and (C) Effective strain distribution from the center line to the outer radius.

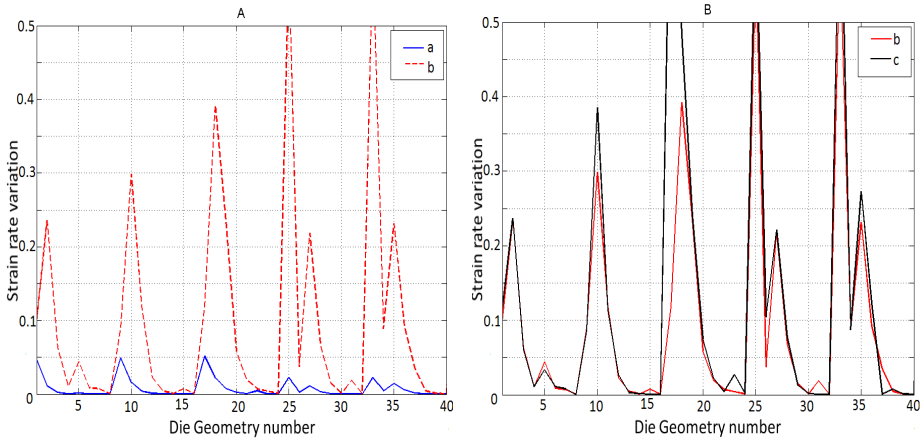

Figure 4.11: Strain rate variation at the die exit with die geometry: (A) Comparison with two different ram speeds, (B) Comparison with two different initial temperatures [**a**:$v = 6.3\ mm/s$, $TD_0 = 450^oC$, $TB_0 = 500^oC$, **b**: $v = 25\ mm/s$, $TD_0 = 450^oC$, $TB_0 = 500^oC$, **c**: $v = 25\ mm/s$, $TD_0 = 400^oC$, $TB_0 = 450^oC$.]

4.11B depicts the comparison of average strain rate for two different initial temperatures. Figure 4.12 depicts the strain rate variation along the die neck for five different die geometries. This shows clearly that the strain rate distribution of ge-

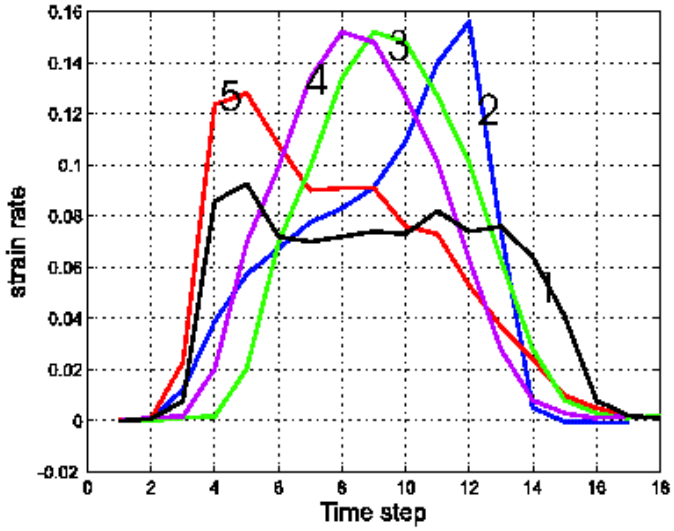

Figure 4.12: Strain rate variation along the die neck for five different dies.

ometry 1 inside the forming zone is more uniform than strain rate graphs of other geometries.

4.4.5 Grain Size

The effects of strain, strain rate and temperature on average grain size of the material are considered here. The relationship between the average recrystallized grain size d and the *Zener-Hollman* parameter Z for the material is expressed in a variety of different ways in the literature[9], [10]. For one type of aluminium alloy (Al-5 wt%Mg), it is given by

$$d = 14.834 - 9.96 \ln\left(\frac{Z}{A}\right). \tag{4.10}$$

Here $\ln A = 19.6$ and Z is

$$Z = \dot{\bar{\varepsilon}} \exp\left(\frac{Q}{RT}\right) \tag{4.11}$$

where A is a constant, Q is an activation energy and is about 135 kJ/mol, $\dot{\bar{\varepsilon}}$ is the average strain rate, T is the temperature and R is the universal gas constant [66]. For AZ31 alloy it is given by [9]

$$\ln d = 9.0 - 0.27 \ln Z. \tag{4.12}$$

and for one type of steel it is given by [76]

$$d = 22600 \dot{\bar{\varepsilon}}^{-0.27} \exp\left(-0.27 \frac{Q}{RT}\right). \tag{4.13}$$

All these equations are based on experimental observations and therefore the uncertainty of constants are high. Further by using regression Equation (4.10) can be written in the form of

$$d = 210 \dot{\bar{\varepsilon}}^{-0.044} \exp\left(-0.044 \frac{Q}{RT}\right). \tag{4.14}$$

All these equations show that the grain size depends mostly on temperature and strain rates. Therefore it is worthwhile to look at the changes of temperature and strain rates at the die exit. Figures 4.13A and 4.13B depict respectively the variation of temperature and strain rate and Figures 4.14A, 4.14B and 4.14C respectively depict the variation of $\exp(0.044\frac{Q}{RT})$ (say Y_1), $\dot{\varepsilon}^{-0.044}$ (say Y_2), and $\dot{\varepsilon}^{-0.044}\exp(-0.044\frac{Q}{RT})$ (say Y_3) across the die exit of die number 8 with two different ram speeds and initial temperatures. These figures clearly demonstrate that the variation in grain size can be minimized by minimizing the temperature and strain rate variation across the die exit. The idea of these figures is to show how the temperature, strain rate and grain size varies across the exit dependent on various different extrusion speeds and initial temperatures.

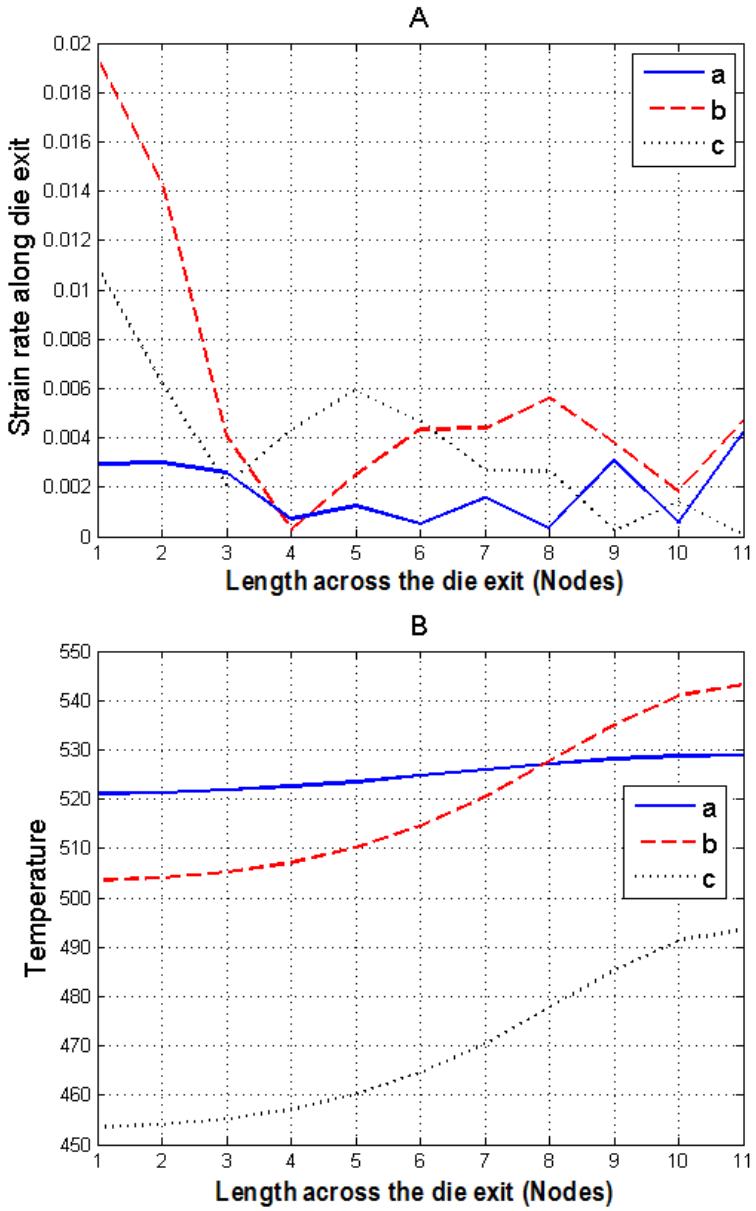

Figure 4.13: Variation of (A) Strain rate and (B) Temperature along the die exit for the die number 8 with different ram speeds and initial temperatures [**a**:v = 6.3 mm/s, $TD_0 = 450^oC$, $TB_0 = 500^oC$, **b**: $v = 25\ mm/s$, $TD_0 = 450^oC$, $TB_0 = 500^oC$, **c**: $v = 25\ mm/s$, $TD_0 = 400^oC$, $TB_0 = 450^oC$.]

4.5 Objective and Constraint Function

The selection of the objective function is associated with the user's specific needs. Here the aim of this study is to extrude a product with given characteristics. There-

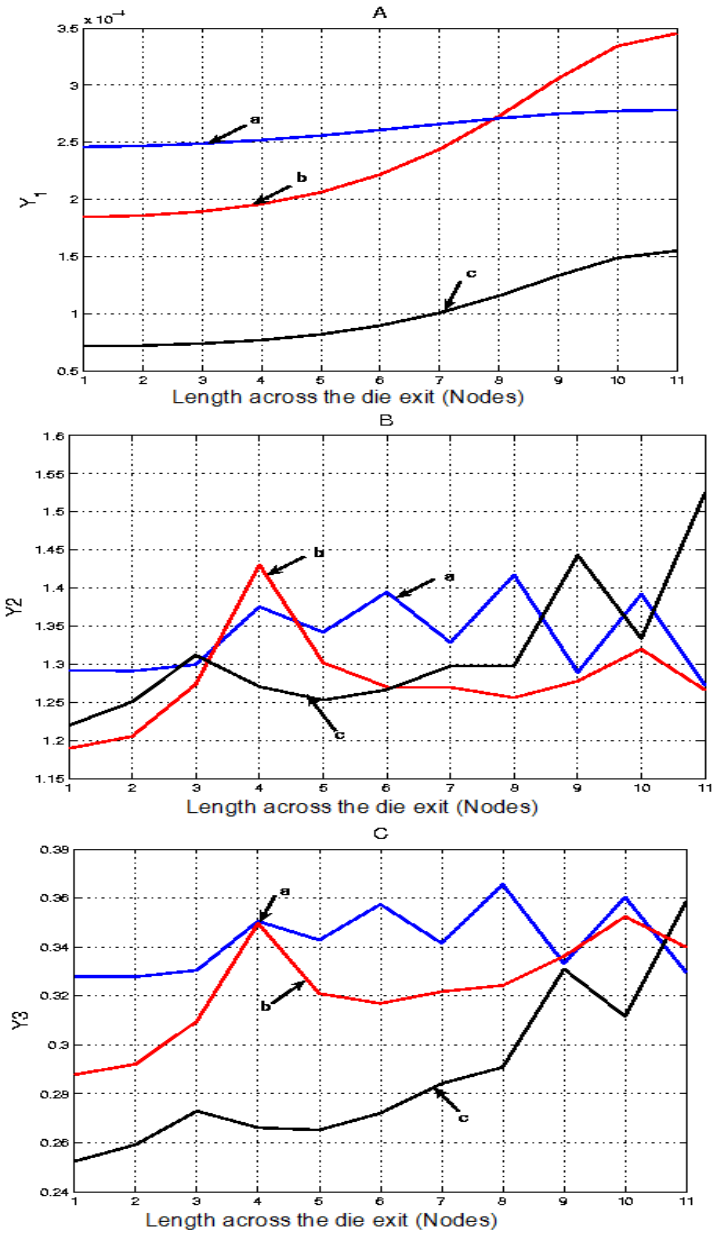

Figure 4.14: Comparison of grain size variation along the die exit for the die number 8 with different ram speeds and initial temperatures:(A) $Y_1 = \exp(-0.044\frac{Q}{RT})$, (B) $Y_2 = \dot{\varepsilon}^{-0.044}$, (C) $Y_3 = \dot{\varepsilon}^{-0.044}\exp(-0.044\frac{Q}{RT})$[**a**:$v = 6.3\ mm/s$, $TD_0 = 450^oC$, $TB_0 = 500^oC$, **b**: $v = 25\ mm/s$, $TD_0 = 450^oC$, $TB_0 = 500^oC$, **c**: $v = 25\ mm/s$, $TD_0 = 400^oC$, $TB_0 = 450^oC$.]

fore the objective function must involve the microstructure (grain size) of the final product. The optimal strain rate, strain and temperature trajectories can be obtained to get a desired value of grain size by minimizing [77]

$$\mathbf{J} = W(\varepsilon(t_f) - \varepsilon_0) + \int_0^{t_f} (d(t) - d_0) \tag{4.15}$$

where ε_0 is a desired strain, W is a weighting factor, t_f is the extrusion time, d_0 is a desired value of average grain size and the average grain size d is [77]

$$d = \alpha \left(\dot{\bar{\varepsilon}} \exp\left(\frac{Q}{RT} \right) \right)^{\beta}. \tag{4.16}$$

The objective function to determine the optimal die profile is the least square deviation between the results obtained using Equation 4.15 and the finite element solution of Equations 2.14-2.26. If the time interval $[0, t_m]$ is subdivided into m partitions then the objective can be expressed by

$$\lambda_1 \min_{\mathbf{Y}} \sum_{1}^{m+1} (\varepsilon_i - \bar{\varepsilon_i})^2 + \lambda_2 \min_{\mathbf{Y}} \sum_{1}^{m+1} (\dot{\varepsilon}_i - \dot{\bar{\varepsilon}}_i)^2 + \lambda_3 \min_{\mathbf{Y}} \sum_{1}^{m+1} (T_i - \bar{T_i})^2 \tag{4.17}$$

Further if die life and flow balance are considered then the Equations 4.3 and 4.5 can be included as constraints with the objective function 4.17.

4.6 Schema of the Design

Let us now consider the technical design details of the algorithm to solve Equation 4.17. The solution will be arrived at through several steps as shown in Figure 4.15. They consist of:

(i) The input data define the physical structure by its dimensions, material properties and boundary conditions.

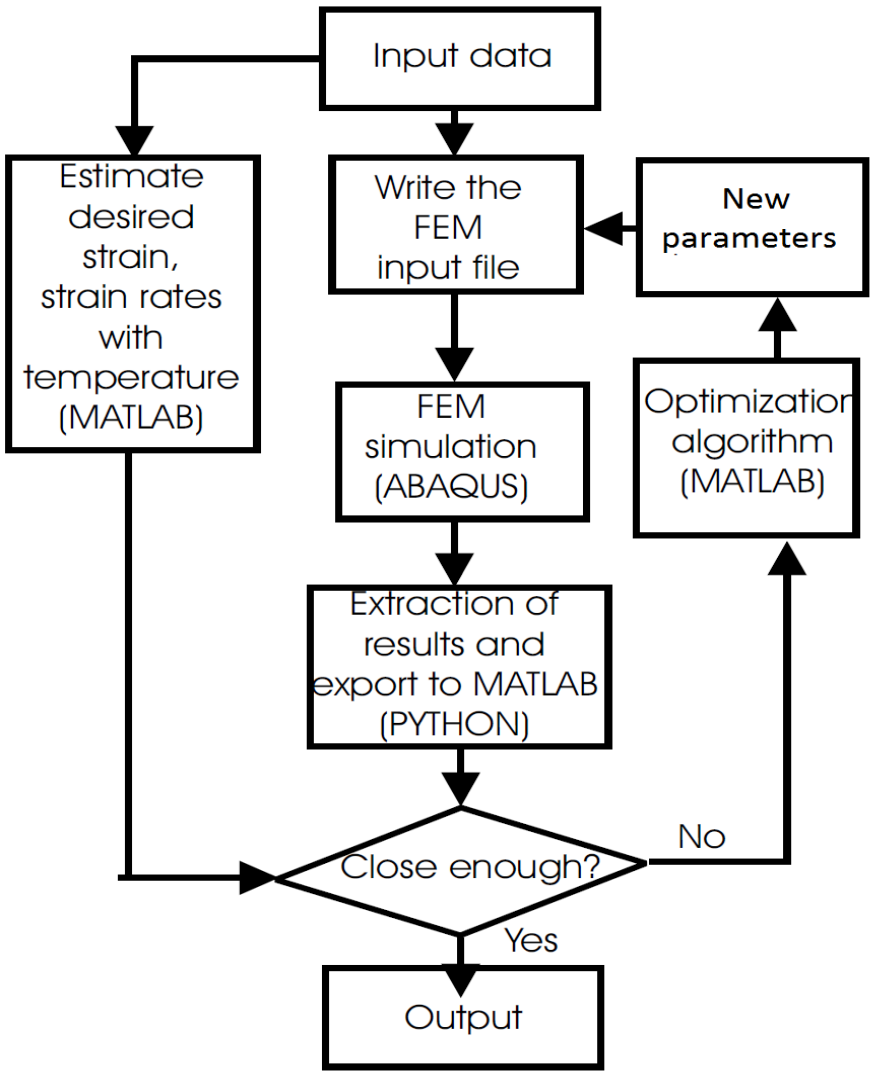

Figure 4.15: Illustration of design process.

(ii) *MATLAB's lsqnonlin* optimization algorithm is applied to obtain the optimal values of strain-rate, strain values and temperature for given microstructure properties of the material.

(iii) The input file module creates a model for the finite element analysis. It consists of geometry of the model, material properties, contact definitions and loading sequence etc. This is done with a *MATLAB* script which creates an

input file for the *ABAQUS* program. The reason for choosing this approach is the possibility of easy modification of the die geometry for each iteration process in the optimization routine.

(iv) FEM simulation part executes the created input file using *ABAQUS* explicit.

(v) The extraction module retrieves results from the *ABAQUS* ODB database. Here the interface is set up between *MATLAB*'s optimization procedure and *ABAQUS* finite element simulation. This is achieved through the use of *PYTHON* scripts to retrieve necessary results from the ABAQUS output (ODB) database. It is saved in a different file with an *EXCEL* file format and then processed with *MATLAB* to obtain the results for optimization.

(vi) The optimisation part is implemented using *MATLAB*'s *lsqnonlin* built-in function which uses the Levenberg-Marquardt algorithm. This approach ensures an easy implementation of multiple runs of *ABAQUS* within an optimization routine.

Unlike the linear problem, the non-linear objective function given by Equation 4.17 may have more than one minimum. Therefore, the solution process should include finding the global minimum. To deal with these problems first all or most of the local minima of Equation 4.17 are found for a sequence of design variables at a larger interval. Then the lowest value of the minima is picked. In the next step the minimum obtained from the previous step is used as the starting value to solve Equation 4.17.

4.7 Results and Discussion

In order to study the optimum results of an aluminium extrusion process, a FE-simulation is carried out using MATLAB and ABAQUS. The process here is a

hot extrusion process with heat transfer between the work-piece and die being considered. The work-piece and die have an initial temperature of $T = 450^oC$. The extrusion ratio is 1.33. The friction factor at the die-material interface is assumed to be 0.1. The die is considered as a deformable body. Ram velocity is 6.25 mms^{-1}. The flow stress-strain relationship of the work-piece (aluminium alloy) material is [83]

$$\bar{\sigma} = 209\,(\bar{\varepsilon})^{0.122} \;\; N/mm^2 \tag{4.18}$$

Other data values used in the simulation of the work-piece are: Young's modulus of $E = 7 \times 10^{10}\ Pa$, coefficient of expansion= $8.4 \times 10^{-5}\ ^oC^{-1}$ at $T = 20\ ^oC$, Poisson's ratio= 0.35, inelastic heat fraction = 0.9, specific heat = 910 $Jkg^{-1}K^{-1}$, density= 2750 kgm^{-3}, conductivity = 204 $Wm^{-1}K^{-1}$ when $T = 0\ ^oC$, = 225 $Wm^{-1}K^{-1}$ when $T = 300\ ^oC$ and the values used for the die material are Young's modulus of $E = 20 \times 10^{10}\ Pa$, coefficient of expansion= $8.4 \times 10^{-5}\ ^oC^{-1}$ at $T = 20\ ^oC$, Poisson's ratio= 0.30, inelastic heat fraction = 0.9, specific heat = 450 $Jkg^{-1}K^{-1}$, density= 7200 kgm^{-3}, conductivity = 204 $Wm^{-1}K^{-1}$ when $T = 0\ ^oC$, = 225 $Wm^{-1}K^{-1}$ when $T = 300\ ^oC$.

First extrusion pressure, die pressure, temperature variation inside the deformation zone, velocity variation at the die exit, distortion variation, strain variation and strain rate variation at the die exit are minimized separately to study how each property vary with the process and design parameters. It is interesting to find that the optimal parameter values were not the same (eg. the parameters which minimizes the extrusion pressure are not same as the parameters which minimizes temperature variation inside the die) for all categories.

Secondly the circumferential, axial stress and hydrostatic pressure at the die exit are compared. The contour plot of circumferential stress, axial stress and hydrostatic pressure at the die entrance for three different dies (A: which needs minimum extrusion pressure, B: which minimizes the velocity variation at the exit,

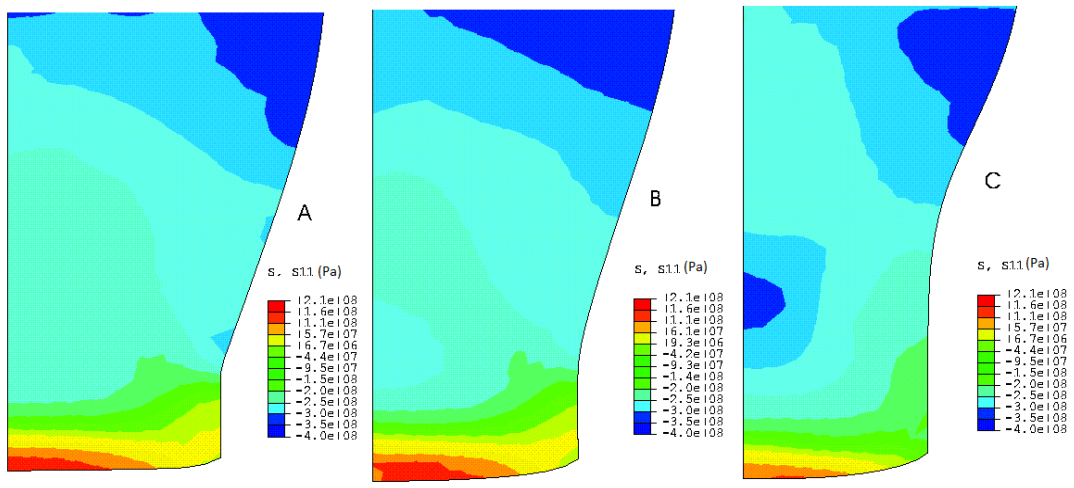

Figure 4.16: Circumferential stress (Pa) when :(A) Extrusion pressure, (B) Velocity variation at exit, (C) Strain-rate variation at exit are lowest.

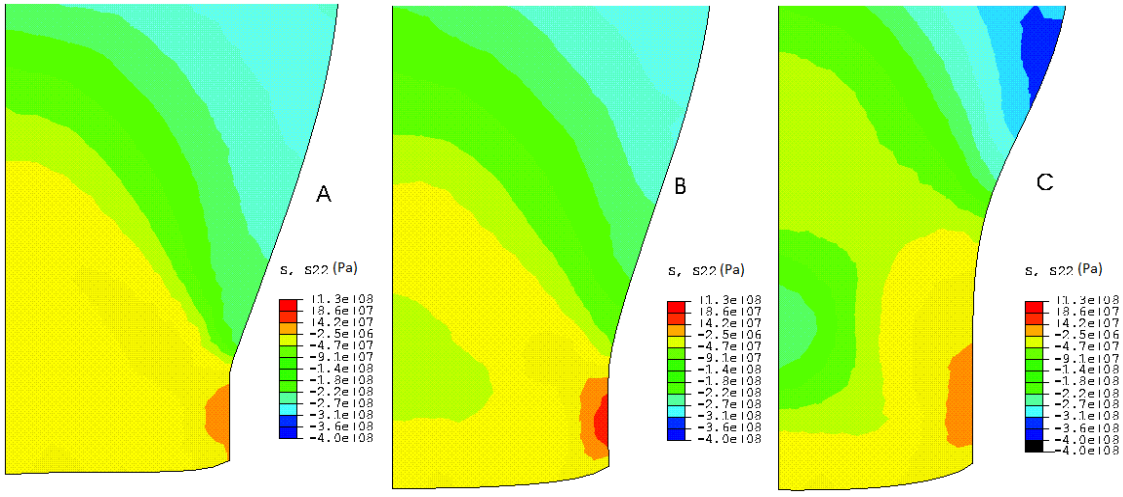

Figure 4.17: Axial stress (Pa) when :(A) Extrusion pressure, (B) Velocity variation at exit, (C) Strain-rate variation at exit are lowest.

C: which minimizes strain rate variation), are shown respectively in Figure 4.16, 4.17 and 4.18. It has been found, that the die, which minimizes the strain rate variation at the exit also produces the profile with lowest circumferential stress and the die, which minimizes the extrusion pressure, produces the profile with minimum axial stress, which can be expected. The review of literature [67] showed, that the

possibility of cracking increases with increasing tensile circumferential stresses and chevron(or central) bursts increase with increasing axial stress. Therefore it is important and necessary to include the minimization of circumferential and axial stress during the optimization process.

The tendency toward chevron cracking increases, if plastic zones do not meet together inside the forming zone. The probability of chevron cracking increases with decreasing extrusion ratio. If this happens the hydrostatic pressure at that region is zero. It can be shown that the hydrostatic pressure is not zero inside the forming zone for any of the above mentioned cases (which minimizes extrusion pressure, die pressure, temperature variation, and strain rate variation etc) and in certain non optimal cases as shown in Figure 4.19 (eg. when extrusion pressure is maximum) the hydrostatic pressure inside the forming zone is zero.

The average grain size is proportional to

$$\frac{d}{\alpha} = \left(\dot{\bar{\varepsilon}} \exp\left(\frac{Q}{RT}\right)\right)^{\beta}. \tag{4.19}$$

Here d is an average grain size and α is a constant. The variation of the four most optimized d/α values along the die exit with different process conditions are shown in Figure 4.20. Most optimal (in terms of uniformity) d/α values of four different cases and their respective die surface which gives the optimum are shown in Figure 4.21. These figures clearly show that the grain size is more sensitive to extrusion speed and the initial temperature than the die geometry. Further the uniformity of the grain size is more influenced by the shape of the die surface than initial temperature or ram speed. Therefore, a certain grain size with uniformity could be achieved by trading off between these parameters.

Finally the grain size variation with various desired grain sizes for a sequence of design and process parameters are considered and it is found that values of

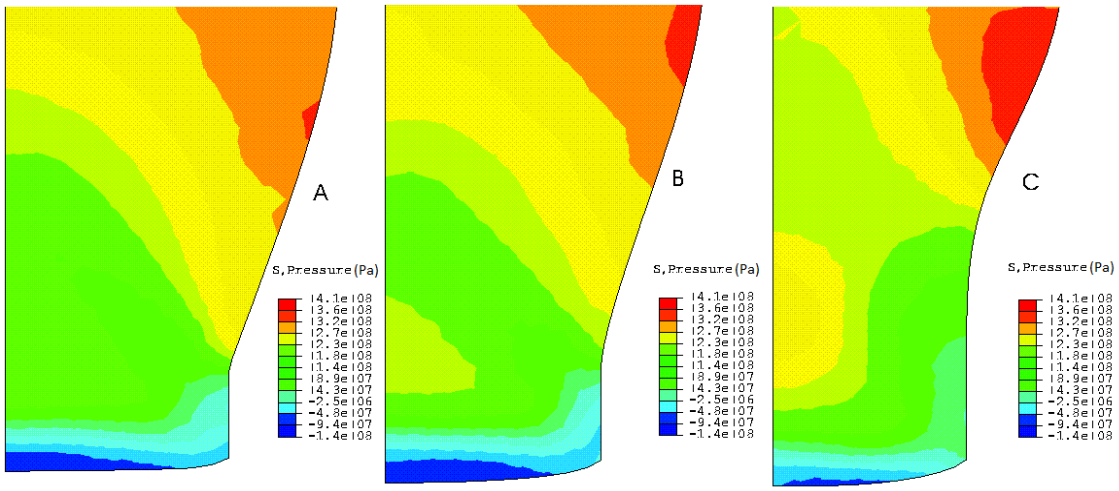

Figure 4.18: Hydrostatic pressure (Pa) when :(A) Extrusion pressure, (B) Velocity variation at exit, (C) Strain-rate variation at exit are lowest.

parameters (design and process) exist to satisfy equations 4.6– 4.9.

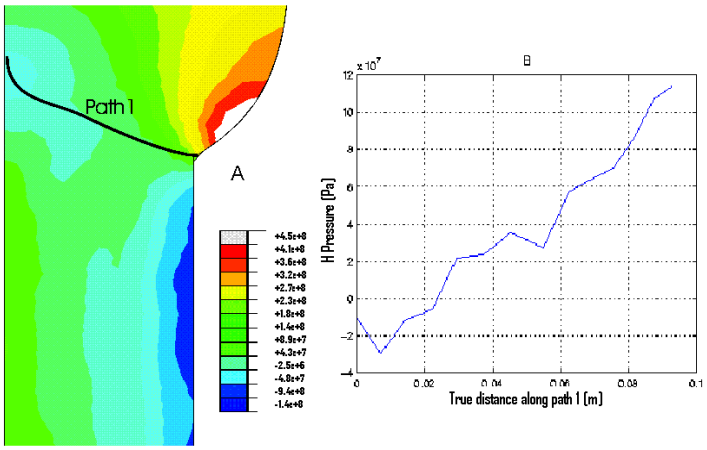

Figure 4.19: Hydrostatic pressure (A) inside the forming zone, (B) along the Path 1 .

4.8 Summary

The goal of the work presented here is to investigate a numerical technique which is capable of simultaneously estimating the optimal die profile and the process

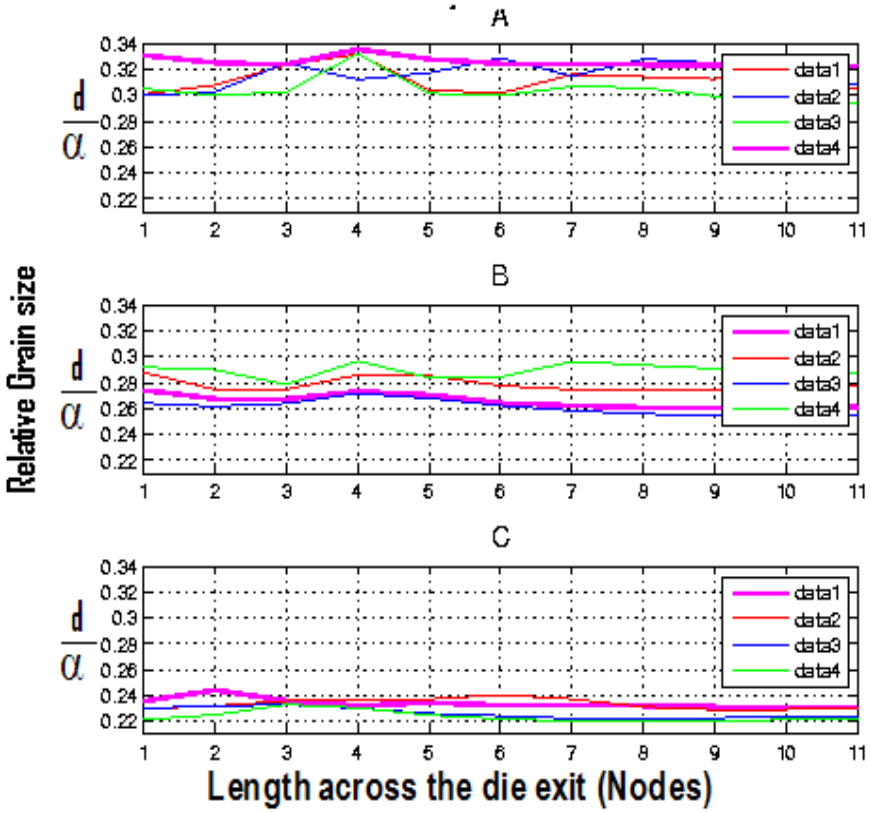

Figure 4.20: Grain size variation along the die exit (d/α) (A) when $v = 6.3\ mm/s$, $T_{D_0} = 450^oC$, $T_{B_0} = 500^oC$, (B) when $v = 25\ mm/s$, $T_{D_0} = 450^oC$, $T_{B_0} = 500^oC$, (C) when $v = 25\ mm/s$, $T_{D_0} = 400^oC$, $T_{B_0} = 450^oC$.

parameters such as extrusion speed and initial temperatures. The approach is based on a non-linear least squares estimation using the desired properties of the product which is extruded.

The examples considered in the above section describe how values of the design and process parameters influence the optimization process. The results from these examples suggest that the proposed technique is capable of estimating the optimal values well.

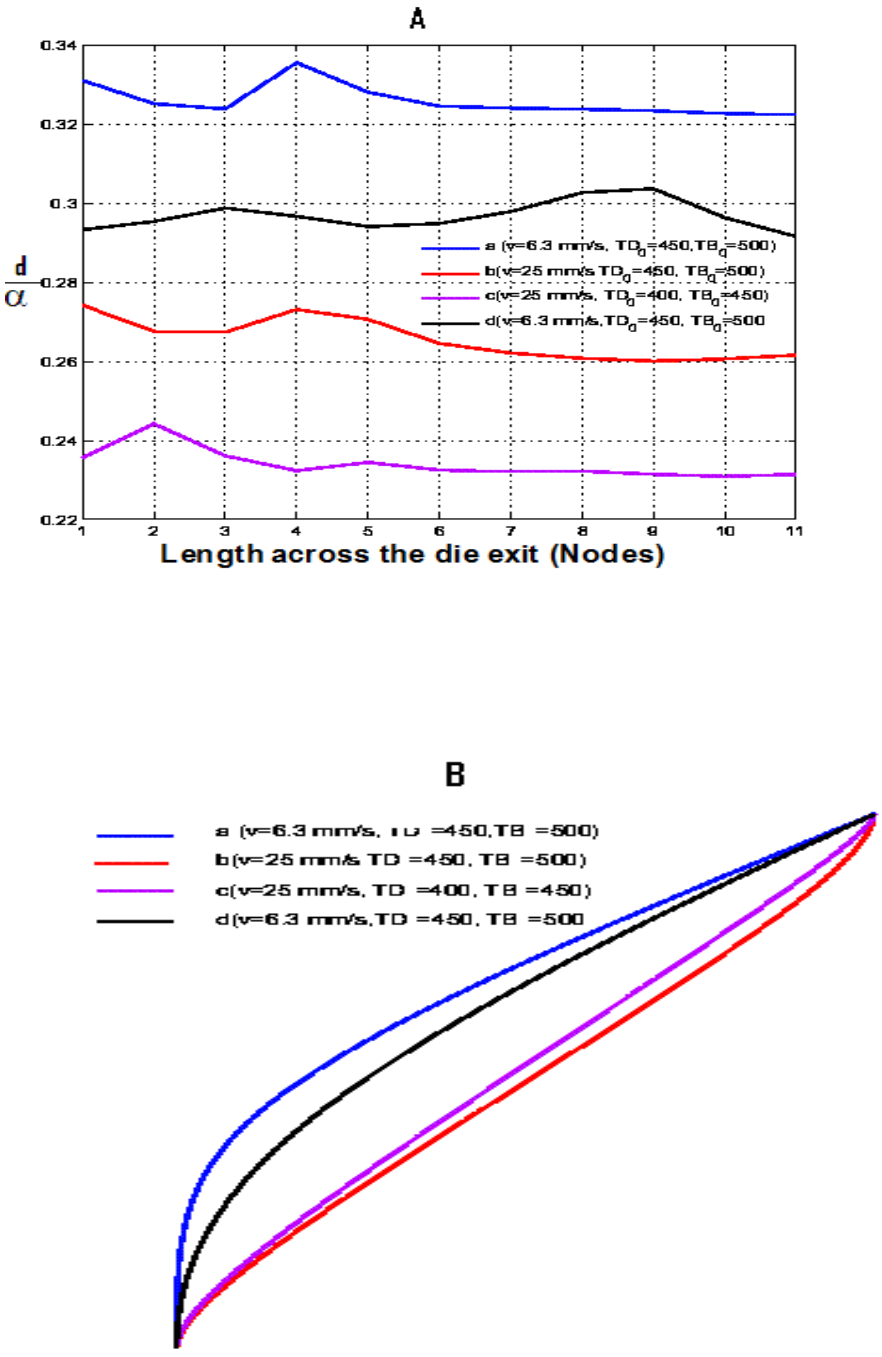

Figure 4.21: Grain size variation along the die exit (d/α):(A) Optimal vales with different process conditions, (B) Optimal die shape with different process conditions .

Chapter 5

Estimation of Average Grain Size and Material Constants

5.1 Introduction

Numerical modelling of extrusion may be used during a design process to assess the extruded material properties. The extrusion simulation describes the material flow through the die. An extrusion model, which is capable of describing the behaviour of material flow, requires the following input data: (a) material data such as Young's modulus, coefficient of expansion, Poisson's ratio, inelastic heat fraction, specific heat, density, conductivity, flow stress-strain relationship, (b) die design variables and (c) process variables such as ram speed, initial temperature and friction factors.

In reality, material data can be measured using available measuring instruments, but the optimal values of die design variables and process variables are often unknown. In the previous chapters, a non-linear least squares inverse model is formulated in which the optimal values of die design variables and process variables were estimated to achieve a certain grain size. In this approach the following

average grain size equation [76], [77]

$$d = \alpha \left(\frac{d\varepsilon}{dt} \exp\left(\frac{Q}{RT} \right) \right)^{\beta} \tag{5.1}$$

was used as optimizing criteria to terminate the problem. In equation 5.1, Q is an activation energy, d is the average recrystallized grain size, T is the temperature, $\frac{d\varepsilon}{dt}$ is the strain rate and R is the universal gas constant.

The values of constants α and β are based on experimental observations and therefore the uncertainty of the constants can be very high. Small changes in these values can cause variation in the grain size estimation. The successful application of equation (5.1) depends on the accuracy of the parameters. Methods to identify the optimal values of α and β are therefore an important part of modelling extrusion processes to increase the reliability of the numerical simulation.

In this chapter an alternative method is proposed. The idea is to develop an inverse model for estimating grain size history, using inverse modelling techniques available in the literature. Inverse modelling avoids the use of α and β for the grain size history estimation. To do so the problem in which the material properties of the billet as well as process and die design parameters are known but the material constants α, β and grain size d are not known is considered. The accuracy of the model is examined by using simulated temperature and strain data (generated by the forward model) to which normally-distributed relative noise has been added. The inverse model is designed as a least squares minimisation problem associated with an ABAQUS finite element solution of an extrusion process. This is an ill-posed problem and it is solved using regularisation methods.

5.2 Forward Problem

The thermo-mechanical behaviour of the extrusion process can be described mathematically using equations (2.14-2.26). The solutions can be obtained with finite element methods. The solution procedure is implemented using ABAQUS to obtain temperature and strain histories during the deformation process. Once the temperature and strain values are obtained, the average grain size at a nodal point can be calculated with equation 5.1.

5.3 Inverse Problem

The goal of inverse modelling is the extraction of model parameter information from data. It is a subject, which supplies tools for the proficient use of data in the estimation of constants appearing in the models. In this inverse problem, the structure of the equation is known; outputs, temperature (T) and strain (ε) values are available. Average grain size history and parameters α and β are the unknowns.

In this section a model is formulated to obtain the best estimate of grain size history, α and β appearing in equation 5.1 from temperature and strain estimations made at some nodes in the material inside the forming zone. The microstructural model given by equation (5.1) can be rewritten to solve for strain rate as follows.

$$\frac{d\varepsilon}{dt} = \left(\frac{d}{\alpha}\right)^{1/\beta} \exp\left(\frac{-Q}{RT}\right) \tag{5.2}$$

Therefore the strain is

$$\begin{aligned} \varepsilon(t) &= \int_0^t \left(\frac{d(\tau)}{\alpha}\right)^{1/\beta} \exp\left(\frac{-Q}{RT(\tau)}\right) d\tau \\ &= \int_0^t K(t,\tau) D(\tau) d\tau \end{aligned} \tag{5.3}$$

where the kernel $K(t,\tau)$ is:

$$K(t,\tau) = \exp\left(\frac{-Q}{RT(\tau)}\right) \tag{5.4}$$

and

$$D(\tau) = \left(\frac{d(\tau)}{\alpha}\right)^{\frac{1}{\beta}} \tag{5.5}$$

If n temperature and strain values are available at the node (X_1, Y_1, Z_1) between 0 and t_f and supposing that $D(\tau)$ at times $\tau_0 = 0, \ldots, t_f$ are to be determined, then discretising (5.3) by the trapezoidal rule gives a system of linear equations

$$\mathbf{e} = \mathrm{A}(\mathbf{p})\mathbf{q} \tag{5.6}$$

where $\mathbf{e} = [\varepsilon(\mathbf{0}), \ldots, \varepsilon(\mathbf{t_f})]^{\mathbf{T}}$, $A_{ij} = K(t_i, \tau_j)\beta_{ij}$, $\mathbf{q} = [D(\tau_0), \ldots, D(\tau_f)]^T$ and $\mathbf{p} = [\mathbf{Q}]$, and β_{ij} is a quadrature weight. Generally, minimising an objective function solves inverse problems. The objective function Z that provides minimum variance estimates is the ordinary least squares function

$$minimize \quad Z(\mathbf{p},\ \mathbf{q}) = \|A(\mathbf{p})\mathbf{q} - \mathbf{e}\|_2^2 \tag{5.7}$$

If the value of activation energy Q is known then the problem becomes a linear least square problem and can be solved easily. But the coefficient matrix of problem 5.7 always has a very large condition number and is ill posed. Therefore well posed situation must be restored by restricting the class of admissible solutions. This can be achieved using regularisation methods [29]. With Tikhonov's regularisation, the regularised objective function

$$Z(\mathbf{q}) \quad = \quad \|A\mathbf{q} - \mathbf{e}\|_2^2 + \lambda^2\|L\mathbf{q}\|_2^2 \tag{5.8}$$

is introduced where $\|A\mathbf{q} - \mathbf{e}\|_2^2$ is the residual norm (or data misfit function), and $\|L\mathbf{q}\|_2^2$ is the solution norm. The minimisation of the function $Z(\mathbf{q})$ for different values of λ will be interested. Note that the objective function Z is the 2-norm of the following system of equations

$$\begin{bmatrix} A \\ \lambda L \end{bmatrix} \mathbf{q} = \begin{bmatrix} \mathbf{e} \\ 0 \end{bmatrix},$$

where L is the regularisation operator and is defined by

$$\|L\mathbf{q}\|^2 = \int_0^t \left(\frac{d^N \mathbf{q}}{d\tau^N}\right)^2 d\tau, \tag{5.9}$$

and λ is the regularisation parameter. The regularisation parameter λ has to be altered in such a way that the solution fits well in some optimal way.

If the value of Q is not known then the problem becomes a nonlinear least square problem as follows.

$$Z\left(\mathbf{q},\ \mathbf{p}\right) = \|A(\mathbf{p})\mathbf{q} - \mathbf{e}\|_2^2 + \lambda^2 \|L\mathbf{q}\|_2^2. \tag{5.10}$$

Since the equation (5.10) has a combination of linear parameters $\mathbf{q}$ and non-linear parameters $\mathbf{p}$, the solution process is separated into two steps. The non-linear parameter $\mathbf{p}$ is found by constructing an iterative procedure, where at each iteration a linear sub-problem is solved to estimate the linear parameter $\mathbf{q}$ corresponding to that particular value of $\mathbf{p}$.

Now taking natural logarithms of both sides of the equation 5.5 and rearranging gives

$$\ln(D) = m \ln(d) + C \tag{5.11}$$

where $m = \dfrac{1}{\beta}$ and $C = \dfrac{1}{\beta} \ln\left(\dfrac{1}{\alpha}\right)$. Now supposing $n+1$ D values are available the

corresponding d values are to be determined. This gives

$$K\mathbf{y} = \mathbf{f}, \tag{5.12}$$

where

$$\mathbf{K} = \begin{pmatrix} m & 0 & \dots & 0 & 0 \\ 0 & m & \dots & 0 & 0 \\ \vdots & \vdots & \vdots & \vdots & \vdots \\ 0 & 0 & \dots & m & 0 \\ 0 & 0 & \dots & 0 & m \end{pmatrix}$$

$$\mathbf{y} = \begin{pmatrix} \ln\left(\frac{d_1}{d_0}\right) \\ \ln\left(\frac{d_2}{d_0}\right) \\ \vdots \\ \ln\left(\frac{d_{n-1}}{d_0}\right) \\ \ln\left(\frac{d_n}{d_0}\right) \end{pmatrix}, \ \mathbf{f} = \begin{pmatrix} \ln\left(\frac{D_1}{D_0}\right) \\ \ln\left(\frac{D_2}{D_0}\right) \\ \vdots \\ \ln\left(\frac{D_{n-1}}{D_0}\right) \\ \ln\left(\frac{D_n}{D_0}\right) \end{pmatrix}$$

Now the minimisation problem for estimating $\mathbf{y}$ is formulated as

$$\min_{\mathbf{y}} \|K\mathbf{y} - \mathbf{f}\|_2^2. \tag{5.13}$$

It is a linear problem and therefore the grain size history $d_1, d_2, \dots, d_n$ can be calculated with reasonable accuracy provided the initial grain size is known.

5.4 Applications

In this section, numerical simulations to demonstrate the solution process are presented and the accuracy of the model is evaluated. To do so, an input of temperature and strain value data generated are considered at three elements A, B,

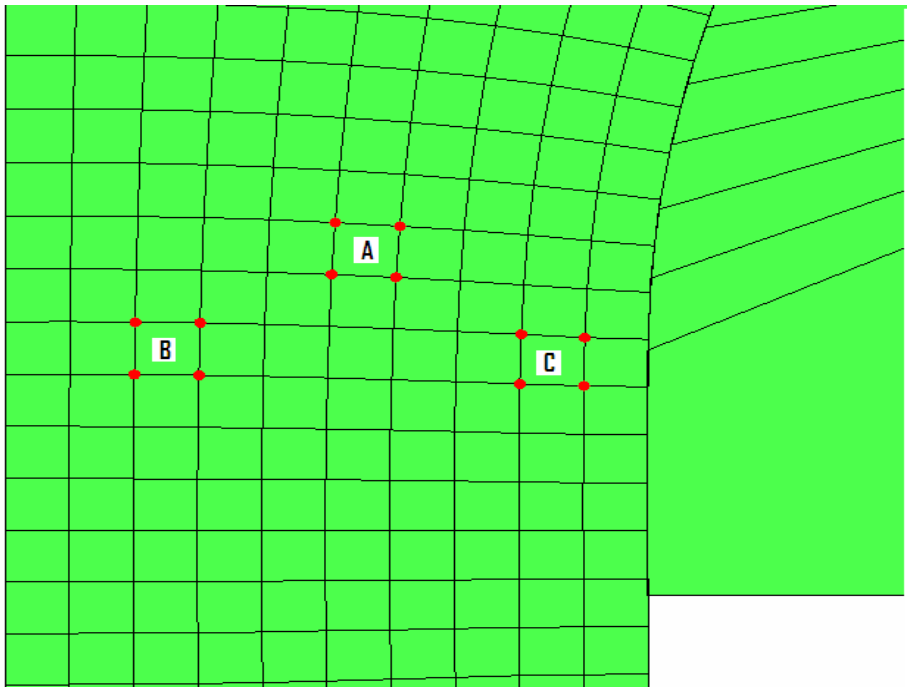

Figure 5.1: Three considered elements of a deformed mesh

C as shown in Figure 5.1 from a FE-simulation of extrusion using ABAQUS. The data values used in the simulation of extrusion are: initial temperature of work piece and die respectively are $T = 500^oC$ and $T = 450^oC$, work piece's Young's modulus $E = 7 \times 10^{10}\ Pa$, coefficient of expansion $8.4 \times 10^{-5}\ {}^oC^{-1}$ at $T = 20\ {}^oC$, Poisson's ratio 0.35, inelastic heat fraction 0.9, specific heat 910 $Jkg^{-1}K^{-1}$, density= 2750 kgm^{-3}, conductivity 204 $Wm^{-1}K^{-1}$ when $T = 0\ {}^oC$, 225 $Wm^{-1}K^{-1}$ when $T = 300\ {}^oC$, die material's Young's modulus $E = 20{\times}10^{10}\ Pa$, coefficient of expansion $8.4 \times 10^{-5}\ {}^oC^{-1}$ at $T = 20\ {}^oC$, Poisson's ratio 0.30, inelastic heat fraction 0.9, specific heat 450 $Jkg^{-1}K^{-1}$, density 7200 kgm^{-3}, conductivity 204 $Wm^{-1}K^{-1}$ when $T = 0\ {}^oC$, 225 $Wm^{-1}K^{-1}$ when $T = 300\ {}^oC$.

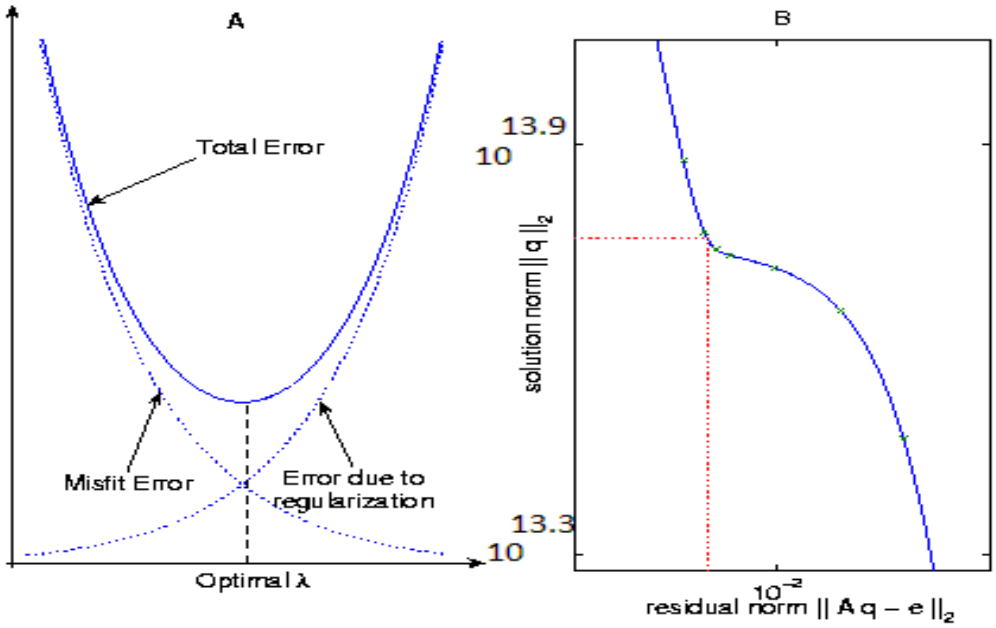

Figure 5.2: (A):Total error, (B) L-curve.

5.4.1 Estimation of Grain Size $d(t)$ for Known Value of Activation Energy Q

If the value of Q is known, the Equation 5.8 has to be solved to estimate the grain size. The minimization problem given by Equation 5.8 depends on the optimal value of the regularization parameter λ. A number of techniques have been discussed in the literature[30] for estimating an optimal value of a regularization parameter. Here the L-curve criterion is used to estimate the parameter values. It is based on minimizing the total error equation 5.8 as shown in Figure 5.2. A good regularization parameter λ should provide a fair balance between data misfit error and regularization error. The L-curve method shown in Figure 5.2B is based on minimizing total error as shown in Figure 5.2A.

Once the optimal value of λ is known, $\mathbf{q} = [D(\tau_0), \ldots, D(\tau_f)]^T$ are easily estimated and then using equation 5.13 values $\mathbf{y} = \left[\frac{D_1}{D_0}, \ldots, \frac{D_n}{D_0}\right]^T$ are calculated.

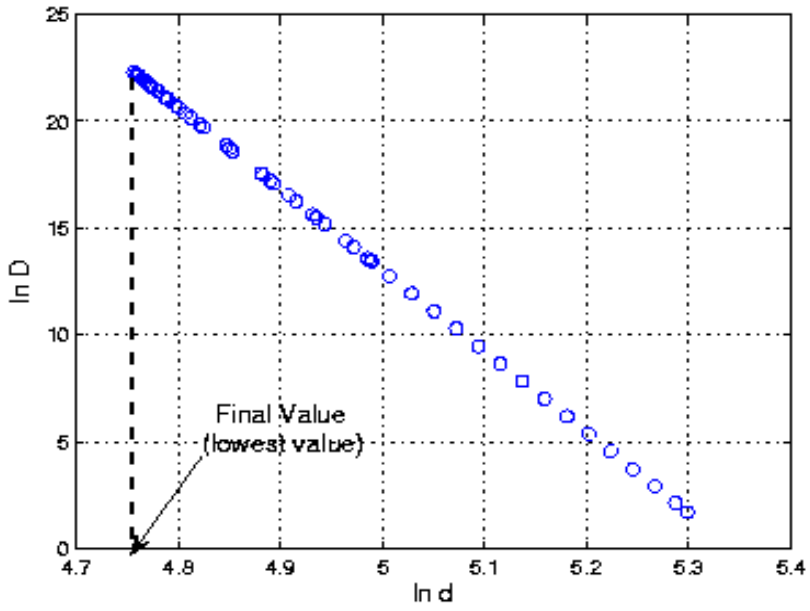

Figure 5.3: Graph of Equation 5.11

Figure 5.3 shows the graph of equation 5.11 for the initial grain size $d_0 = 200\ \mu m$ and the activation energy $Q = 100\ KJm^{-1}$.

The accuracy of value Q in Equation 5.1, may or may not be very high since it is based on experimental observations and the accuracy of estimation of d is also subject to error. Therefore it is appropriate to analyze the effect of inaccuracy of the Q value. To investigate, the Q values are changed, while all other values are unchanged. Table 5.1 shows the optimal values of α and β for the respective values of Q obtained using the proposed method. Figure 5.4 depicts the comparison of grain size variation. Data 4 in this graph is the grain size estimation using the proposed method and data 5 is the grain size variation obtained by Equation 5.1 for the respective α and β values given in Table 5.1. Data 1, Data 2 and Data 3 respectively are the grain size values for ($\alpha = 278$ & $\beta = -0.080$), ($\alpha = 200$ & $\beta = -0.020$) and ($\alpha = 279$ & $\beta = -0.018$) by Equation 5.1. When Q is

	Q	α	β
Data1	20	140	-0.044
Data2	50	278	-0.080
Data3	100	209	-0.026
Data4	140	200	-0.020
Data5	180	240	-0.019
Data6	220	279	-0.018
Data7	300	412	-0.019

Table 5.1: Variation of α and β with Q values

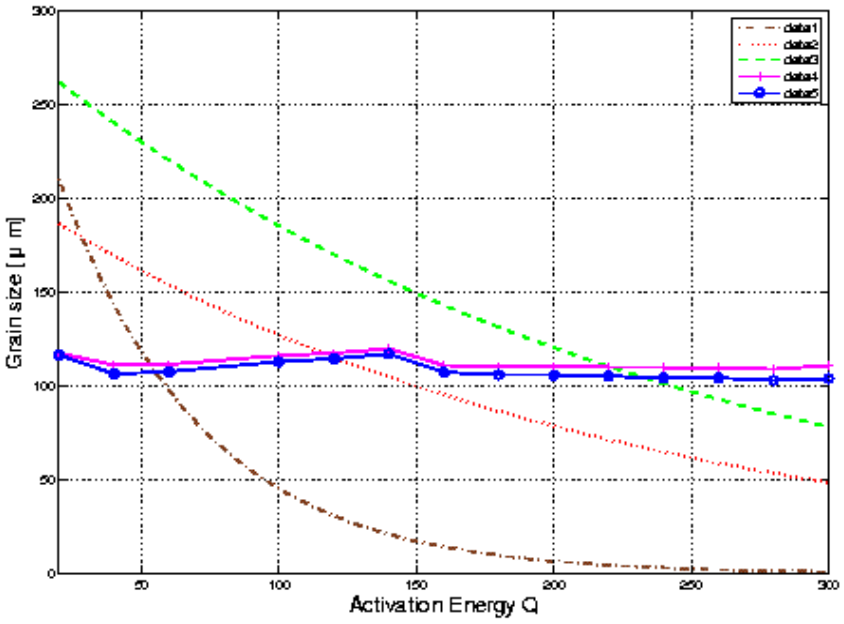

Figure 5.4: Grain size vs activation energy for different material constants

underestimated, the average grain size estimated value using Equation 5.1 is higher than it used to be and increases approximately quadratically with decreasing Q value. When Q is overestimated, the average grain size estimated value is lower than it used to be and decreases approximately quadratically with increasing Q value. The graph of Data 4 and Data 5 are approximately the same. This shows that even if the Q value is wrong, it is possible to estimate d accurately using

Equation 5.1 if appropriate α and β values are available. These results can't be gained by practical experiments, but can only be achieved through inverse modelling techniques.

5.4.2 Estimation of $d(t)$ for Unknown Value of Activation Energy

Here the problem is concerned with the estimation of grain size $d(t)$ values and the activation energy (Q). This estimation process contains a combination of a nonlinear parameter (Q) and linear parameters ($d(t)$). This is different from a linear problem and therefore linear algebra cannot be used to solve this problem. This problem can be solved by constructing an iterative procedure as mentioned above. Alternatively the Equation 5.10 can be solved for a sequence of Q values to get a best value for Q which minimizes Equation 5.10, since there is only one nonlinear parameter. Figures 5.5A, 5.5B respectively show the variation of Z with Q at the nodes A (data 1), B (data 2), C (data 3) for the ram speed 12.5 $mm\ s^{-1}$ and 6.5 $mm\ s^{-1}$. The graphs clearly show that the best value of Q is not the same for all cases. In the literature it can be found that the activation energy of the material varies with temperature. During the extrusion process the temperature inside the deformation zone is not constant everywhere. Therefore using a constant Q value in Equation 5.1 will not give an accurate result unless appropriate values of α and β are used. Again the estimation of α and β which suits the Q value is not achievable in a real practical environment.

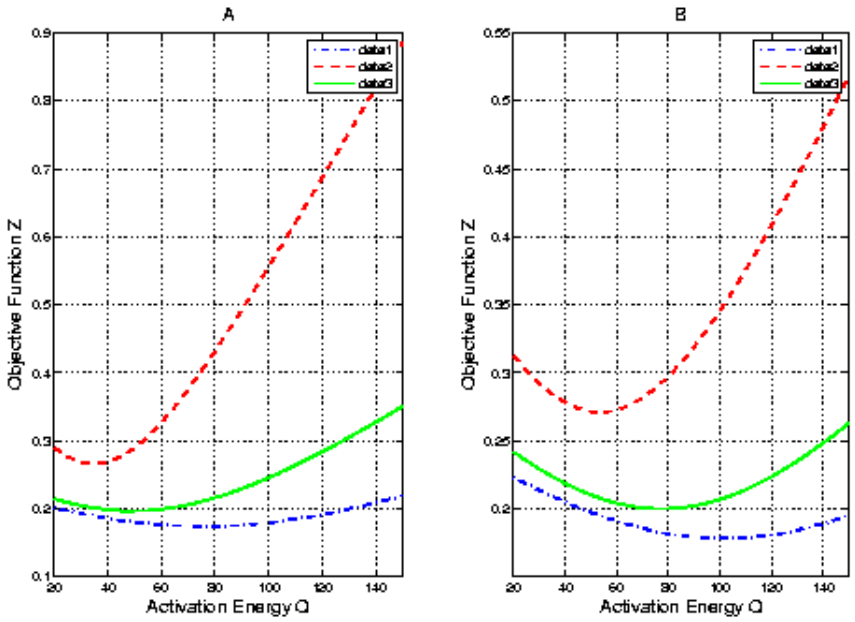

Figure 5.5: Objective function Z vs Activation energy Q

5.5 Summary and Conclusion

The objective of the work demonstrated in this chapter is to develop an inverse model capable of concurrently estimating the average grain size, activation energy and other material constants appearing in the model. The approach is based on a non-linear least squares estimation using simulated temperature and strain value history inside the deformation zone. Since the problem is ill-posed, Tikhonov's regularisation method is applied to stabilise the solution process. Some of the parameters in the problem are linear and some are nonlinear. The linear parameters are determined using simple linear algebra and for the computation of non-linear parameters M_{ATLAB}'s routine *lsqnonlin* is used. The optimal value of the regularisation parameter is obtained using the linear L-curve for the linear problem.

To summarize three points can be made: Firstly, the usefulness of an inverse modeling technique in the grain size estimation process has been demonstrated. The

inverse modelling technique has been applied to Equation 5.1 with the situation in which α, β and Q values are unknown. Secondly, it has been shown that the error in traditional d estimation increases quadratically with the error in Q if the α and β values are adjusted accordingly to cater for Q. The appropriate values of α and β can only be found using the above mentioned inverse modelling technique. Thirdly, it has been demonstrated the optimal value of the activation energy inside the deformation region is not constant and varies with the temperature. Therefore the traditional d estimation using Equation 5.1 with constant values of Q, α and β will not give the accurate value, if the temperature inside the deformation zone is not constant.

Chapter 6

Optimization of Pocket Design to Produce a Thin Shape Complex Profile

6.1 Introduction

The surface qualities of extruded products depend on process and die design parameters. In order to produce appropriate shapes with good surface quality and homogenous structure the metal flow through the die should be as uniform as possible. Therefore the estimation of an optimal set of process and die design parameters for a particular product geometry is an important part of an extrusion process.

The geometry of the product considered for the investigation is a current production part. The profile geometry is shown in Figure 6.1. Since it is symmetry about the axis and therefore only half of the part is considered as shown in Figure 6.1 is considered. This specific die geometry was selected because the extruded product showed surface quality problems. After anodizing it has white lines along the extrusion direction that make an uneven visual surface. These lines tend to

appear at different places on different production runs. They seem to be random in whether they appear or not and when they do, it could be anywhere on the profile. These lines are seen as flow–lines.

Flow–lines are distinctive surface marks and tangential to the machine direction. They are very irregular in size, shape and position. According to the available literature it is a region of highest shear stress. A poor temperature and velocity uniformity inside the forming zone leads to a change in flow characteristics and layer distribution.

Figures 6.3 and 6.4 depict the velocity, temperature and shear stress distribution of the extruded product between the entrance and exit of a die for the given geometry. It shows that the temperature and velocity distributions are not homogenous. Further the location of the higher stress area was found moving with different initial billet temperatures. All these results demonstrate the importance to improve the die design. If the profile geometry is simple then the flow can be adjusted by using a curved die. But here the profile geometry is complex and the die is flat. There are several methods available to alter metal flow and temperature distribution through a flat die. More reliable methods are (1) assigning a different bearing length at different locations and (2) inclusion of a pocket (or pre-chamber) in front of the die bearing. Even though the variation of the bearing length at different locations is an effective method to control the metal flow the tendency for extruded surface defects to occur will increase since more heat generates from friction in certain regions of the interaction between billet and die bearing.

6.2 Finite Element Model

The finite element program DEFORM 3D is used in this analysis to simulate the extrusion process as shown in Figure 6.5. It is based on the Lagrangian method and

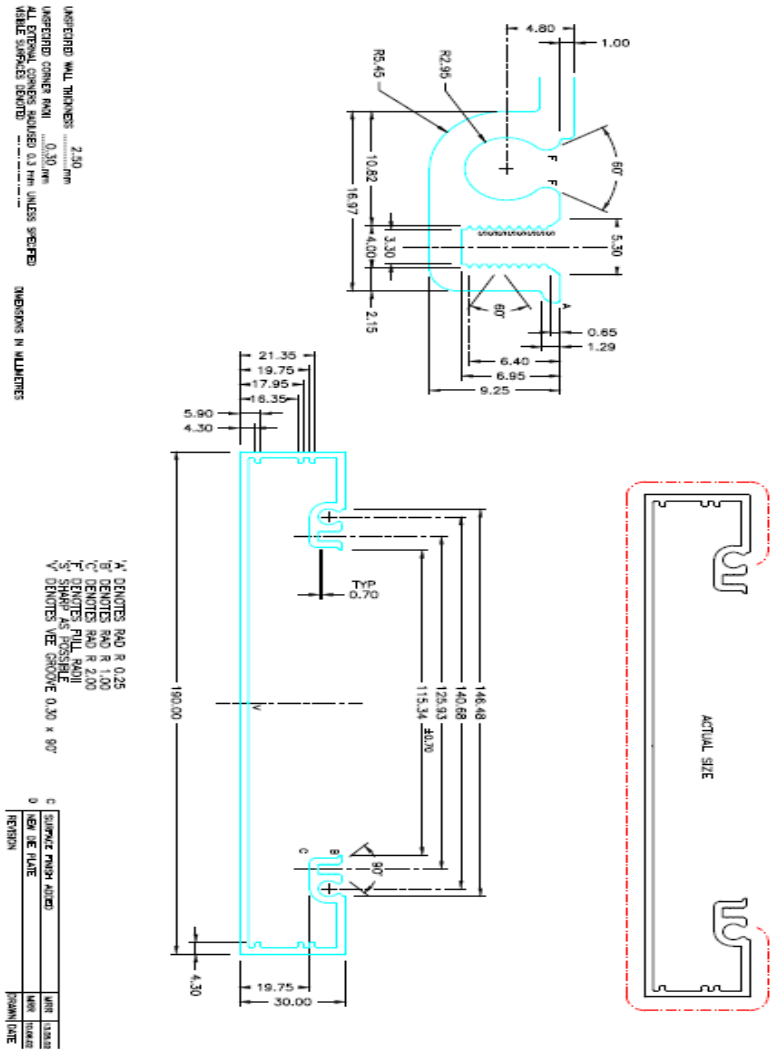

Figure 6.1: CAD model of the die

capable of being applied to most metal forming simulation processes. DEFORM's forming modules are used to set up the extrusion process. The geometry of billet and die are created using SolidWorks and imported into the DEFORM platform. Aluminium AA6061 and AA7075 was used as a billet material. The die and container are assumed to be rigid and made of H13 steel. The physical properties of die and billet are given in Table 6.1.

In addition, DEFORM has an automatic mesh generator which produces an

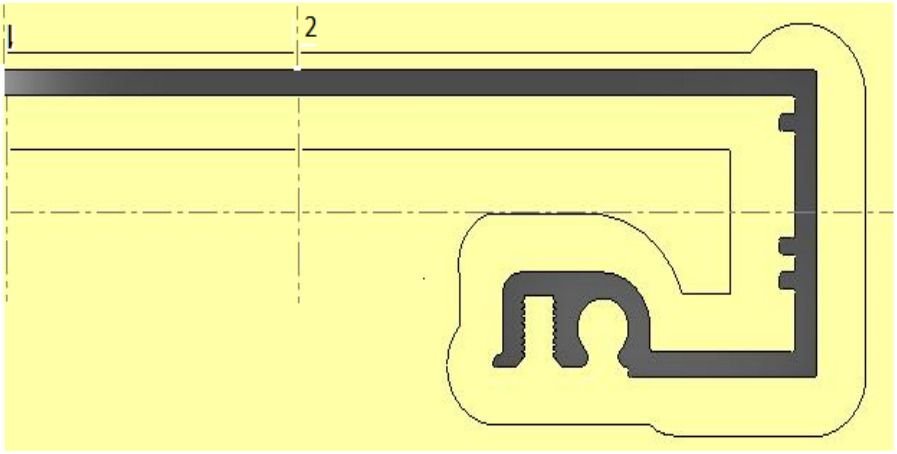

Figure 6.2: Geometry of the die

Material properties	AA6061	AA7075	H 13
Heat capacity $N/mm^2\,^\circ C$	2.4	2.39	5.6
Thermal conductivity $W/m\,^\circ C$	166	130	28.4
Heat transfer coefficient between die and billet $N/\,^\circ C smm^2$	11	11	11
Emissivity	0.1	0.1	0.7

Table 6.1: Material properties of billet and die

optimized mesh with local element size control. More elements are used where there are large deformations and fewer elements are used where little deformation takes place.

In this study of simulation of extrusion, Coulomb friction is used when contact occurs between billet and die. The frictional force in the Coulomb law model is defined by

$$f_s = \mu p$$

where f_s is the frictional stress, p is the interface pressure between two bodies and μ is the friction factor. A friction factor of 0.1 was used for most simulations

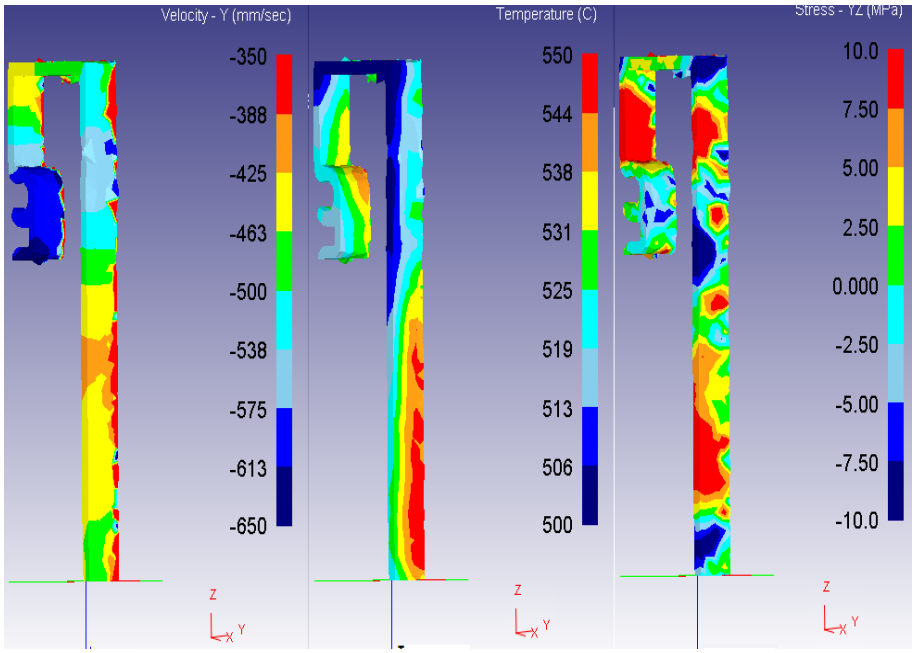

Figure 6.3: Velocity, Temperature and Shear stress, distribution inside the die land

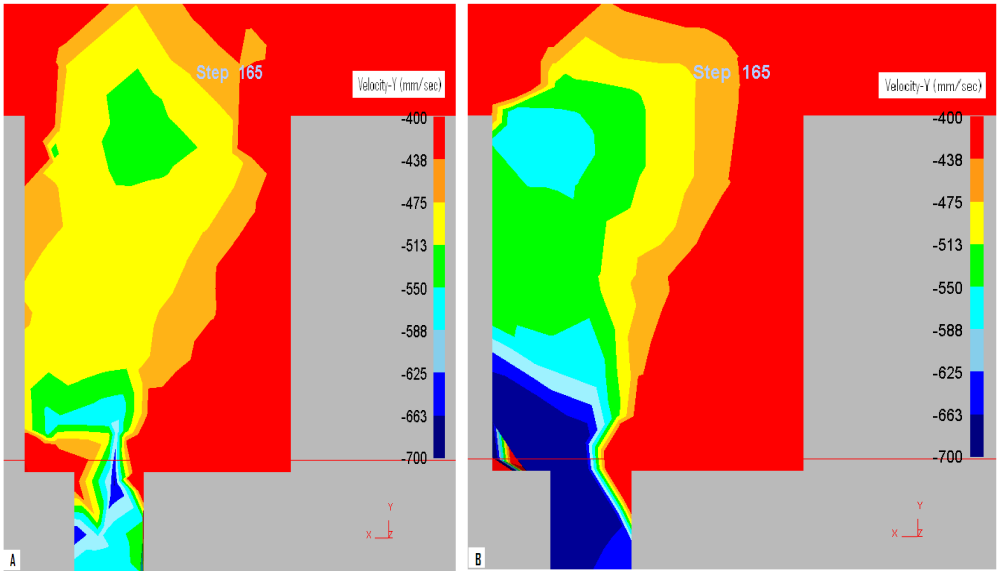

Figure 6.4: Velocity distribution at two different locations along the die channel: (A) Location 1, (B) Location 2 of Figure 6.2

following a recommendation in the DEFORM 3D manual to use a friction factor between $0.1 - 0.2$ for warm forming processes.

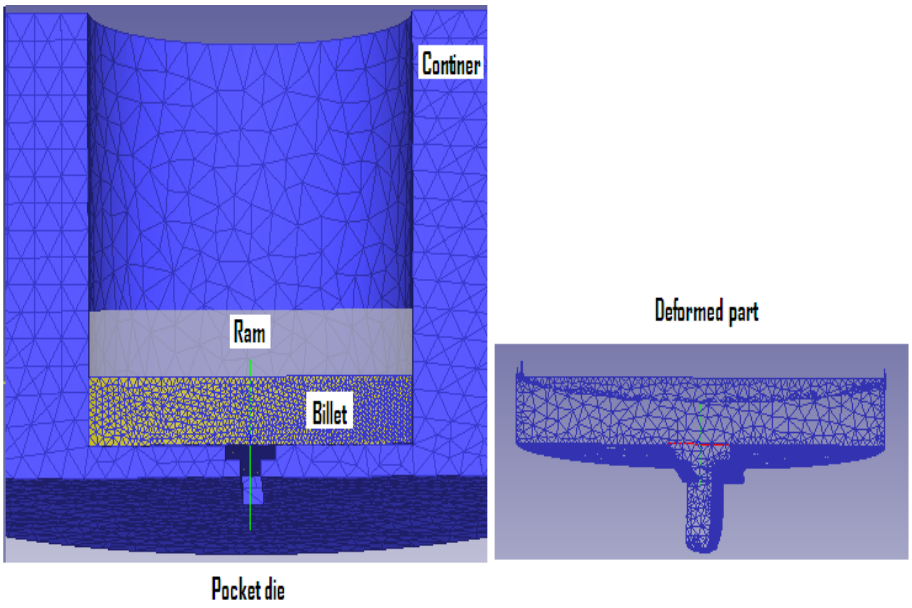

Figure 6.5: Finite element model

6.3 Analysis of the Influence of Pocket Design Parameters

The surface finish of the extruded product is related to the flow pattern. The flow pattern depends on pocket design parameters such as the pocket shape, the distance between the centre axis of the die and centre axis of the pocket (r_p), pocket depth (d) and pocket width (w). In this section the influences of these parameters on the flow pattern were investigated using a simple rectangular pocket die as in Figure 6.6.

6.3.1 Influence of Distance from Die Centre r_p

Figure 6.7 shows the homogeneity of flow when the die channel is not in the middle of the die axis ($r_P > 0$). It can be seen from this figure that the flow through the die channel is more homogeneous when the width of the pocket closer to the

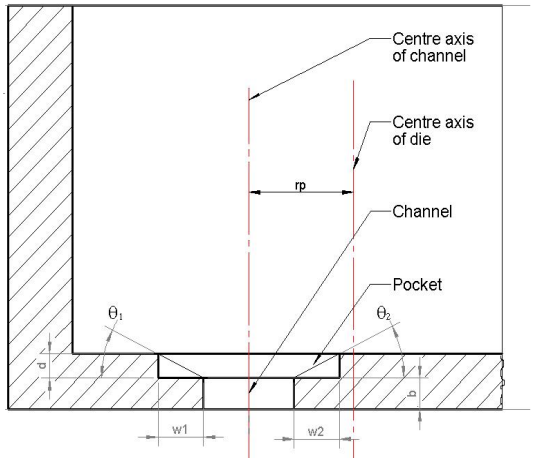

Figure 6.6: Pocket shape 1

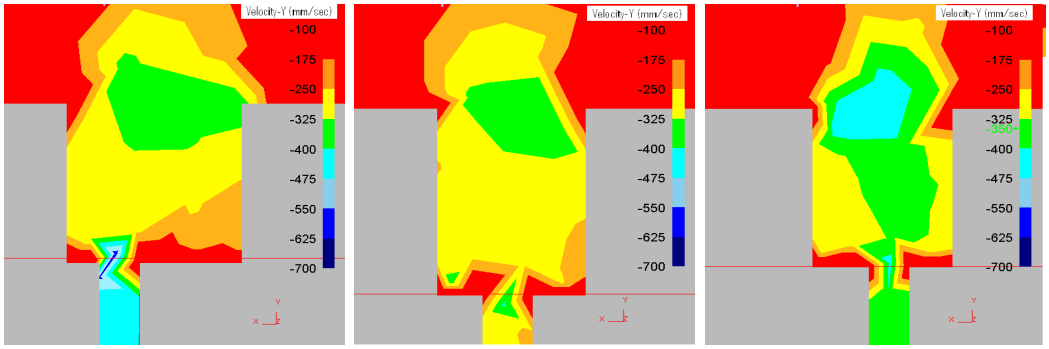

Figure 6.7: Homogeneity of flow with different pocket widths when $r_P > 0$: (A) $w_1 > w_2$ (B) $w_1 = w_2$, (C)$w_1 < w_2$

die center is smaller than the width of the pocket, which is away from the die axis. It clearly demonstrates the importance of finding an optimal ratio of w_1 and w_2. Figure 6.8 shows the homogeneity of flow at two different locations along the channel length. In this figure the flow pattern at the front is more homogeneous than the flow behind. These simulations indicate that the optimal ratio of $w_1 : w_2$ at two locations along the channel is not the same. This increases the number of parameters to be considered and eventually the complexity of the pocket design problem.

Figure 6.9 shows the homogeneity of flow at two different locations along the

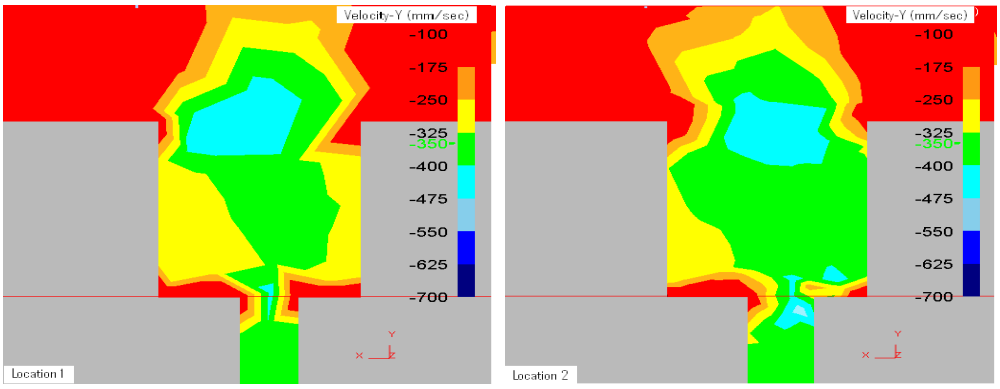

Figure 6.8: Homogeneity of flow across chamber at two different locations along channel when $r_P > 0$

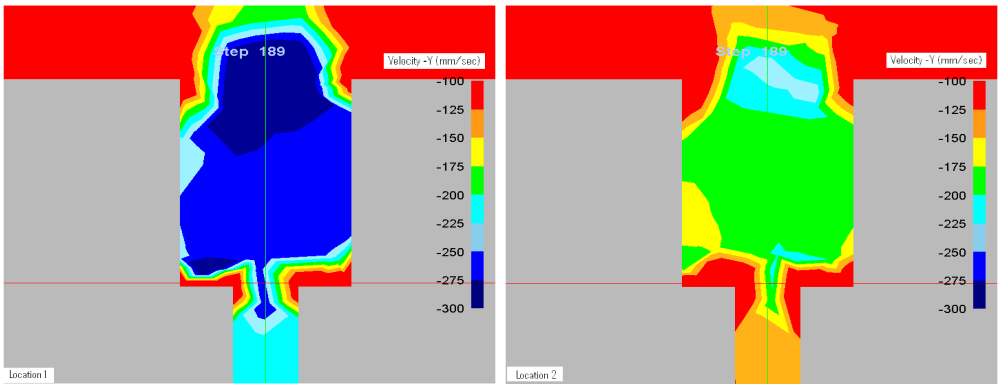

Figure 6.9: Homogeneity of flow across chamber at two different locations along channel when $r_P = 0$

channel length when the axis of the channel and axis of the die are the same ($r_P = 0$). Here it can be seen that the difference between these two are very minimal. These simulations suggest that by keeping the longer channel axis along the die axis it is possible to decrease the complexity of the problem.

6.3.2 Influence of Pocket Shape

The shape of a die pocket in practice is often a rectangle as in Figure 6.6A. Yuan *et al*[81] uses a slant shape pocket geometry during their investigation and have shown that the axial stress at the die exit can be reduced. The surface of the

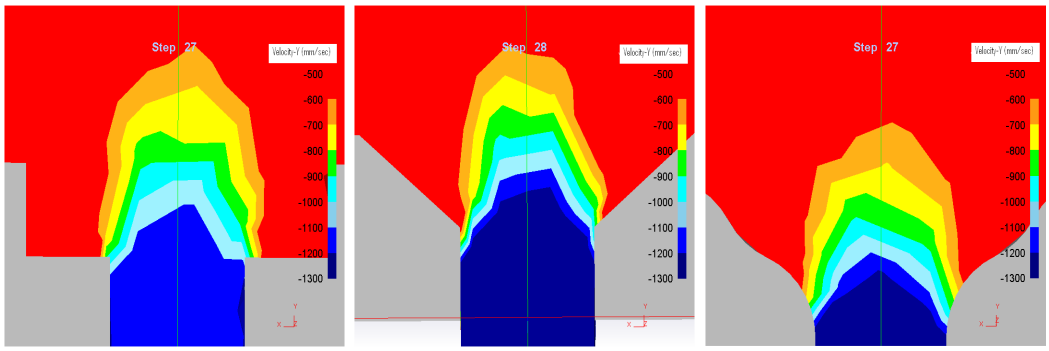

Figure 6.10: Homogeneity of flow with pocket shape: (A) rectangle,(B) slant,(C) curved

pocket can also be constructed using a series of Bezier curves. Figure 6.10 shows the homogeneity of flow for the same condition but with three different types of die. As can be seen from this figure, the homogeneity of flow with a slant pocket die is much better than a rectangular pocket die. The homogeneity of flow is even better in a Bezier curved die than a slant die.

6.3.3 Influence of Pocket Angle

It has been shown in the literature [44], [45] that there is an inverse linear relationship between pocket angle and flow velocity when $\sqrt{d^2 + w^2}$ is constant. Here it has been assumed that $w_1 = w_2 = w$. It is not possible to make a die pocket with constant $\sqrt{d^2 + w^2}$ along the length of the die channel unless the bearing length of the channel is allowed to vary along the length. Die bearing variation along the die channel may increase the tendency of surface defects at certain regions where more heat is generated from friction. In addition this will reduce the die life as well.

Therefore the die bearing length was not varied along the length. There is only the option to change d and w subject to w^2+d^2 being not constant. In order to study the effect of metal flow with different d and w values, two axis symmetry simple geometry dies with extrusion ratio 10 were considered as in Figure 6.11. DEFORM

3D was used to simulate the extrusion process. The billet material used for the investigation is Al 7575 and loaded from the DEFORM 3D database. The initial temperature of die and billet respectively are 350^oC and 400^oC. The ram speed is set as 50 mm/s. The friction coefficient is set as constant and values between $0.1 - 0.4$ have been used for various simulations. Simulations were repeated for various different entry angles and friction coefficients.

The velocity variation with pocket angle for a rectangular pocket and a slant pocket respectively are plotted in Figures 6.12A and 6.12B. As can be seen from Figure 6.12, the velocity is not linearly increasing or decreasing. In Figure 6.12B, simulation results of velocity for a slant pocket are shown for various coefficients of friction values. When the die angle increases flow will also increase but on the other hand a changing surface area will influence the flow due to the friction between die and work-piece. This surface area depends on the formation of dead metal zone for the rectangle pocket die. There won't be any dead metal zone for the slant pocket die and hence the increase of frictional contact area will be proportional to the angle. This is why it can be clearly seen that there is approximately a linear relationship between the pocket angle and corresponding velocity when the design of the pocket is slant.

6.3.4 Influence of Channel Length

In the literature [22] it has been mentioned that if the channel length is significantly long, it will result in an essential difference of flow speeds along the channel length. To investigate this effect a die as in Figure 6.13 was considered and then the extrusion flow was simulated without any pockets. The billet material used for the investigation is Al 7575, initial temperature of die and billet respectively are 400^oC and 450^oC, ram speed is set as 50 mm/s, and the friction coefficient is 0.1.

The extrusion speed at the die exit along the channel is plotted in Figure 6.16.

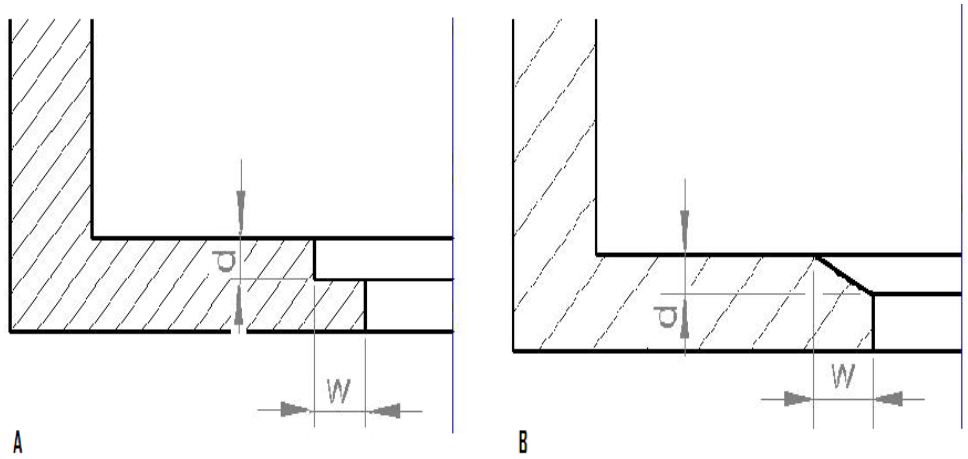

Figure 6.11: Layout of pocket geometry: (A) rectangular pocket, (B) slant pocket

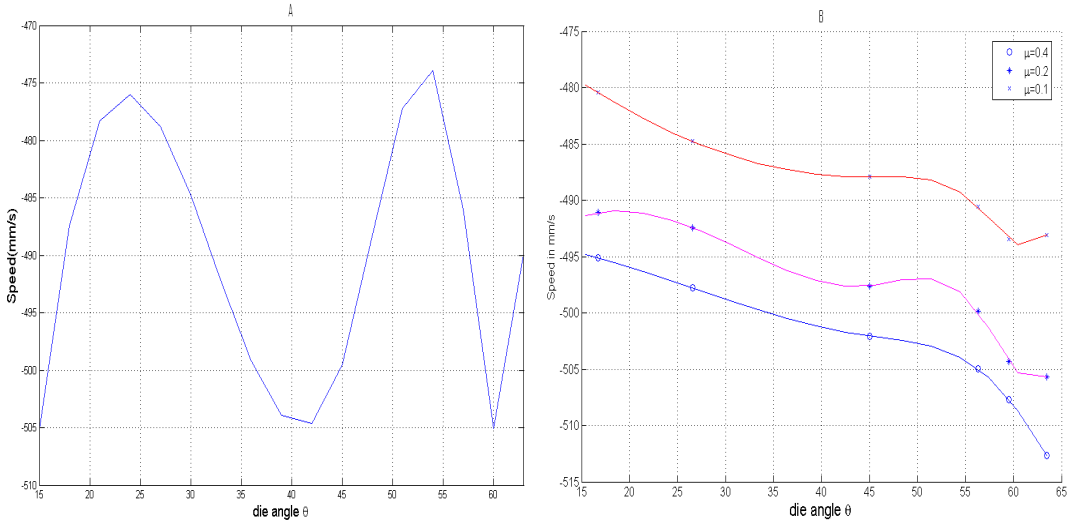

Figure 6.12: (A) Rectangular pocket, (B) Slant pocket

As can be seen from this figure (line data 1–old die), the velocity along the channel length tends to vary when the channel is reasonably long. This might be because the metal away from the die axis tend to flow more slowly as a result of a billet-die interface friction.

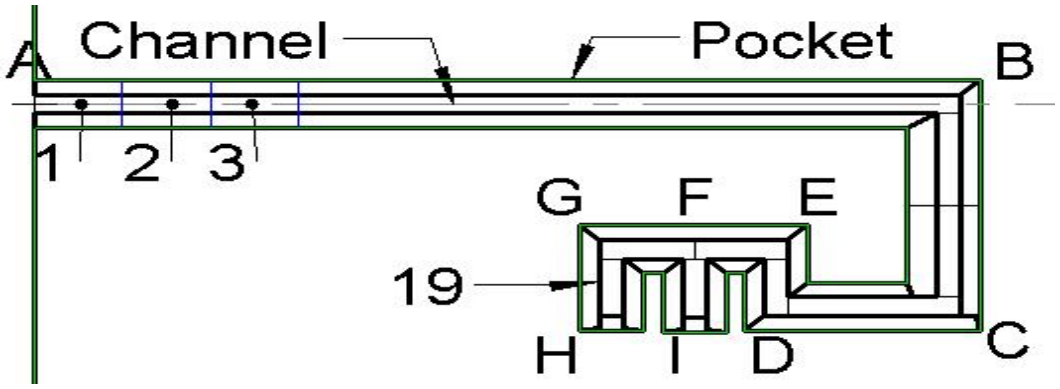

Figure 6.13: Sample die with extrusion ratio 1:51

6.4 Proposed Optimization Algorithms

From our investigation it has been found that (1) if the length of the channel is large, it results in a great difference of flow speed along the length of channel; (2) if the width ratio of the pocket at each side of a channel is not optimum, it will result in a non homogeneous velocity distribution across the die width. Further the width closer to the axis should be smaller than the width which is away from the die axis. If the channel is symmetrical about the die axis, an equal pocket width at each side will lead to a homogeneous velocity distribution across the width along the channel.

The novel concept of this research is to determine the optimal geometry of the pocket to achieve homogenous metal flow in terms of speed, temperature and shear stress distribution inside the forming zone to extrude a product with the geometry given in Figure 6.2. To deal with these problems two algorithms have been developed to determine the best geometry of the pocket.

6.4.1 Algorithm -1

The solution is arrived at through three steps. In the first step, the channel was divided into n elements as shown in Figure 6.13 and the flow velocity across each

element was found when the width of each pocket is zero.

In the second step, width sizes used in each element are not the same. Simulations have been done with the width of the first element equal zero and the widths of all other elements are equal but greater than zero. The value of width has been changed (say w_2) until the velocity across elements 1 and 2 are approximately equal. Then the widths of elements 1 and 2 respectively were kept as zero and w_2 and all other elements were kept equal to a constant value (say w_3) which is greater than w_2. The value of w_3 was altered until the velocity across elements 1, 2 and 3 were approximately equal. This procedure was continued until an appropriate pocket width for all elements was found.

In the third and final step, the outer boundary of each element was smoothed by joining mid points of the outer boundary of each element with a spline. Then the simulations were done by moving the outer boundary of the pocket away from the channel center until the velocity variation across the channel is within a tolerance level.

This procedure is computationally very expensive. In a real situation die designers have to complete their work within 2-3 days. Therefore algorithm 2 has been developed.

6.4.2 Algorithm -2

It has been already demonstrated that there is a near linear relationship between pocket angle and flow velocity. Therefore the simulation was done for a sequence of only 3 or 4 $w-$ values and then linear regression was used to estimate the appropriate w value which gives a certain exit velocity for either side of each element.

In this section, an algorithm was built as a faster alternative to the above method. The inspiration behind this algorithm is based on observations shown in Figure 6.12B. In the first step, after dividing a channel into n elements, at least

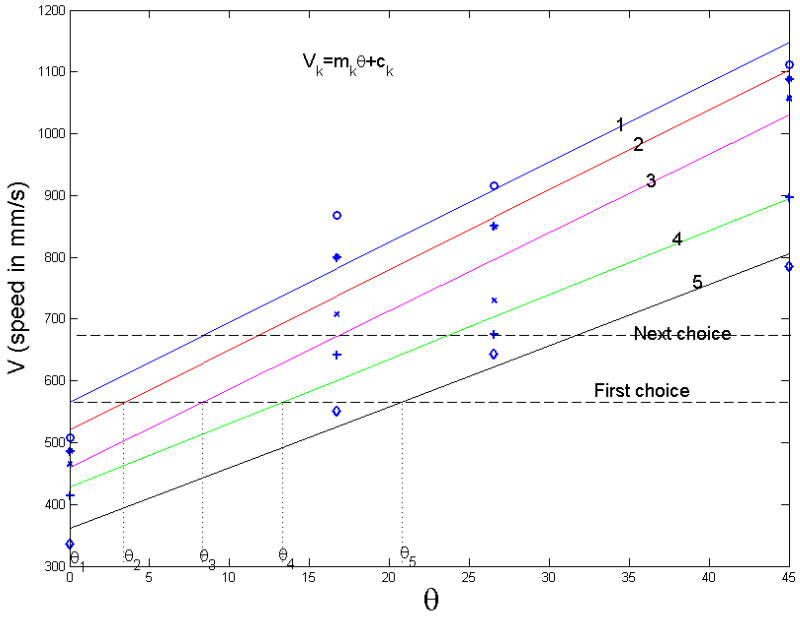

Figure 6.14: Velocity variation with angle θ

three simulations were done with different pocket widths but every element has equal width value and the flow velocity across each element was noted.

In the second step, each element's velocity is changed with w (or θ) which is obtained from the first step to calculate m and C of equation $v = m\theta + C$ by using linear regression as in Figure 6.14. Then for each element respective θ values have been picked for which their velocity is equal to the velocity of the first element.

In the third step, the outer boundary of a pocket was formed by joining mid points of the outer boundary of each element for the respective θ (or w) values with a spline. This process was repeated (step 2 and 3) for various different velocities of the first element until the velocity variation along the channel is minimum. Two of many choices are shown in Figure 6.14 as first choice as well a next choice and their pocket geometries are shown in Figure 6.15.

The shape of the orifices of both dies (selection 1 and 2) are exactly the same

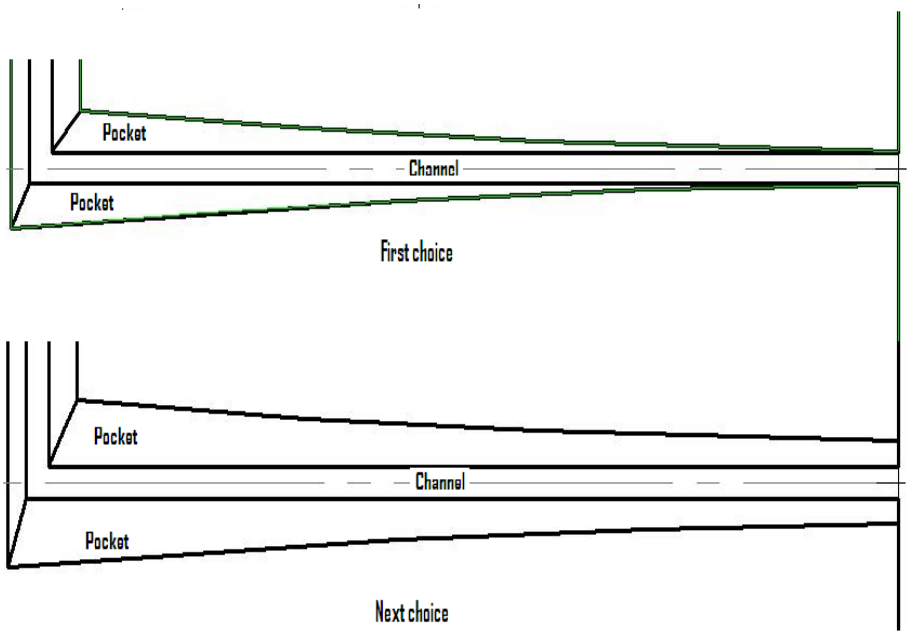

Figure 6.15: Pocket geometries for first and next choice

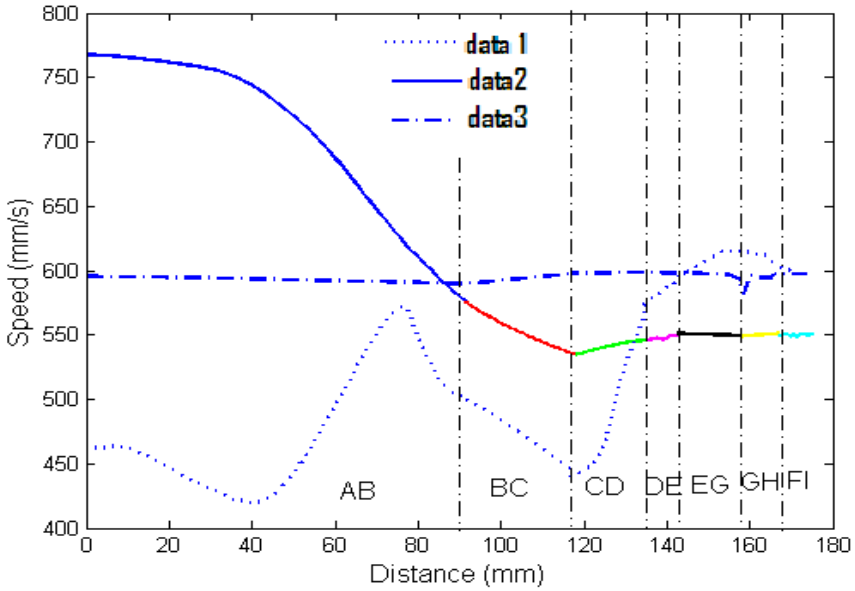

Figure 6.16: Velocity distribution of the extrudate through original die, optimal pocket die and die with no pocket: data 1- old die, data 2- without pocket, data 3- optimal die

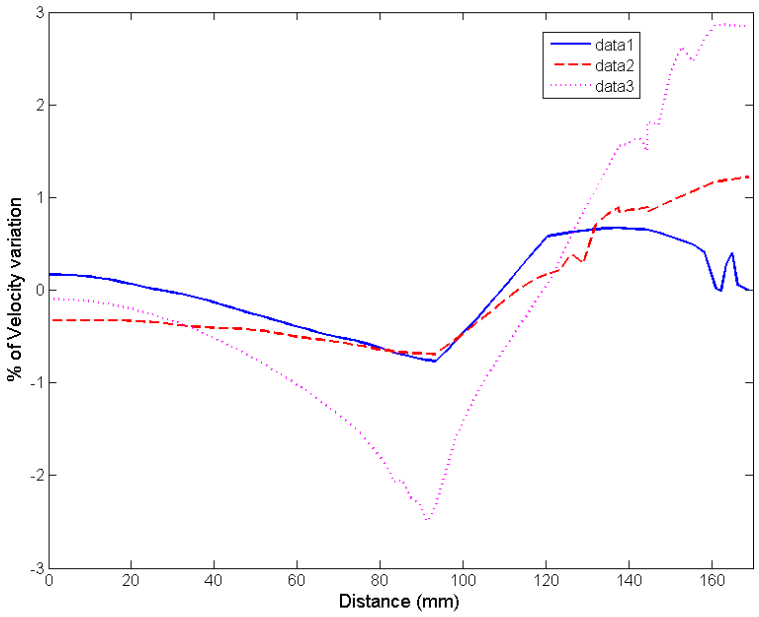

Figure 6.17: Relative comparison of velocity variation along the die channel with optimal pocket geometry for different process conditions ($v = 25,\ 50$ and $T = 400^oC,\ 450^oC$)

but the pocket area of selection 2 is larger than that of selection 1. This is especially obvious at the half symmetry line of the dies. The pocket width of die 1 (selection 1) at the half symmetry line is zero and the width of die 2 (selection 2) at the half symmetry line has a certain dimension. The greater value for the width is a result of minimising the velocity variation along the channel.

Figure 6.16 shows the velocity at just outside the die exit along the channel length for the optimal die together with the die without pocket and the original die.

A comparison of the relative variation for the optimal die geometry with different process conditions are shown in Figure 6.17. In the figure data 1 is obtained when the ram speed is 25 mm/s, the initial billet is 400^oC, data 2 is obtained when the ram speed is 50 mm/s, the initial billet is 400^oC, and data 3 is obtained when the

ram speed is 25 mm/s, and the initial billet is 450^oC. Based on these observations it can be said that the initial temperature is slightly more sensitive to the geometry than the ram speed, although the overall variation from the optimum value is small. Figures 6.18-6.19 depict the velocity, temperature and shear stress distribution of the extruded product of material AA7075 between the entrance and exit of an optimal die for different initial temperatures. Figure 6.20 depicts the velocity, temperature and shear stress for the material AA6061. These figures show that the velocity distributions at the die exit is approximately constant and temperature variation along the channel is very small compared to Figure 6.3. Shear stress just inside the die exit is also reduced. These figures also demonstrate an optimal die is invariant to material variations. The optimal die geometry is shown in Figure 6.21A. For the comparison purposes the original die geometry also shown in Figure 6.21B. There are number of differences between the original pocket geometry and optimal pocket geometry. It can be seen very clearly seen in the figure. Firstly the optimal die pocket walls are not vertical. Secondly the pocket cross sectional area increases from die centre to edge.

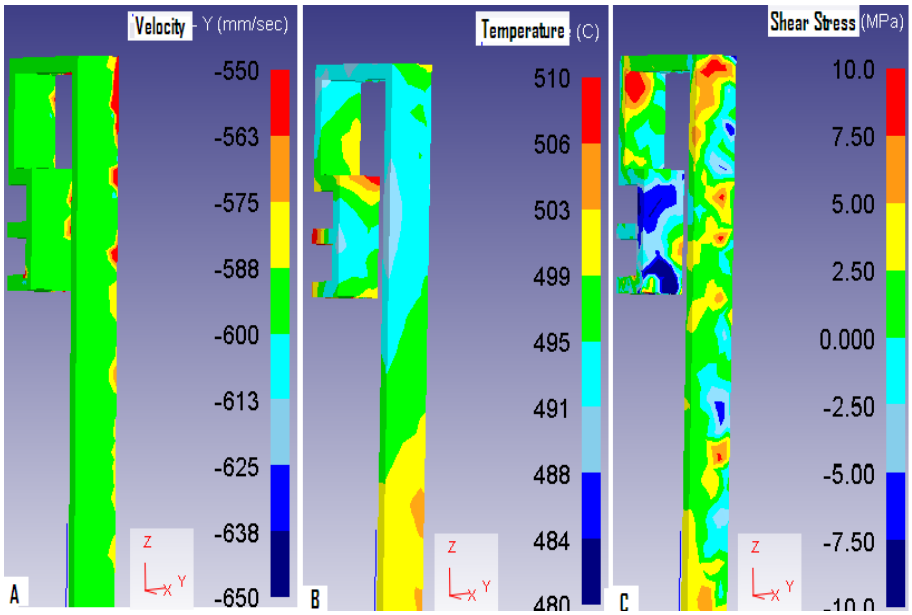

Figure 6.18: (A) Velocity, (B) Temperature, (C) Shear stress distributions of material AA7075: when ram speed 25 mm/s, initial temperature 400^oC.

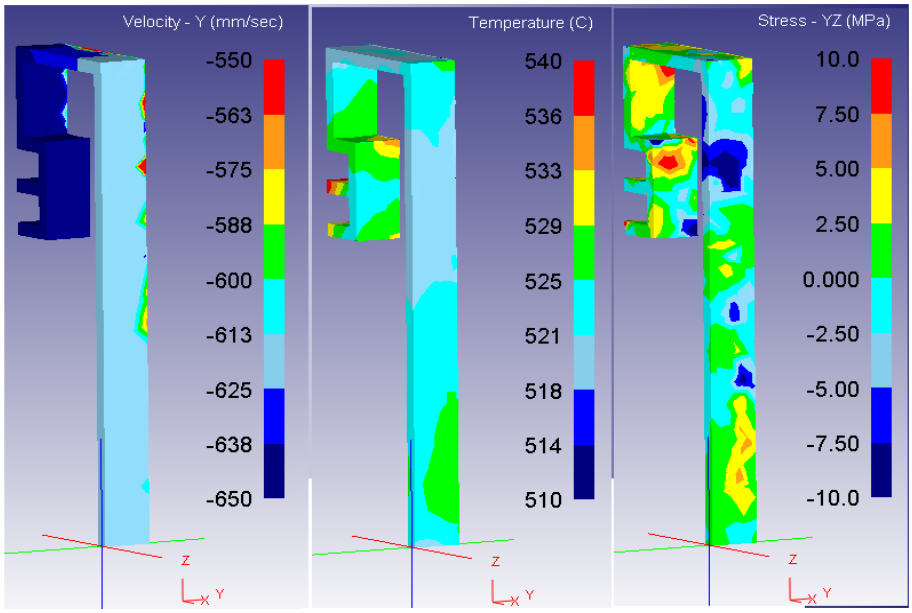

Figure 6.19: Optimal pocket: (A)velocity, (B) temperature, (C) shear stress distributions of material AA7075: when ram speed 25 mm/s, initial temperature 450^oC.

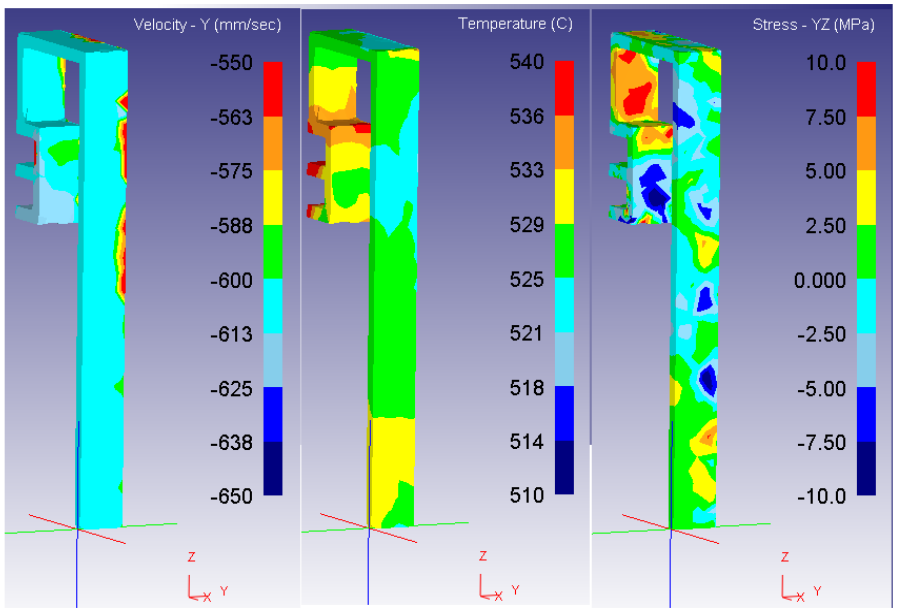

Figure 6.20: Optimal pocket: (A)velocity, (B) temperature, (C) shear stress distributions of material AA6061: when ram speed 25 mm/s, initial temperature 450^oC.

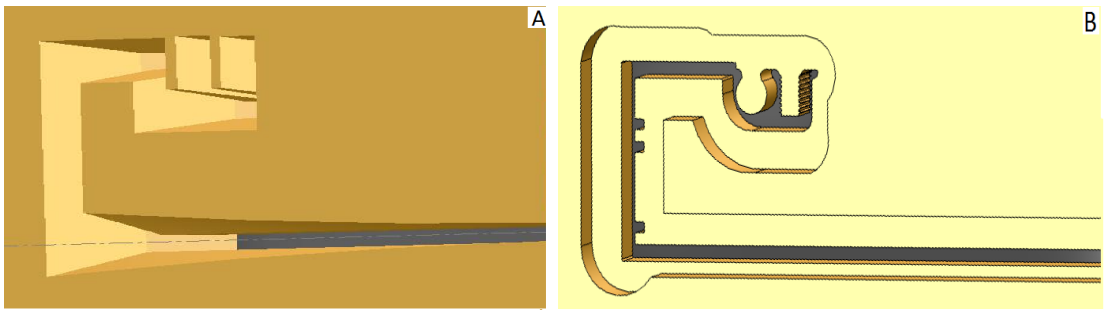

Figure 6.21: Pocket geometry: (A) Optimal, (B) Original.

6.5 Die with Feeder (or Welding) Chamber

A feeder chamber is introduced in front of extrusion dies mainly

(a) to produce a shape larger than the billet diameter,

(b) to allow continuous extrusion,

(c) to pre–form as well as equalize the material flow in front of the die aperture,

and

(d) to spread the material flow [4].

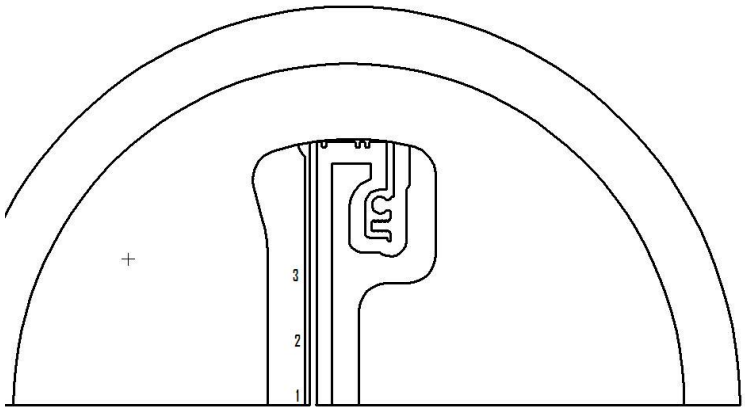

Figure 6.22: Die with feeder chamber

The geometry of the die with feeder chamber considered for the investigation is shown in Figure 6.22. The cross section of the feeder chamber is not very thin and therefore the velocity across the surface is approximately constant everywhere. Just before entering the die opening the aluminium inside the feeder chamber looks like a slab of feeder chamber shape.

Figures 6.23 shows the velocity, temperature and shear stress distribution of the extruded product between the entrance and exit of a die for the geometrical set unit shown in Figure 6.22. It can be seen that the shear stress is very high at certain positions and the velocity is not homogeneous. Figure 6.24 shows the homogeneity of flow at three different locations(1, 2 and 3 as in Figure 6.22) along the longer channel length. In this figure the flow patterns at the forming zone are not all

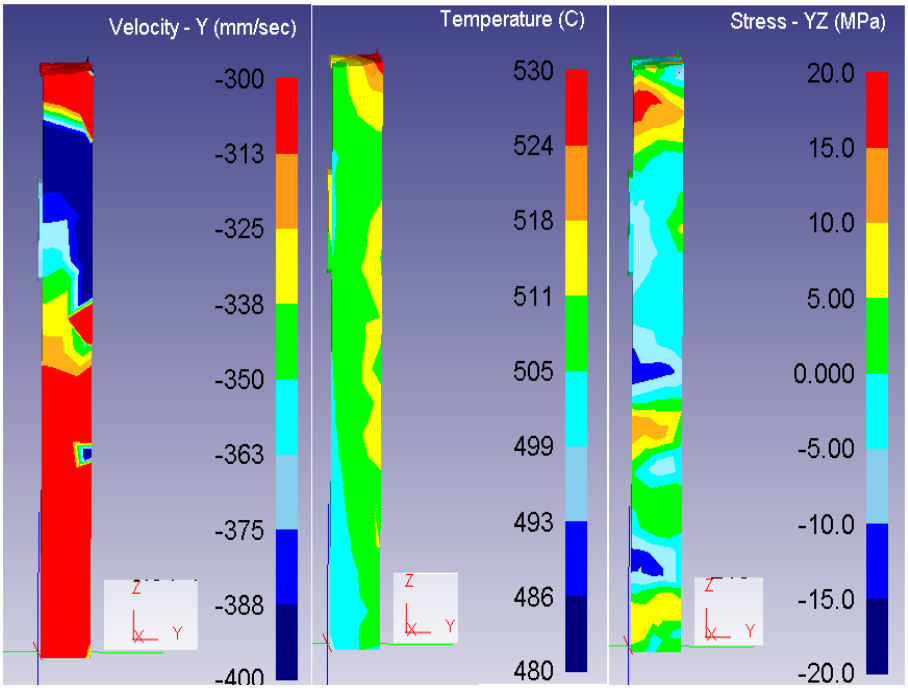

Figure 6.23: (A) Velocity, (B) Temperature, and (C) Shear stress inside the die land

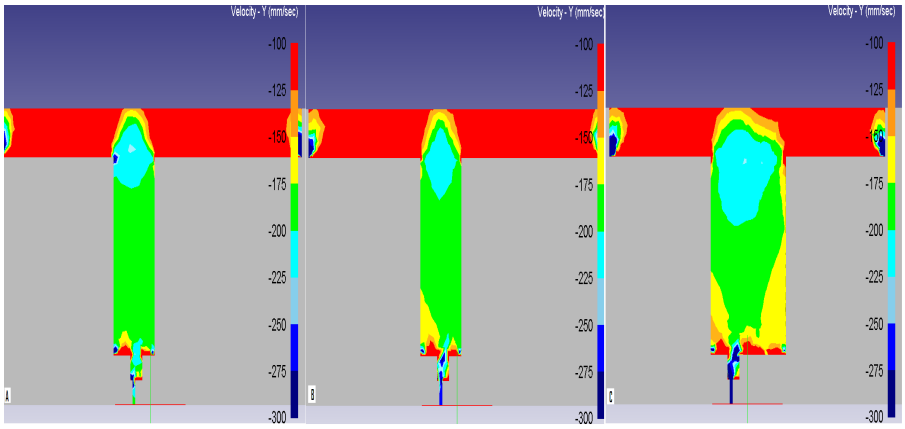

Figure 6.24: Velocity distribution at two different locations along the die channel, cut plane XY: (A) location 1, (B) location 2 , (C) location 3 of Figure 6.22

homogeneous and indicate that the ratio of $w_1 : w_2$ is not optimal to produce a homogeneous flow. Further it has been found that the location of the higher shear stress area is not the same for other simulation runs with different initial billet

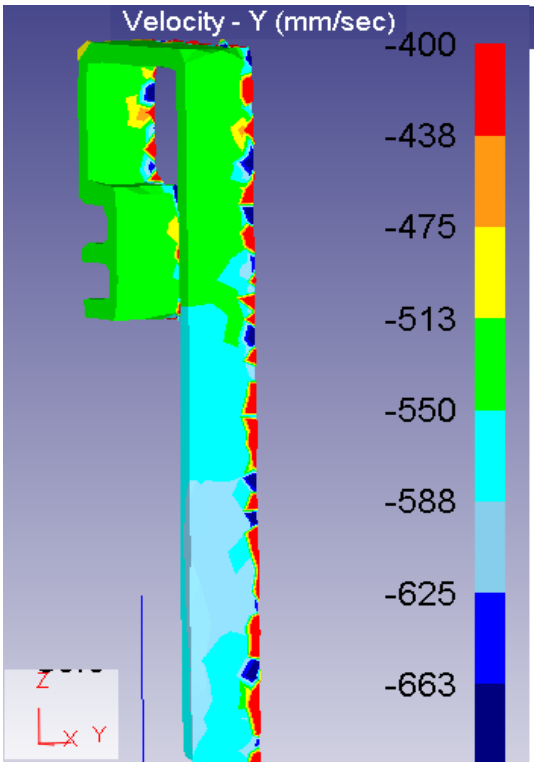

Figure 6.25: Velocity distribution along the die channel without pocket

temperatures and ram speeds. Figure 6.25 shows the velocity distribution inside the die land region for the die without pocket. Here it can be seen that even if the channel length is significantly long, it did not result in such a big difference of flow speeds along the channel length as in Figure 6.16 for the same die without feeder chamber.

In the previous sections it has been already demonstrated that the homogeneity of flow with a slant pocket die is much better than a rectangular pocket die and therefore an investigation was conducted with a slant pocket and a procedure was developed to determine the best possible geometry of a pocket to regulate the flow through a die.

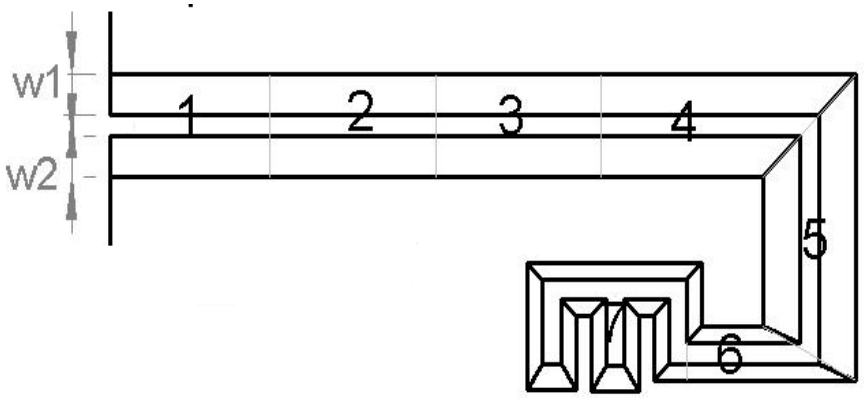

Figure 6.26: Sample die 2

6.5.1 Algorithm -3

The procedure consists of two steps. In the first step, the channel was divided into 7 elements as shown in Figure 6.26. Since the velocity variation along the longer channel is not very large compared to algorithm 1 and algorithm 2, only 4 elements along the longer channel were considered to save computation time. For each element the optimal ratio $w1 : w2$ for well balanced flow is calculated by running at least three simulations for various different $w1$ values for a fixed $w2$ value (or for various different $w2$ values for fixed $w1$ value). One such example is shown in Figure 6.27. In this figure A, B, C and D respectively show the flow velocity at either sides of elements 1, 2, 3 and 4.

In the second step, actual optimal values of $w1$ and $w2$ are calculated. It is done by maintaining the same ratio obtained at step 1 for each element and running simulations for various different $w1$ and $w2$ values until the velocity of flow across each of seven elements are approximately the same. The algorithm consists of the following steps:

1. Initialisation

   (a) choose pocket depth d, bearing length b and one width $w1$;

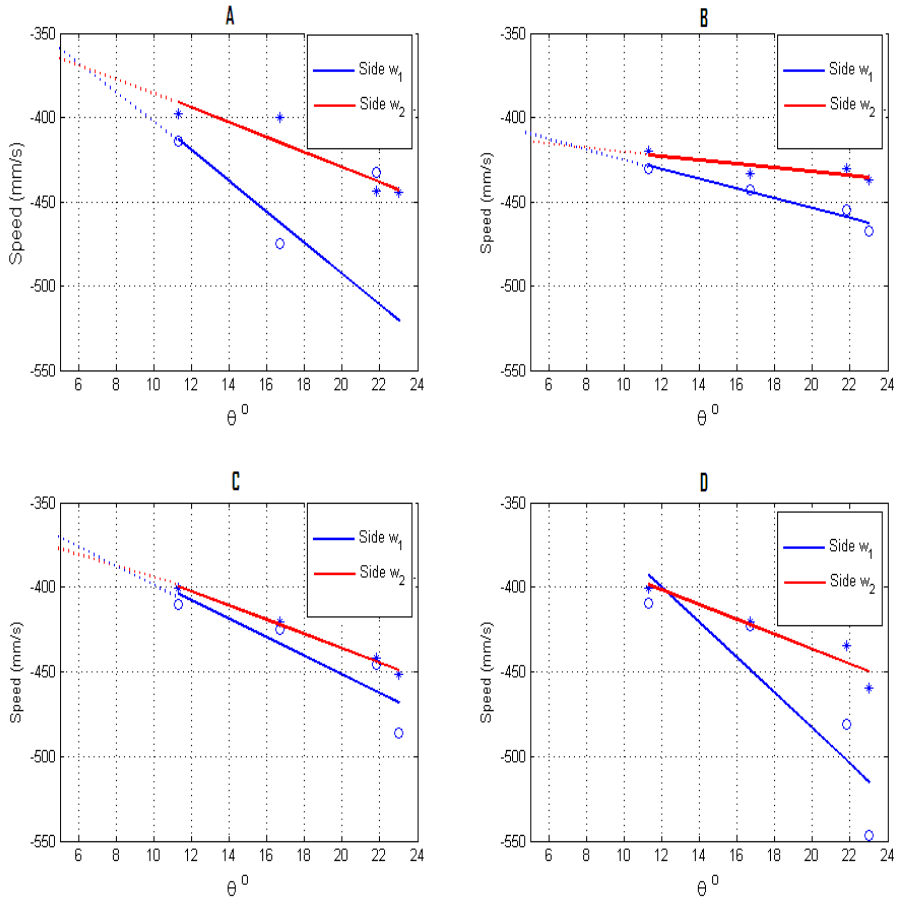

Figure 6.27: Step 1 of Algorithm 3

(b) number of elements to be considered N.

(c) Initialize an array **w2** of different $w2$ values with length of at least 3.

2. Calculate optimal ratio $r = w1 : w2$ for each element for which the velocity across either side of the elements is equal.

(a) for $i = 1 \ldots 3$

- $w2 = \mathbf{w2}(i)$
- Run simulation and store velocity across either side of each element.

(b) Use linear regression to estimate the slope $\mathbf{m}[1 : N]$ of flow velocity vs $w2$ for each element.

(c) Estimate $w2$ for each element such that the velocity $\mathbf{V}[1:N]$ across either side of element is equal.

3. (a) $Vave = \dfrac{\sum \mathbf{V}[1:N]}{N}; \quad w1 = rw_2$

   (b) for $i = 1:N$

   - if $\mathbf{V}[i] - Vave > tol$
     - $\mathbf{w2}[i] = \mathbf{w2}[i] - \delta$
   - else if $\mathbf{V}[i] - Vave < tol$
     - $\mathbf{w2}[i] = \mathbf{w2}[i] + \delta$

4. Go to step 3 if $\|\mathbf{V} - Vave\| > 0$ else Stop.

Figure 6.28 depicts the comparison of the shear stress distribution of the extruded product of material AA7075 between the entrance and exit of an optimal die and the original die. It can be seen that the shear stress distribution just outside the forming zone has been reduced dramatically. The optimal die is shown in Figure 6.29.

6.6 Summary and Discussion

The goal of the work presented here is to identify the design and process parameters which are more important for surface quality and to develop a suitable technique to modify a die to minimize surface defects. It is an inverse problem and solved by a finite element model and linear regression. In the process, three different algorithms were developed, and applied to test cases.

A series of examples describes how the homogeneity of flow depends on the geometry of the die pocket, and how the process parameters such as initial temperature and ram speed influence the homogeneity of flow through a die which is optimal for certain values of process parameters. The results from these examples

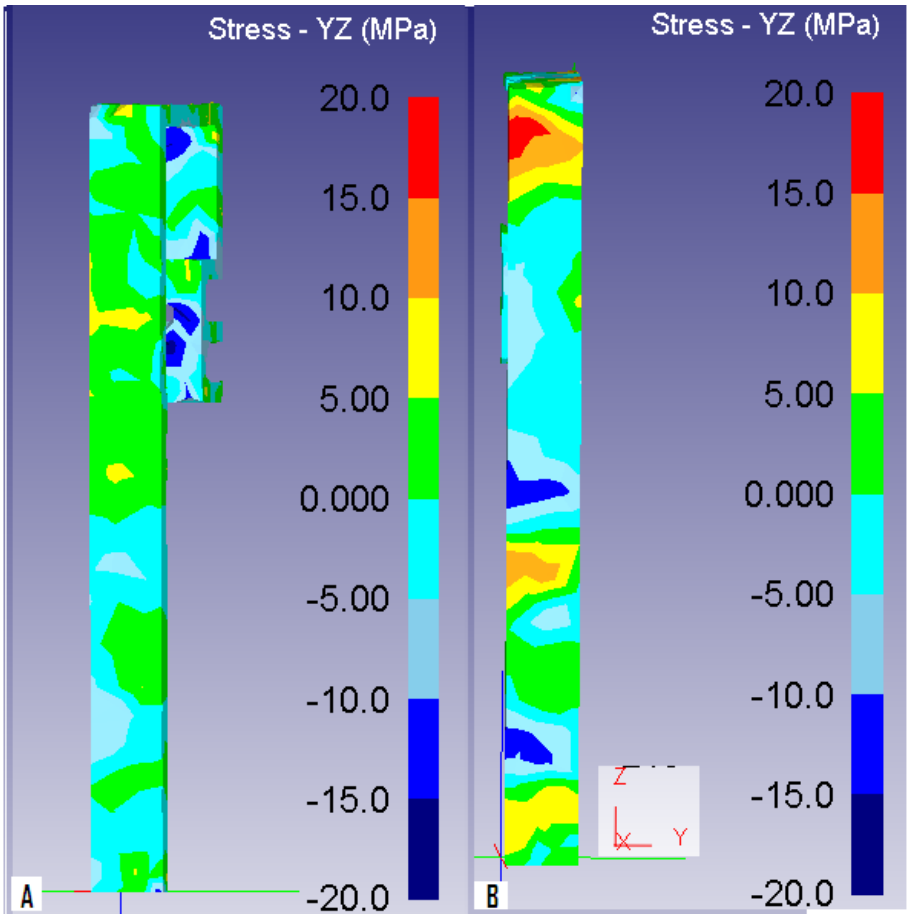

Figure 6.28: Shear stress distribution: (A) optimal die, (B) original die

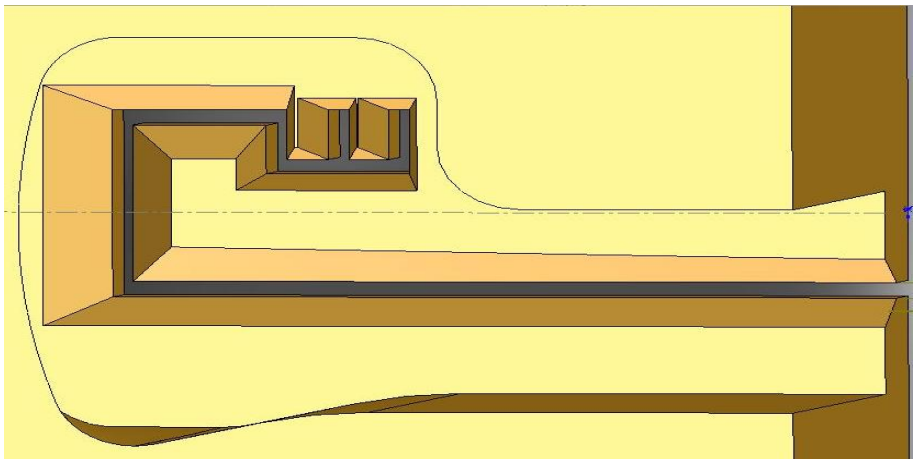

Figure 6.29: Optimal die 2

suggest that the presented algorithms are capable of minimizing the velocity, temperature and shear stress variation along the channel. Four factors which can be used to alter the homogeneity of the flow are:

(i) initial temperature of billet,

(ii) channel length,

(iii) distance between die axis and channel axis, and

(iv) shape of the pocket.

From observations it can be noticed that the major factor that influences the flow is the pocket geometry. Therefore it can be concluded that the surface quality of the product can be optimised by designing a pocket suitable for the respective process conditions.

Chapter 7

Comparison with Experimental data

7.1 Experimental Trial

Experimental trials at an industrial plant were organised and conducted. This chapter describes the equipment, trial procedure and sample preparation as well as evaluation. For verification purposes a die optimized according to the design algorithms mentioned in previous chapters has subsequently been manufactured and run in a production extrusion press. The aim was to establish whether the optimised die design delivers a high quality product free of flow lines on the flat surface.

A billet being loaded in the extrusion press is shown in Figure 7.1. The billet is a cylindrical shape of cast metal which is pushed through a die to extrude desired shapes of uniform cross section. In this experimental investigation AA6061 alloy which has a magnesium concentration of 0.40% was used. Before extrusion the billet was preheated to 470^oC by loading it into a preheating furnace for 40 minutes.

Figure 7-2 shows the extrusion profile extruding from the die exit. After extrud-

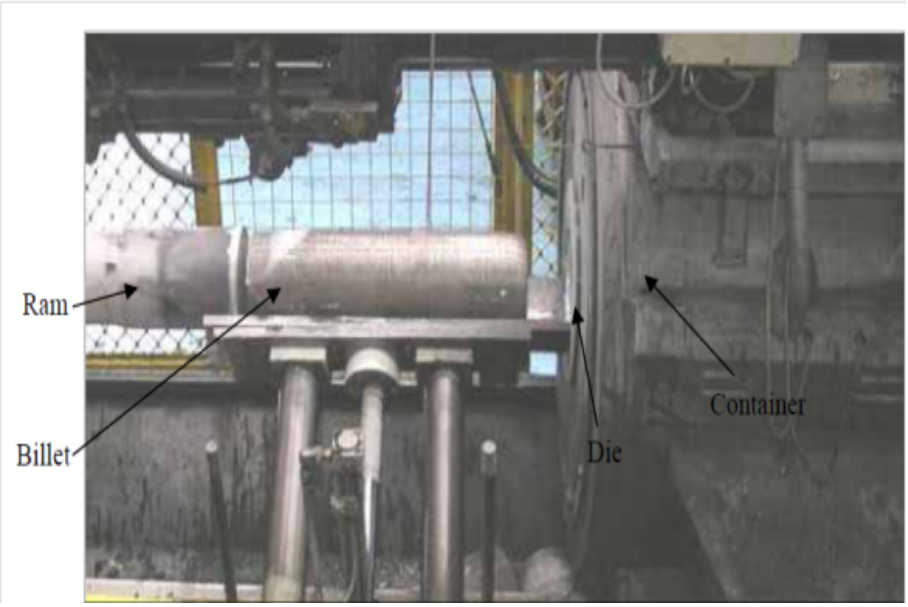

Figure 7.1: Cylindrical billet at the extrusion press.

Figure 7.2: Extrusion at the plant.

ing the part is clamped at either end lengthwise and a horizontal force is applied to straighten it.

7.2 Investigation of Product Surface

Figure 7.3, and 7. 4 respectively show the photograph of the actual newly produced part and the original old part. It can be seen with the naked eye that the usual die lines appear and some slight streaks are also visible in the direction of the material flow in the old and new part, although they are far less pronounced with the new design. Streaks are differentiated by differences in the glossy appearance from their surrounding surfaces. The surface gloss of materials is judged to be the amount of incident light that is reflected at the specular reflectance angle of that surface. The specular gloss is proportional to the reflectance of the surface. Materials with smooth surfaces appear glossy and rough surfaces appear matte. All these are dependent on the microstructure of the surface and any extent of flow-lines can only be confirmed through micrographs.

Figure 7.3: Photograph of the newly produced part

Figure 7.4: Photograph of the original part.

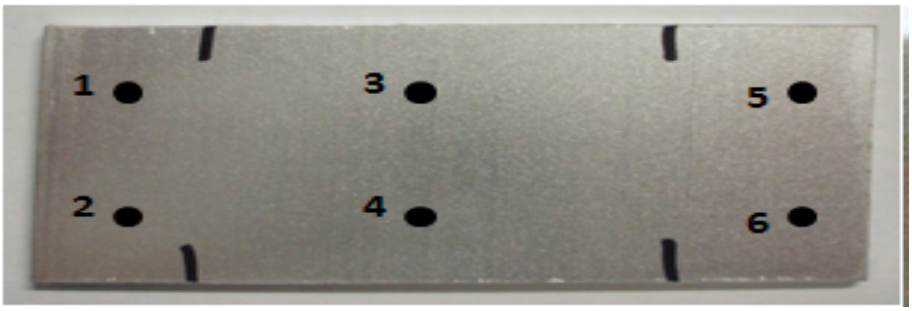

Figure 7.5: Photograph of the newly produced part (which was etched for 20 min).

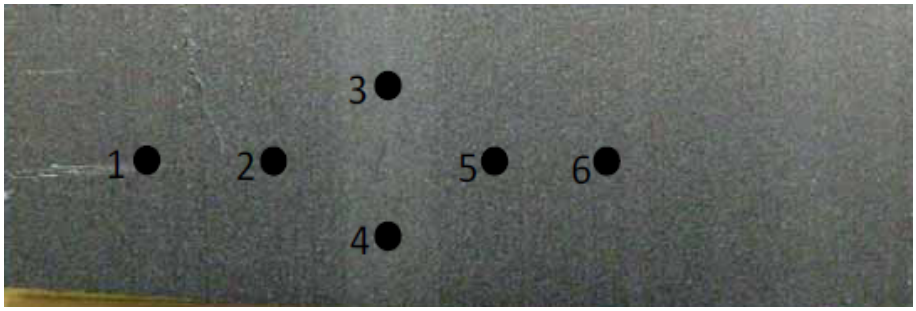

Figure 7.6: Photograph of the original part (which was etched for 17.5 min).

The next step of the examination is to find whether any grain size differences exist in and out of the streak region. To examine that the surfaces of the extruded samples had been etched for 5–20 minutes in a 10 % sodium hydroxide solution and then their microstructure was analyzed with a scanning electron microscope (SEM). Figure 7.5 and 7.6 respectively show the surfaces of samples given in figure 7.3 and 7.4 after etching with a sodium hydroxide solution. Samples considered of each piece are labelled from 1 to 6 as shown in the figures 7.7-7.11 at 300X and 1000X magnification. In Figure 7.7, the areas 3 and 4 were judged as being the most streaky ones, while areas 1 and 2 on the left hand side as well as areas 5 and 6 on the right hand side were seen as streak free surfaces.

The SEM pictures underneath reveal that the surface topography varied in and out of the streak region in terms of surface matteness. The difference in mi-

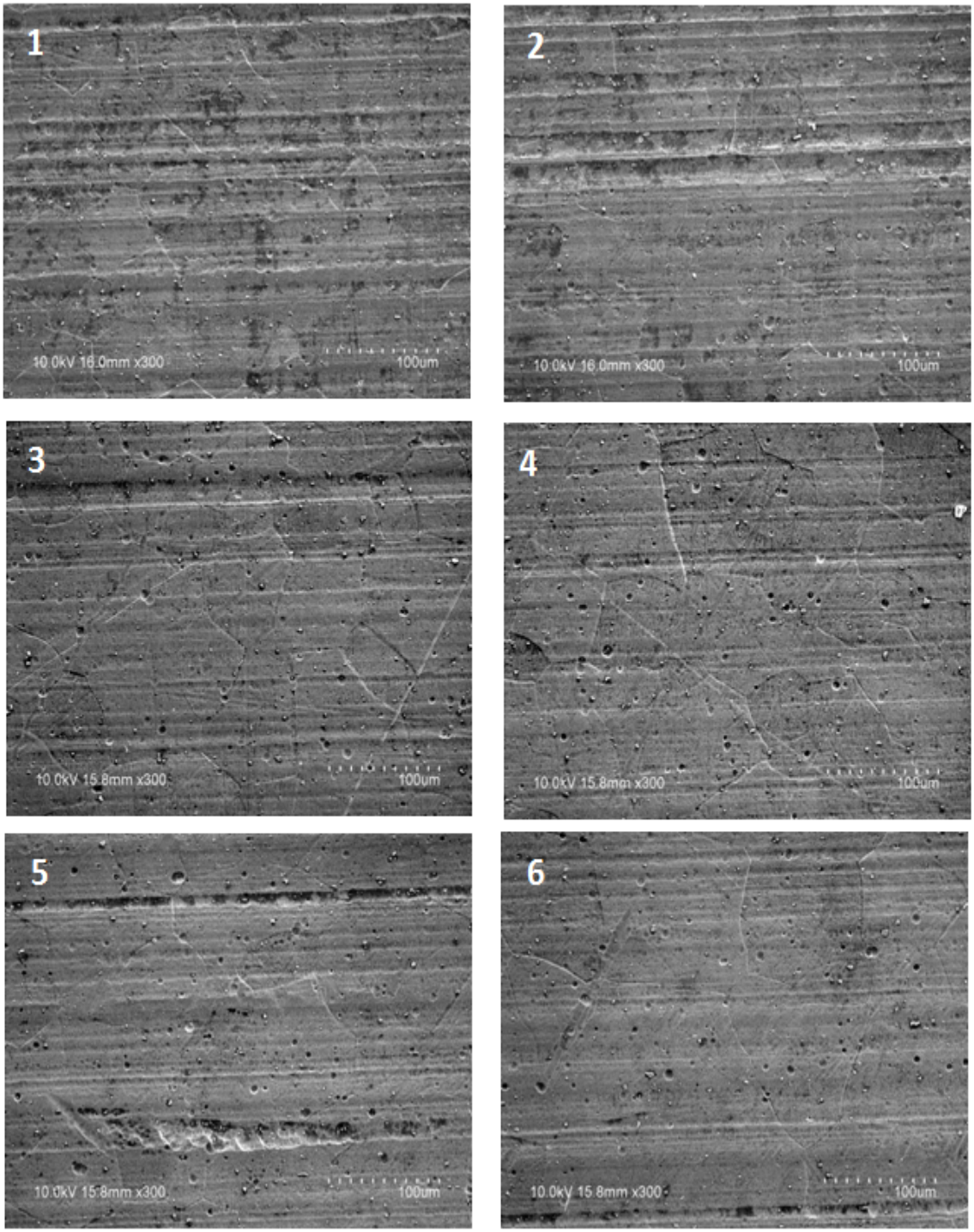

Figure 7.7: New product: SEM images taken from six fields of view on the surface at 300X magnification. (5 minute etching in 10% Sodium Hydroxide).

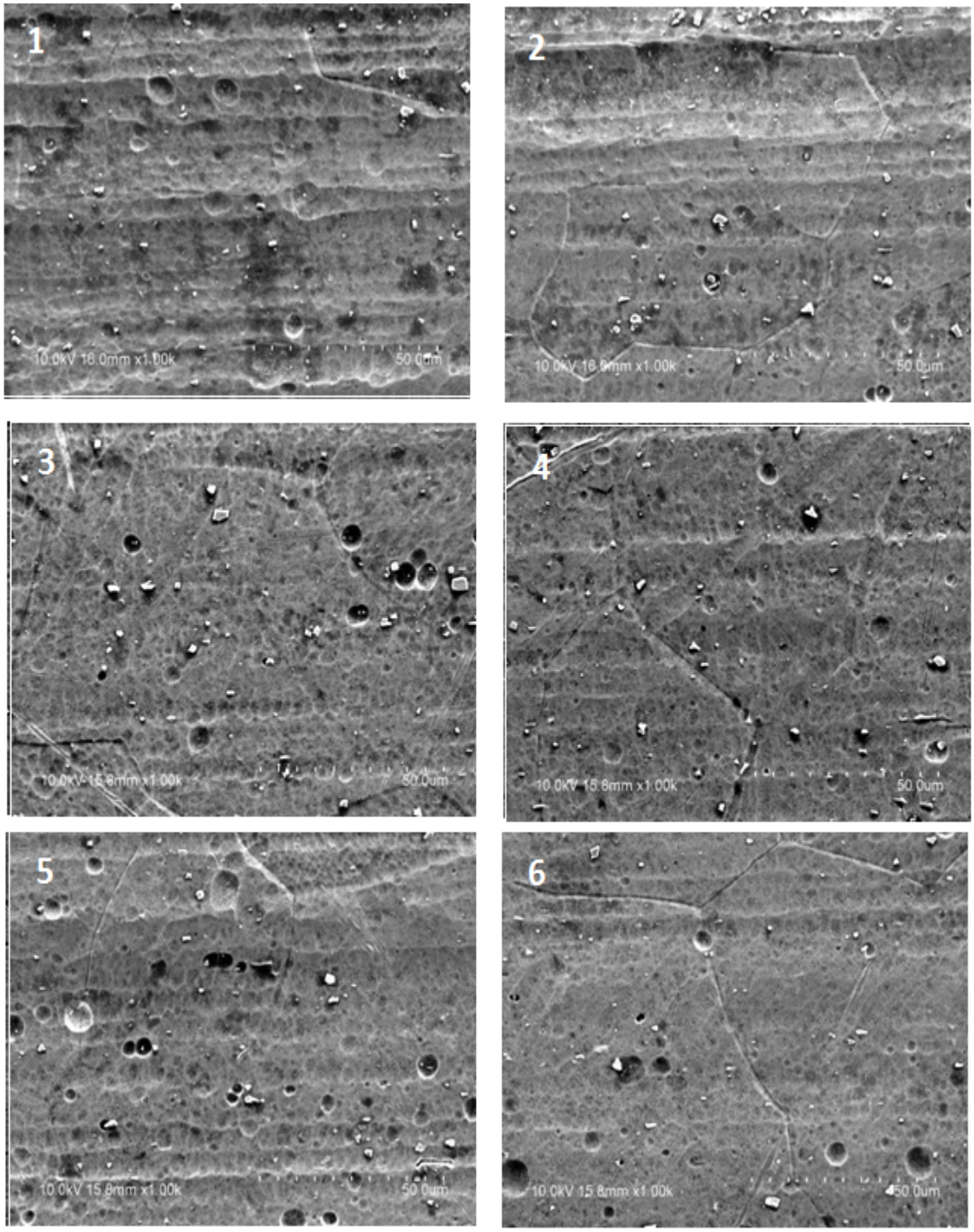

Figure 7.8: New product: SEM images taken from six fields of view on the surface at 1000X magnification. (5 minute etching in 10% Sodium Hydroxide).

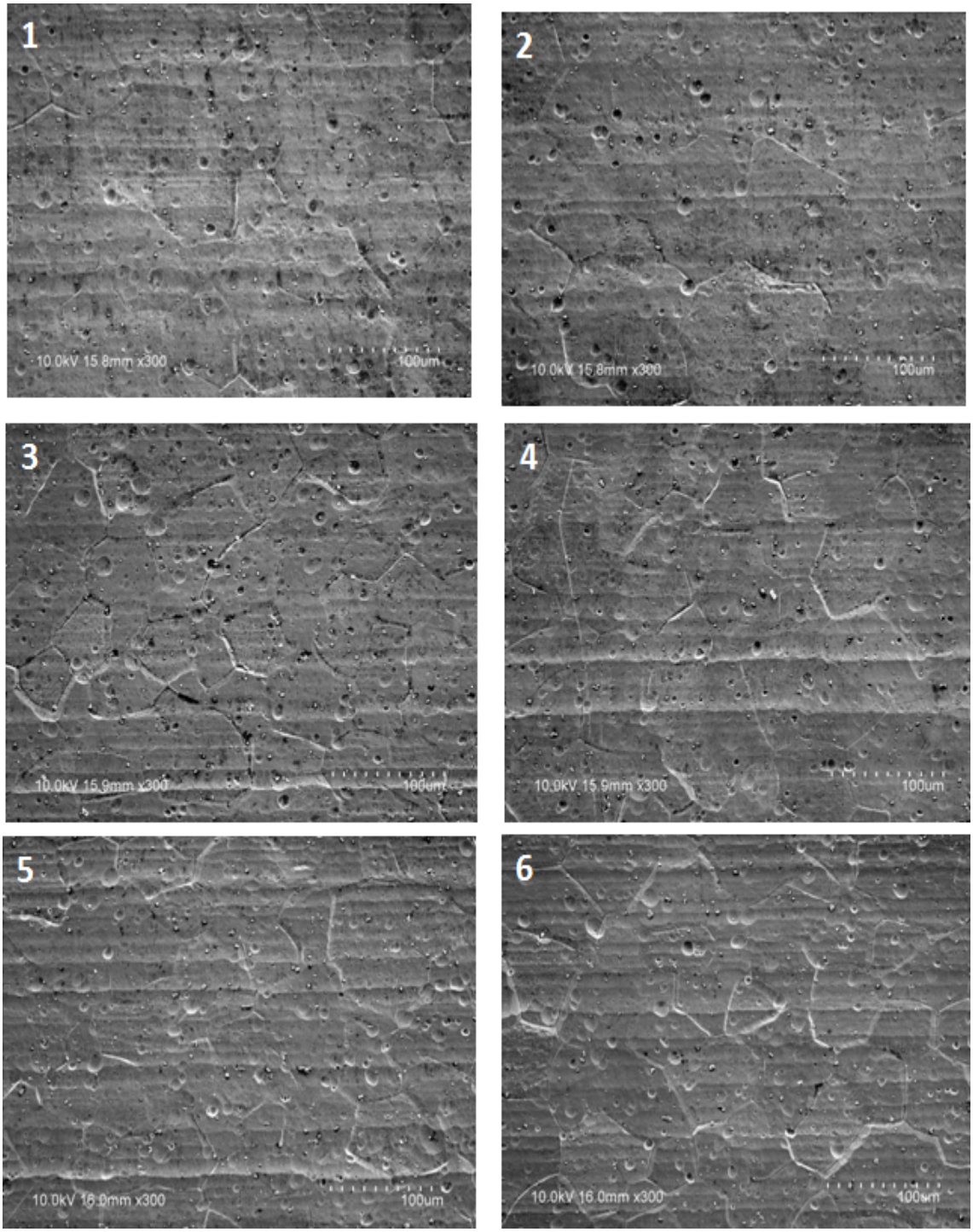

Figure 7.9: New product: SEM images taken from six fields of view on the surface at 300X magnification. (20 minutes etching in 10% Sodium Hydroxide).

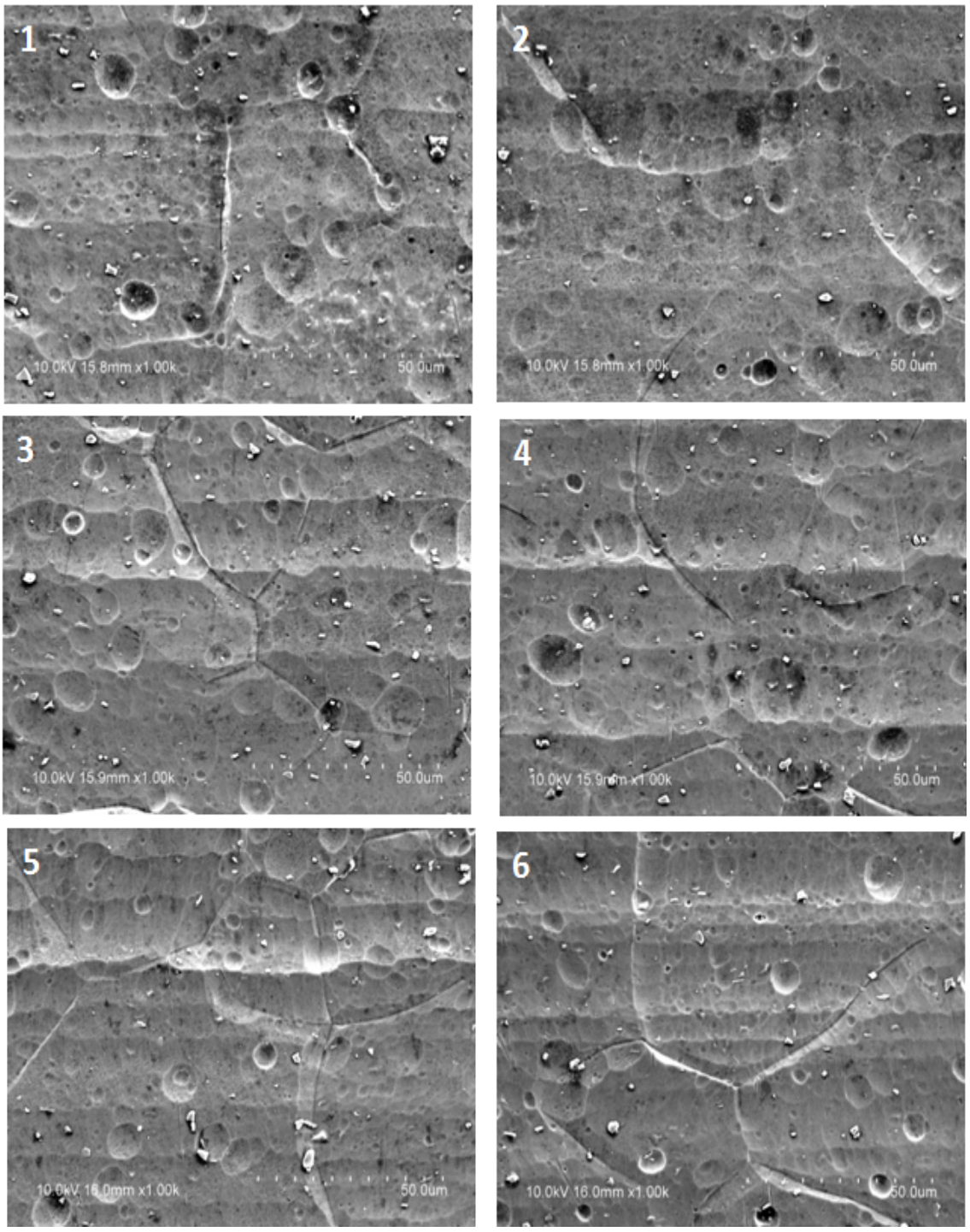

Figure 7.10: New product: SEM images taken from six fields of view on the surface at 1000X magnification. (20 minutes etching in 10% Sodium Hydroxide).

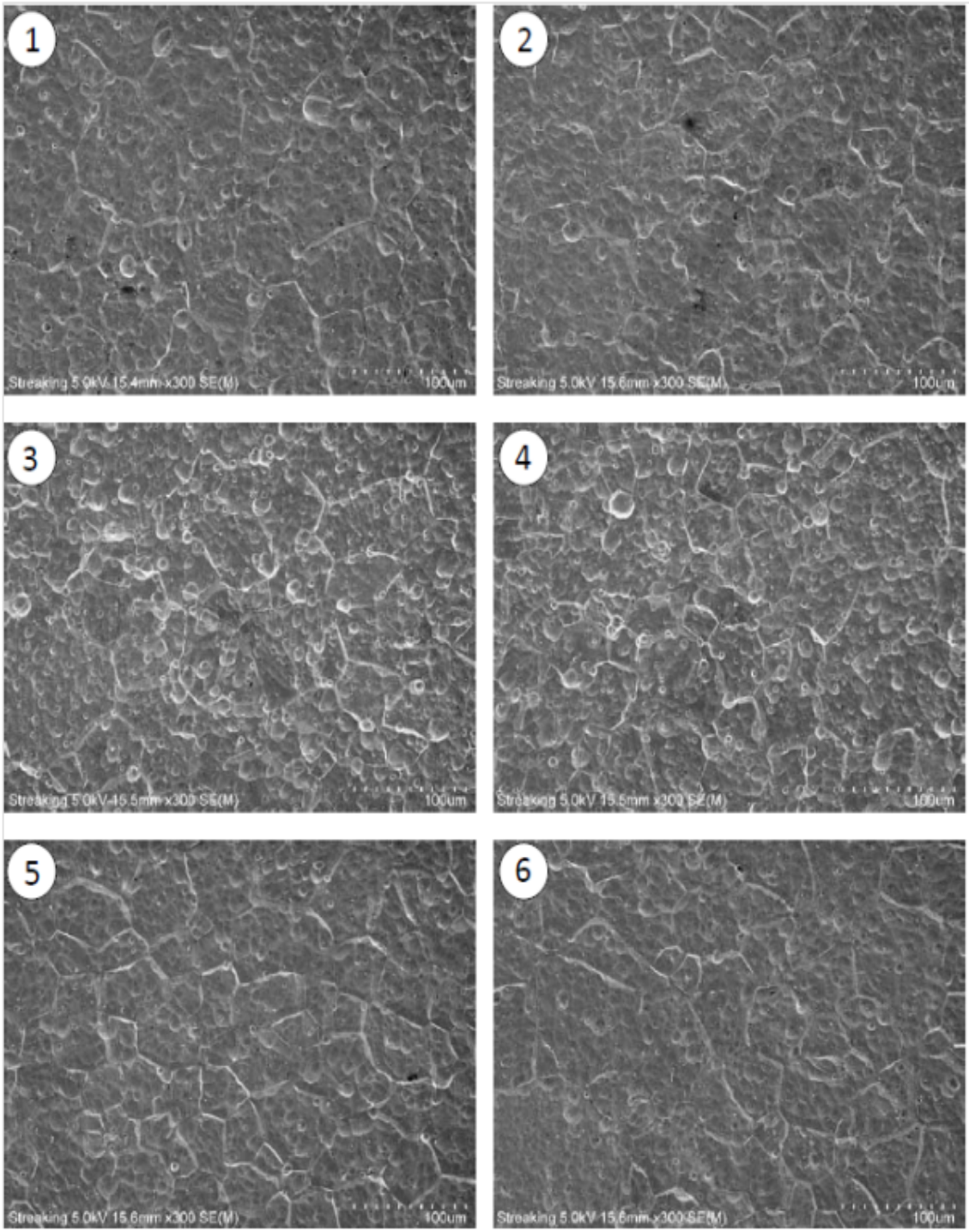

Figure 7.11: Original product: SEM images taken from six fields of view on the surface at 300X magnification.

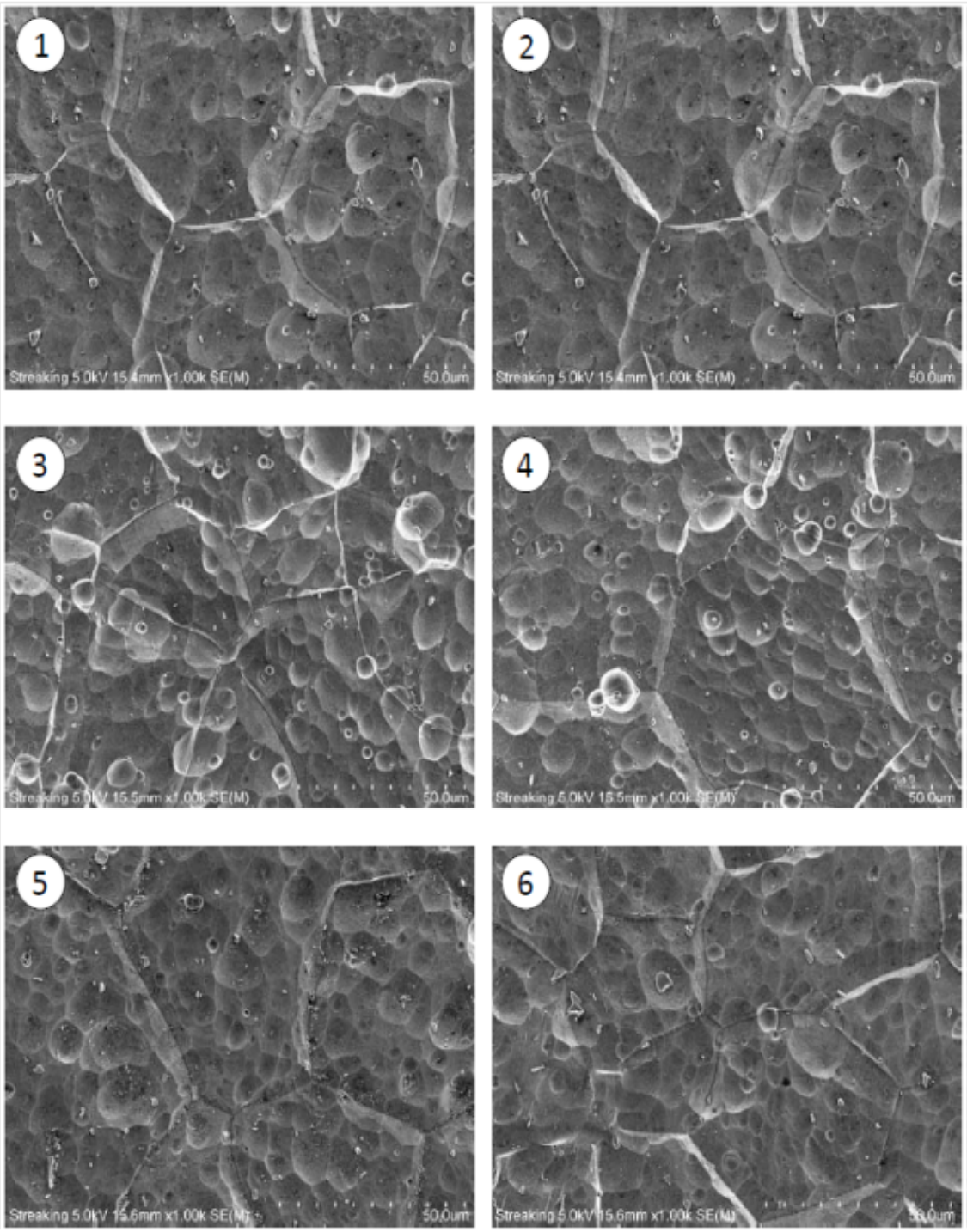

Figure 7.12: Original product: SEM images taken from six fields of view on the surface at 1000X magnification.

crostructure within areas of the new piece are relatively small compared to within the original piece. Therefore the optimised design has achieved its goal of providing a more even material flow, which leads to a more homogeneous microstructure.

7.3 Image processing tool box - Matlab

Image processing generally involves extraction of useful information from an image. The techniques used here are based on available literature [23]. Matlab's image processing tool box was used to investigate the SEM images from the previous section. Initially Matlab's in-built function, 'im2bw' was used to convert the images to binary images; however the resulting images failed to distinguish between the boundary and grain particles. The three colour channels (RGB) were found to give better judgement to identify boundaries and grains. For each channel, intensity thresholds were set above or below which pixels were defined as boundary or grains. Boundary pixels were set to black and grain pixels to white to obtain a binary image.

Image restoration resulted in the boundaries between particles in very close contact being lost. To repair this, holes in the images are filled by adjusting the intensity levels of the surrounding pixels using morphological reconstruction. Once the repair work is completed an in-built Matlab image segmentation algorithm was used to detect particle edges and re-establish particle boundaries. The image segmentation algorithm is a process of sorting a digital image into a number of parts based on pixels properties. Each of the pixels in a region is similar with respect to some characteristics, such as intensity, gradient and texture. Closest regions are considerably different with respect to the same feature. The goal here is to simplify the illustration of an image into objects that are more accurate and easier to investigate.

The final binary image used for this investigation is shown in Figure 7.13. Par-

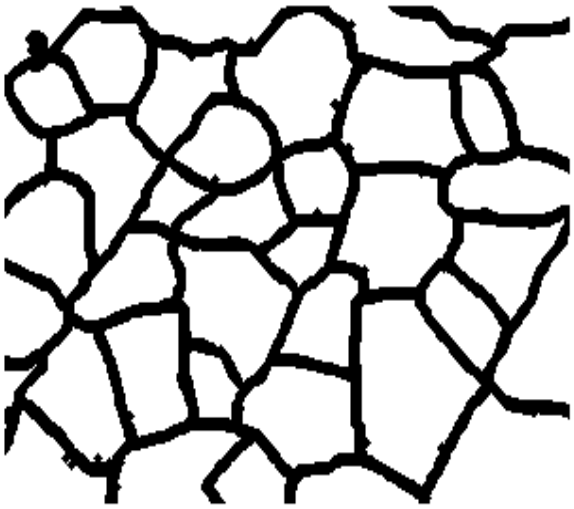

Figure 7.13: Binary image of Figure 7.7-3 after image reconstruction.

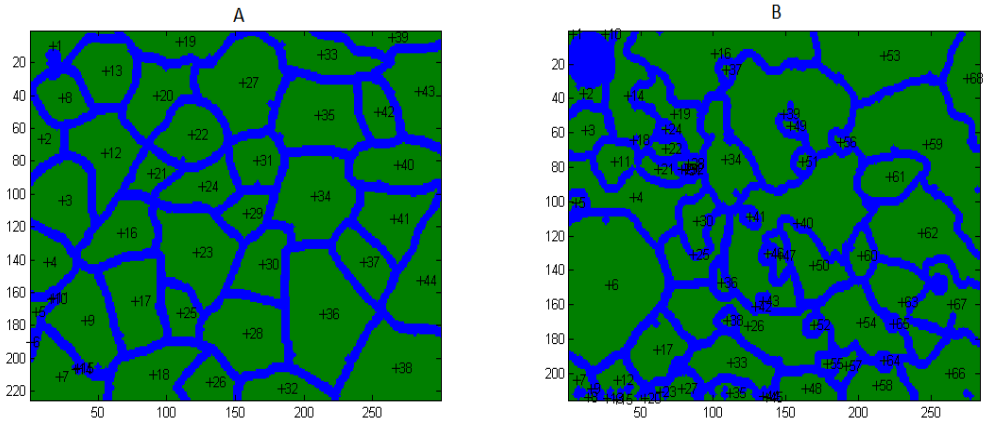

Figure 7.14: Final processed image of (A) Figure 7.7-3 and (B) Figure 7.11-3 used for investigation.

ticle centroids are marked with a cross and the particle index number in Figure 7.14. Once the grain particle cross section images were separated, the area of each grain particle was calculated. The total number of particles identified and used in the investigation of Figures 7.7-1, 7.7-2, 7.7-3, 7.11-1, 7.11-2 and 7.11-3 are given in Figure 7.15A, 7.15B, 7.15C,7.15D, 7.15E and 7.15F respectively. It can be seen that the difference in grain size area of the workpiece from the modified die is relatively

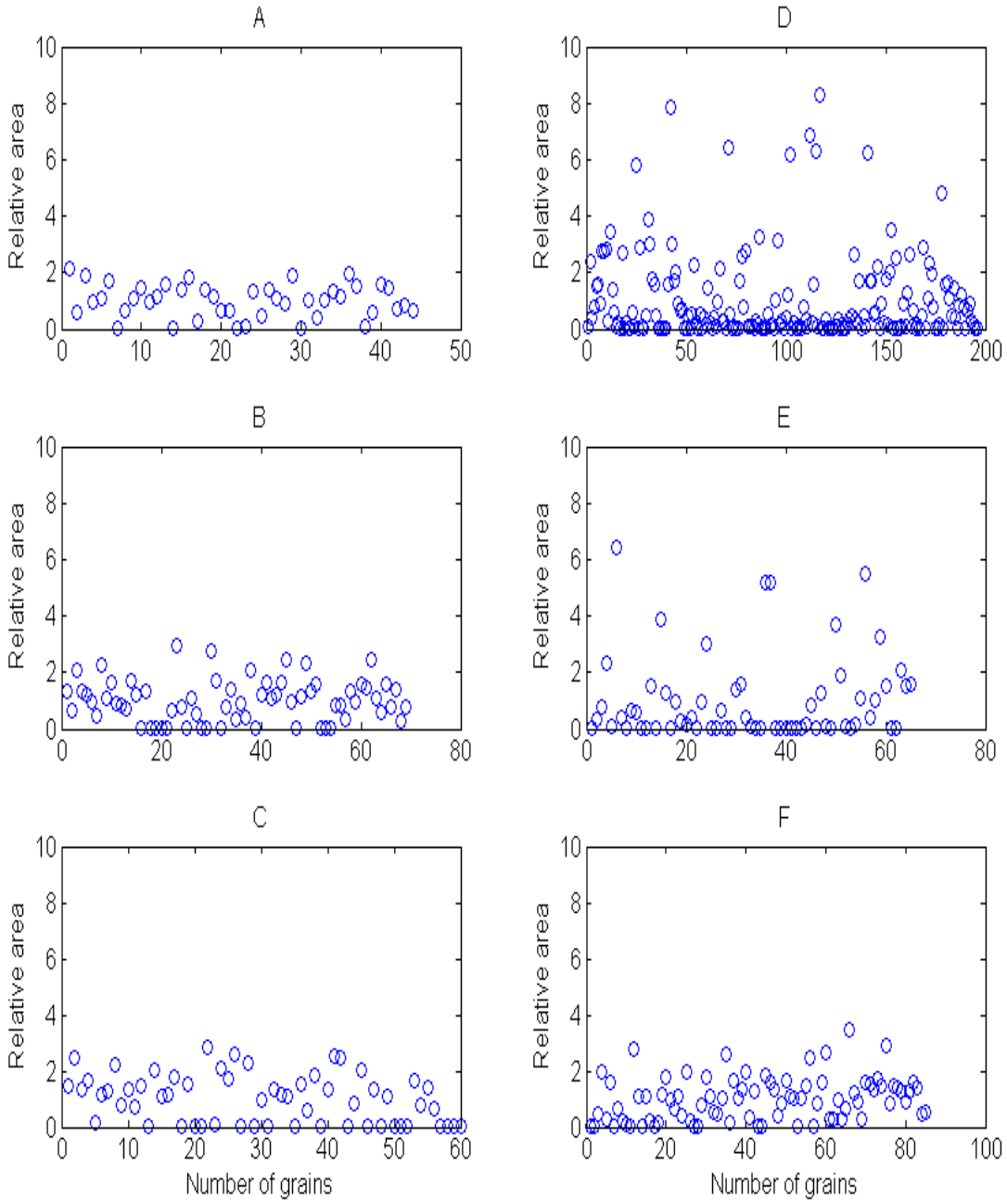

Figure 7.15: Particle counts from processed images of:(A) Figure 7.7-1, (B) Figure 7.7-2, (C) Figure 7.7-3, (D) Figure 7.11-1, (E) Figure 7.11-2 and (F) Figure 7.11-3.

uniform compared to pictures of the workpiece manufactured with the old die.

7.4 Validation of FEA calculation

The following checks were done to confirm the accuracy and reliability of finite element simulation work.

1. Initially similar problems given in the software manuals (Abaqus and Deform 3D) were compared with the simulation results in the manuals.

2. A very simple geometry model was solved using both software (Abaqus and Deform 3D) and the simulation results were compared against each other.

3. The same model given in the literature [6], [18], [50] was modelled and the simulation results were compared.

4. Implicit and explicit schemes were used and in different attempts yielding the same results.

5. Inclusion of adaptive meshing improved the simulation speed maintaing accuracy.

6. Element type and mesh density evaluated: Increased number of elements to approach convergence. Same results obtained with different element types.

7. Model is solved using two different contact algorithms and yielding similar results.

7.5 Summary and Discussion

The goal of this chapter is to examine whether the optimised die design delivers a high quality product free of flow lines on the flat surface. To do that, the optimal

die shape which showed very even flow characteristics during the simulation has been manufactured and run in a production extrusion press. The surface of the extruded part shows the improved surface properties and a subsequent scanning electron microscope analysis revealed very little variation in microstructure between different surface regions of the final product.

Chapter 8

Summary and Conclusions

8.1 Summary

This thesis presents the development of procedures that can be used to find an optimal set of conditions for an isothermal process to extrude a product for a given shape and material properties with minimal defects. The solution process is classified into the following:

1. Simple die geometry,

   (a) Optimization of process and design parameters for given product qualities.

   (b) Estimation of grain size and material constants.

2. Complex die geometry.

   Optimization of process and design parameters

   (a) without feeder chamber

   (b) with feeder chamber.

The developments of solution procedures for these cases are presented in chapters 4, 5 and 6. The developed procedures use the product geometry and material data such as flow curve and microstructure during dynamic recrystallization as its inputs.

Firstly, a small scale extrusion model was simulated using ABAQUS to study the extrusion process in general. The following items were investigated.

1. How temperature, stress, strains and velocity changes during the extrusion and how these quantities are related to die angle, die land length, friction, material properties, initial billet temperature and extrusion speed.

2. How different solution schemes, adaptive meshing, different element type and different contact algorithms influence the efficiency of the simulation.

Secondly a numerical technique to estimate the optimal die profile and the process parameters for a simple geometry die was investigated. It is based on a non-linear least squares coupled with finite element techniques. Nonlinear least squares optimization is done by constructing an iterative procedure using $MATLAB$'s inbuilt function *lsqnonlin* and at each iteration, finite element solutions to the extrusion flow are obtained using the $ABAQUS$ FEA program.

Thirdly an inverse model to concurrently estimate the average grain size, activation energy and other material constants appearing in the above optimization function was developed. This method is not dependent on experimental observation and it only uses simulated temperature and strain value history inside the deformation zone. The method of the approach is based on a non-linear least squares and Tikhonov's regularisation method.

Fourthly, a complex geometry problem was considered. The finite element program DEFORM 3D, which efficiently uses adaptive meshing controls to accommodate high workpiece deformations, is used to identify design and process parameters.

Three methods have been developed:

	Method 1		Method 2		Method 3
(i)	Obtained the flow velocity across each element (1:n) for the die with no pocket.	(i)	Obtained a linear relationship between widths and speeds for each element.	(i)	Obtained a ratio between the pocket widths for each element which gives well balanced flow across the die opening.
(ii)	Obtained the widths of the elements 2 to n which gives the same flow as element 1	(ii)	Obtained widths of each element which gives the same speed across the die opening.	(ii)	By maintaining the ratio obtained from step 1 calculated the optimal values of pocket widths for each element to achieve a uniform speed across the opening.
(iii)	Pocket shape is obtained for the well balanced uniform flow across the die opening.	(iii)	Obtained the outer shape of the pocket which gives well balanced uniform speed across the. die opening.		

All three methods perform well; one particular approach does not always predict a better result than the other method. Therefore all three methods are equally useful. If only the amount of computation time is considered, then method 3 is a

better choice than the other two methods.

Finally experimental trials at an industrial plant were conducted. These experiments were done to verify the theoretical prediction described in previous chapters.

8.2 Conclusions

The main objective of the work presented here is to identify the design and process parameters which are most important for surface quality to extrude a complex geometry product with 6XXX and 7XXX series aluminium alloys. In the process suitable computational techniques were developed to modify an existing die to minimize surface defects. Then the newly designed die has been manufactured and run in a production extrusion press. The main contributions towards resolving this problem are:

1. The surface of the extruded part shows more homogeneous surface properties and a subsequent scanning electron microscope analysis revealed very little variation in microstructure between different surface regions of the newly developed product.

2. The newly developed die is capable of extruding a product with relatively small variation of velocity, temperature and shear stress across the channel.

3. Four factors which can be used to alter the homogeneity of the flow are (i) initial temperature of billet, (ii) channel length, (iii) distance between die axis and channel axis, and (iv) shape of the pocket. It can be noticed from observations that the major factor that influences the flow is the pocket geometry. Therefore it can be concluded that the surface quality of the product can be optimised by designing a pocket suitable for the respective process conditions.

4. The efficiency of the simulation results hugely depends on (a) solution methods (b) iteration method and (c) step controls since the problems considered here have a complex geometry and thin profiles, which necessitate large billet area reductions and sharp corners which require frequent remeshing during the simulation of the extrusion process.

5. It has been demonstrated that finite element analysis is an efficient tool to predict the deformation behaviour and the following has been established:

   (a) The tendency toward chevron cracking is not observed (hydrostatic pressure inside the forming zone is not zero) with a die shape that minimizes one or more of the following: extrusion pressure, temperature variation, and strain rate variation.

   (b) The possibility of surface cracking can be avoided by designing a die, which minimizes the strain rate variation, velocity variation at the exit and the extrusion pressure.

   (c) The optimal parameter values are not the same (eg the parameters which minimizes the extrusion pressure are not same as the parameters which minimizes temperature variation inside the die) for all categories.

   (d) The grain size is more sensitive to extrusion speed and the initial temperature than die geometry.

   (e) The uniformity of the grain structure is more influenced by the shape of the die surface than the initial temperature or ram speed.

   (f) Surface quality of the simple geometry product can be optimised by altering the flow through the die using Bezier curves with five control points and optimising process conditions.

8.3 Future Experimental work

The main purpose of this thesis was a theoretical study of the process of aluminium extrusion and the results have been verified towards the end of the project in a factory trial of an improved version of a production die. The original production die had created surface imperfections in terms of flow lines and was a difficult profile to extrude because of a high extrusion ratio. Since the verification took place in a factory environment, the opportunities for gathering ample process data were limited.

To further confirm the accuracy of the simulation work it would be desirable to conduct a similar extrusion process in a laboratory environment and record and compare a number of process input and output parameters.

1. The speed and force of the extrusion press should be continuously recorded. The billet temperature profile should be measured as well as the exit temperature of the extruded material behind the die.

2. The process conditions of press speed and billet temperature should be varied within feasible limits to be able to assess, whether the simulation model shows the same sensitivity as the real process.

3. After each trial run the grain sizes should be determined on the surface of the product as well as internally and the uniformity or lack of it should be assessed.

8.4 Future Research

This research establishes a foundation for future work. In particular, the following items are still requiring clarification:

(i) In Chapter 6 it has been learned that the homogeneity of flow with a curved pocket die is much better than a slant or rectangular pocket die. The curved pocket can be constructed using a series of Bezier curves along the channel sides as in Figure 8.1 and therefore it is possible to extend the method developed for a simple geometry die. This can be incorporated into our algorithm easily, but considering more Bezier curves along the channel will increase the number of design parameters considerably and it is computationally currently very expensive and it is not possible to complete the task within a resonable time frame. This is one area where the model could be improved.

(ii) A model developed for one specific geometry cannot be directly applied for another geometry. If a parameterised model can be developed suitable for a wide range of geometries then by changing necessary parameter values it will be possible to predict an optimal set of values of process and design parameters. This would be of further benefit for industrial applications.

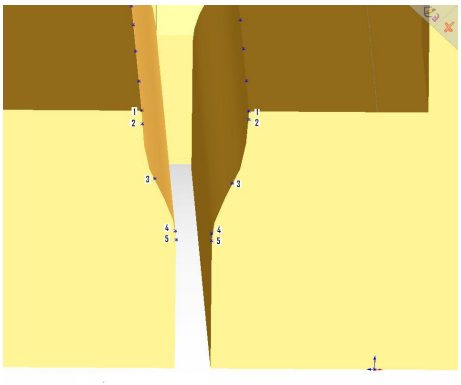

Figure 8.1: Bezier curved die

Appendix A

Appendix: Programming Codes

Python programming codes

```
from abaqus import *
from abaqusConstants import *
session.Viewport(name='Viewport: 1', origin=(0.0, 0.0), width=225.0,
height=186.46875)
session.viewports['Viewport: 1'].makeCurrent()
session.viewports['Viewport: 1'].maximize()

from driverUtils import executeOnCaeStartup
executeOnCaeStartup()
import visualization
import xyPlot
import displayGroupOdbToolset as dgo
o2 = session.openOdb(name='Abaqus-file-name.odb')
session.viewports['Viewport: 1'].setValues(displayedObject=o2)
```

```
odb = session.odbs['Abaqus-file-name.odb']

session.xyDataListFromField(odb=odb, outputPosition=NODAL, variable=
(('S',  INTEGRATION_POINT, ((INVARIANT, 'Pressure'), )), ),
nodeSets=('PART-1-1.TOP', ),steps=('Step-1','Step-2'))
###
xy1 = session.xyDataObjects['S:Pressure PI: PART-1-1 N: 831']
xy2 = xy1*1
session.XYData(name='S', objectToCopy=xy2,
    sourceDescription='"S:Pressure PI: PART-1-1 N: 831" * 1')
xy1 = session.xyDataObjects['S']
session.writeXYReport(fileName='TOPpressure.xls', appendMode=OFF,
xyData=(xy1, ))
####
session.xyDataListFromField(odb=odb, outputPosition=NODAL, variable=
(('NT11',  NODAL,), ), nodeSets=('PART-1-1.ALL',
),steps=('Step-1','Step-2'))

xy1 = session.xyDataObjects['NT11: PI: PART-1-1 N: 574']
xy2 = xy1*1
session.XYData(name='NT11', objectToCopy=xy2,
    sourceDescription='"NT11: PI: PART-1-1 N: 574" * 1')
xy1 = session.xyDataObjects['NT11']
session.writeXYReport(fileName='Tem574.xls', appendMode=OFF,
xyData=(xy1, ))
####
session.xyDataListFromField(odb=odb, outputPosition=NODAL, variable=
```

```
(('PEEQ',  INTEGRATION_POINT, ), ), nodeSets=('PART-1-1.ALL',
),steps=('Step-1','Step-2'))
xy1 = session.xyDataObjects['PEEQ: PI: PART-1-1 N: 574']
xy2 = xy1*1
session.XYData(name='PEEQ', objectToCopy=xy2,
    sourceDescription='"PEEQ: PI: PART-1-1 N: 574" * 1')
xy1 = session.xyDataObjects['PEEQ']
session.writeXYReport(fileName='peeq574.xls', appendMode=OFF,
xyData=(xy1, ))
####
session.xyDataListFromField(odb=odb, outputPosition=NODAL, variable=
(('S',  INTEGRATION_POINT, ((COMPONENT, 'S22'), )), ),
nodeSets=('PART-1-1.ALL', ),steps=('Step-1','Step-2'))
xy1 = session.xyDataObjects['S:S22 PI: PART-1-1 N: 538']
xy2 = xy1*1
session.XYData(name='S', objectToCopy=xy2,
    sourceDescription='"S:S22 PI: PART-1-1 N: 538" * 1')
xy1 = session.xyDataObjects['S']
session.writeXYReport(fileName='s22-538.xls', appendMode=OFF,
xyData=(xy1, ))
session.xyDataListFromField(odb=odb, outputPosition=NODAL, variable=
(('CPRESS', ELEMENT_NODAL,), ), nodeSets=('PART-1-1.CONTACT',
),steps=('Step-1','Step-2'))
####
xy1 = session.xyDataObjects['CPRESS: PI: PART-1-1 N: 1']
xy2 = xy1*1
session.XYData(name='CPRESS', objectToCopy=xy2,
```

```
    sourceDescription='"CPRESS: PI: PART-1-1 N: 1" * 1')
xy1 = session.xyDataObjects['CPRESS']
session.writeXYReport(fileName='CPRESS01.xls', appendMode=OFF,
xyData=(xy1, ))
####
session.xyDataListFromField(odb=odb, outputPosition=NODAL, variable=
(('U',  NODAL, ((COMPONENT, 'U2'), )), ),
nodeSets=('PART-1-1.ALL', ),steps=('Step-1','Step-2'))
xy1 = session.xyDataObjects['U:U2 PI: PART-1-1 N: 496']
xy2 = xy1*1
session.XYData(name='U', objectToCopy=xy2,
    sourceDescription='"U:U2 PI: PART-1-1 N: 496" * 1')
xy1 = session.xyDataObjects['U']
session.writeXYReport(fileName='U2496.xls', appendMode=OFF,
xyData=(xy1, ))
###
session.xyDataListFromField(odb=odb, outputPosition=NODAL, variable=
(('V',  NODAL, ((COMPONENT, 'V2'), )), ),
nodeSets=('PART-1-1.ALL', ),steps=('Step-1','Step-2'))
xy1 = session.xyDataObjects['V:V2 PI: PART-1-1 N: 496']
xy2 = xy1*1
session.XYData(name='V', objectToCopy=xy2,
    sourceDescription='"V:V2 PI: PART-1-1 N: 496" * 1')
xy1 = session.xyDataObjects['V']
session.writeXYReport(fileName='V2496.xls', appendMode=OFF,
xyData=(xy1, ))
####################
```

Matlab programming codes

```
    function [x,y]=Beziergraph(n,X,Y)
%n=number of points required
%(X,Y) are 5 Control points of Beziercurve
N=length(X);
t=0:1/(n-1):1;
x=zeros(1,n);y=zeros(1,n);
for i=1:n
    b=bernstein_basis(N-1,t(i));
    x(i)=sum(X.*b);y(i)=sum(Y.*b);
end


    R0=0.10;Rf=0.0666;m1=2;
P1X=R0;P2X=R0;P4X=Rf;P5X=Rf;
P1Y=-0.01;
P2Y=-0.07;
P3Y=-0.07;
P4Y=-0.16;
P5Y=-0.16;


n2=length(P2Y);n4=length(P4Y);
n5=length(P5Y);n3=length(P3Y);
MY=zeros(n2*n3*n4*n5,5);MX=zeros(n2*n3*n4*n5,5);
MY(:,1)=P1Y;MX(:,1)=P1X;
nn=n2*n3*n4*n5;
s=1;
for i=1:n2
```

```
   for j=1:n3
      for k=1:n4
         for l=1:n5
            MY(s,5)=P5Y(l);MX(s,5)=P5X;
            MY(s,4)=P4Y(k);MX(s,4)=P4X;
            MY(s,3)=P3Y(j);
            MY(s,2)=P2Y(i);MX(s,2)=P2X;
            MX(s,3)=Rf+(R0-Rf)*(MY(s,4)-MY(s,3))/(MY(s,4)-MY(s,2));
            s=s+1;
         end
      end
   end
end
n=23;
z=1:1:165;
EP=zeros(1,nn);
PEEQ=zeros(4,nn);
TEM=zeros(1,nn);
S11=zeros(1,nn);
S22=zeros(1,nn);
DP1=zeros(21,nn);
DP2=zeros(21,nn);
U2=zeros(11,nn);
V2=zeros(11,nn);
PEEQ1=zeros(11,nn);
PEEQ1dot=zeros(11,nn);
for i=1:nn
```

```
    [x,y]=Beziergraph(n,MX(i,:),MY(i,:));

%~~~~~~~~~~~~~~~~~~~~~~~~~~~~~~~~~~~~~~~~~~~~~~~~~~~~~~~~~~~~~~~~~~~~~~~~~~~~

    fid = fopen('dienode1.inp','w');
    fprintf(fid,'%4d, %3.4f, %3.4f\n', z(1), x(1), y(1));
    fprintf(fid,'%4d, %3.4f, %3.4f\n', z(59), x(2), y(2));
    fprintf(fid,'%4d, %3.4f, %3.4f\n', z(60), x(3), y(3));
    --
    --
    --
    fclose(fid);
        %~~~~~~~~~~~~~~~~~~~~~~~~~~~~~~~~~~~~~~~~~~~~~~~~~~~~~~~~~~~~~~~~~~~~~~~~~~~~

   !abaqus job=file-Name interactive

!abaqus cae nogui=filename.py
ncols=2;nhead=2;nlrows=10;

        fin = fopen('Excel-file-name.xls','r');
        for j=1:nhead,  buffer = fgetl(fin);  end
        data = fscanf(fin,'%f');
        nd = length(data);        %  total number of data points
        nr = nd/ncols;
        data = reshape(data,ncols,nr)';   %  notice the transpose operator
        y = data(:,2:ncols);
        nl=length(y);
```

```
EP(1,i)=sum(y)/nl;
```

Bibliography

[1] Arentoft M., Gronostajski Z., Niechajowicz. A., and Wanheim T., Physical and mathematical modelling of extrusion process, *Journal of Materials Processing Technology*, 106, 2–7, 2000.

[2] Antunez H. J., Thermo-mechanical modelling and sensitivity analysis for metal-forming operations, *Computer Methods in Applied Mechanics and Engineering* 161(1-2): 113–125, 1998.

[3] Balendra R., Qin Y., and Chodnikiewicz K., Analysis of temperature and from-error variation with the manufacturing cycle during the forward extrusion components, *Journal of Materials Processing Technology*, 145, 171–179, 2004.

[4] Bauser M., Sauer G., and Siegert K., Extrusion, *ASM publications*, 2006.

[5] Bhattacharyya D., Richards P. J., Modelling of metal extrusion using the phonix package, *Journal of Materials Processing Technology*, 35(1), 93–111, 1992.

[6] Chanda T., Zhou J., and Duszczyk. J., A comparative study on iso-speed extrusion and isothermal extrusion of 6061 Al alloy using 3D FEM simulation, *Journal of Materials Processing Technology*, 114, 145–153, 2001.

[7] Chanda T., Zhou J., and Duszczyk. J., Application of three-dimensional numerical simulation to analysis of development of deformation zone at beginning

of aluminium extrusion process, *Materials science and Technology*, 17, 70–74, 2001.

[8] Chanda T., Zhou J., and Duszczyk. J., FEM analysis of aluminium extrusion through square and round dies, *Materials and Design*, 21, 323–335, 2000.

[9] Chang C. I., Lee C. J., and Huang J. C., Relationship between grain size and ZenerHolloman parameter during friction stir processing in AZ31 Mg alloys, *Scripta Materialia*, 51, 509–514, 2004.

[10] Cho J. R., Bae W. B., Hwang W. J., and Hartley P., A study on the hot deformation behaviour and dynamic recrystallization of Al-5 wt %Mg alloy, *Journal of material processing technology*, 118, 356–361, 2001.

[11] De Pari Jr. L, Misiolek W. Z., Theoretical predictions and experimental verification of surface grain structure evolution for AA6061 during hot rolling, *Acta Materialia* 56, 6174-6185, 2008.

[12] Dieter G. E., Semiatin S. L., and Kuhn H, Handbook of Workability and Process Design, *ASM International*, 2002.

[13] Duan X., and Sheppard T., Simulation and control of microstructure evolution during hot extrusion of hard aluminium alloys, *Materials Science and Engineering*, 351, 282–292, 2003.

[14] Duan X., and Sheppard T., *Modelling and Simulation in Material Science and Engineering*, 10(4), 363–380, 2002.

[15] Fang G., Zhou J., Duszczyk J., and Wu. X. K, FE simulation of extrusion to produce a thin-walled wide profile through a spreading pocket die, *Key Engineering Materials*, 367, 63–70, 2008.

[16] Fang G., Zhou J.,, Duszczyk J., Extrusion of 7075 aluminium alloy through double-pocket dies to manufacture a complex profile, *Journal of Materials Processing Technology*, 209, 3050–3059, 2009.

[17] Fernandes J. L. M., Rodrigues J. M. C., and Martins P. A. F., Combined finite elementboundary element thermo-mechanical analysis of metal forming processes *Journal of Materials Processing Technology*, 87, 247-257, 1999.

[18] Flitta I and Sheppard T., Nature of friction in extrusion process and its effect on material flow, *Materials Science and Technology*, 19, 837–846, 2003.

[19] Gardner J. D., and Dornfeld D., Finite Element Modeling of Drilling Using DEFORM, *Laboratory for Manufacturing and Sustainability, Consortium on Deburring and Edge Finishing*, June, 2006.

[20] Gejadze I., and Jarny Y., An inverse heat transfer problem for restoring the temperature field in a polymer melt flow through a narrow channel, *International Journal of Thermal Sciences*, 41, 528-535, 2002.

[21] Gierzynska-Dolna M., and Lacki P., Some aspects of modelling of metal forming processes, *Computers & Structures*, 81, 605–613, 2003.

[22] Golovko O., Grydin O., Method for pocket die design on the basis of numerical investigations of aluminium extrusion process, *Metalurgija*, 45(3), 155–161, 2006.

[23] Gonzalez R., Wood R., and Eddins S., Digital image processing using MATLAB, 2004.

[24] Gouveia B. P. P. A., Rodrigues J. M. C., Bay. N., and Martins P. A. T., Finite-element modelling of cold forward extrusion, *Journal of Materials Processing Technology*, 94, 85–93, 1999.

[25] Gouveia B. P. P. A., and Rodrigues J. M. C, Physical modelling and numerical simulation of the round-to-square forward extrusion, *Journal of Materials Processing Technology*, 112, 244–251, 2001.

[26] Gouveia B. P. P. A., and Rodrigues J. M. C., Finite-element modelling of cold forward extrusion, *Journal of Materials Processing Technology*, 94, 85–93, 1999.

[27] Gouveia B. P. P. A., and Rodrigues J. M. C., Steady-state finite-element analysis of cold forward extrusion, *Journal of Materials Processing Technology*, 73, 281–288, 1998.

[28] Gouveia B. P. P. A., and Rodrigues J. M. C., Finite element modelling of cold forward extrusion using updated Lagrangian and combined Eulerian-Lagrangian formulations, *Journal of Materials Processing Technology*, 80-81, 647-652, 1998.

[29] Hansen C. P., *Rank-deficient and discrete ill-posed problems*, SIAM, Philadelphia, PA, 1997.

[30] Hansen C. P., *Regularization tools: A MATLAB package for analysis and solution of discrete ill-posed problems*, Danish Computing Center for Research and Education, 1993.

[31] HE You-feng, XIE Shui-sheng, CHENG Lei, HUANG Guo-jie, FU Yao, FEM simulation of aluminum extrusion process in porthole die with pockets, *Trans Nonferrous Met Soc China*, 20, 1067–1071 2010.

[32] Kathirgamanathan P., and Neitzert T., Optimization Method of Extrusion Dies, Submitted to *Production Engineering Research & Development*.

[33] Kathirgamanathan P., and Neitzert T., Optimization of pocket design to produce a thin shape complex profile, *Production Engineering Research & Development*, 3-3, 231–241, 2009.

[34] Kathirgamanathan P., and Neitzert T., Inverse Modelling for Estimation of Average Grain Size and Material Constants - An Optimization Approach, *Lecture Notes in Engineering and Computer Science*, 2, 850–854, 2008.

[35] Kathirgamanathan P., and Neitzert T., Optimal process control parameters estimation in aluminium extrusion for given product characteristics, *Lecture Notes in Engineering and Computer Science*, 2, 1436–1441, 2008.

[36] Kathirgamanathan P., and Neitzert T., Modelling of metal extrusion using ABAQUS, *The Proceedings of 3rd NZ Metals Industry Conference 2006.*

[37] Lee S. K., Ko D. C., and Kim B. M., *Optimal die profile design for uniform microstructure in hot extruded product*, *International Journal of Machine Tools & Manufacture*, 40, 1457–1478, 2000.

[38] Lee G., Kwak D. M, Kim S., Im I., Analysis and design of flat-die hot extrusion process, *International Journal of Mechanical Sciences*, 44, 915-934, 2002.

[39] Li F., Yuan S. J., He Z. B., Research of metal flow behavior during extrusion with active friction, *JMEPEG*, 17, 7-14, 2008.

[40] Li S., Bourke M. A. M., Finite element analysis of the plastic deformation zone and working load in equal channel angular extrusion, *Materials Science and Engineering*, 382(1-2), 217-236, 2004.

[41] Li H. J., Qi L. H., Neural network modeling and optimization of semi-solid extrusion for aluminum matrix composites, *Journal of Materials Processing Technology*, 151(1-3), 126–132, 2004.

[42] Li L., Zhou J., Prediction of temperature evolution during the extrusion of 7075 aluminium alloy at various ram speeds by means of 3D FEM simulation, *Journal of Materials Processing Technology*, 145(3), 360–370, 2004.

[43] Li L., Zhou J., and Duszczyk J., A 3D FEM simulation study on the isothermal extrusion of a 7075 aluminium billet with a predetermined non-linear temperature distribution, *Modelling and Simulation in Materials Science and Engineering*, 11, 401–416, 2003.

[44] Li Q., Smith C. J., Harris C., and Jolly M. R., Finite element investigations upon the influence of pocket die designs on metal flow in aluminium extrusion Part 1. Effect of pocket angle and volume on metal flow, *Journal of Materials Processing Technology*, 135, 189–196, 2003.

[45] Li Q., Smith C. J., Harris C., and Jolly M. R., Finite element investigations upon the influence of pocket die designs on metal flow in aluminium extrusion Part 2. Effect of pocket geometry configurations on metal flow, *Journal of Materials Processing Technology*, 135, 197–203, 2003.

[46] Li L., Zhou J., and Duszczyk J., A 3D FEM simulation study on the isothermal extrusion of a 7075 aluminium billet with a predetermined non-linear temperature distribution, *Modelling and Simulation in Materials Science and Engineering*, 11, 401-416, 2003

[47] Li L. X., and Rao K. P., A study on hot extrusion of Ti-6Al-4V using simulations and experiments, *International Journal of Mechanical Sciences*, 44(12), 2415–2425, 2002.

[48] Lia L. X., Rao K. P., Lou Y., and Peng D. S., A study on hot extrusion of Ti6Al4V using simulations and experiments, *International Journal of Mechanical Sciences*, 44, 2415-2425, 2002.

[49] Lin Z., and Juchen X., Optimization of die profile for improving die life in the hot extrusion process, *Journal of Materials Processing Technology*, 142(3), 659–664, 2003.

[50] Lof J., Developments in finite element simulations of aluminium extrusion, *PhD Thesis, University of Twente, The Netherlands*, 2000.

[51] Lof J., and Blokhuis Y., FEM simulations of the extrusion of complex thin-walled aluminium sections, *Journal of Materials Processing Technology*, 122, 344–354, 2002.

[52] Lu J., and Saluja N., Computer modeling of the continuous forming extrusion process of AA6061 alloy, *Journal of Materials Processing Technology*, 79(1-3), 200–212, 1998.

[53] Malas J. C., Frazier W. G., Venugopal S., Medina A., Medeiros S., Srinivasan R., Irwin D., Mullins W. M., and Chaudhary A., *Optimization of microstructure development during hot working using control theory*, *Metallurgical and Materials Transactions A*, 28, 1921–1930, 1997.

[54] Mathews j. H., and Fink K. D., *Numerical Methods Using Matlab*, *Prentice-Hall Inc*, 4-th Edition, 309–317, 2004.

[55] Muramatsu T., Zhang S., Lim B., and Yong S., Study on Flexi-Extrusion Forging Technique by Using Intelligent Actuating Tooling, *SIMTech Technical Report*, 2005.

[56] Nes E., Marthinsen K., Modelling the evolution in microstructure and properties during processing of aluminium alloys, *Journal of Materials Processing Technology*, 117(3), 333–340, 2001.

[57] Peng Z., and Sheppard T., A study on material flow in isothermal extrusion by FEM simulation, *Modelling and Simulation in Materials Science and Engineering*, 12, 745–763, 2004.

[58] Peris R., Effects of extrusion conditions on "Die Pick-Up" formed during extrusion of aluminium alloy AA6060, *Masters Theses*, 2007.

[59] Reddy V. R., Sethuraman R., Lal G. K., Upper-bound and finite-element analysis of axisymmetric hot extrusion, *Journal of Materials Processing Technology*, 57, pp.14–22, 1996.

[60] Reddy J. N., Energy principles and variational methods in applied mechanics, *NWiley, New York*, 2002.

[61] Rodrigues J. M. C., and Martins P. A. F., Coupled thermo-mechanical analysis of metal-forming processes through a combined finite elementboundary element approach, *International Journal for Numerical Methods in Engineering*, 42, 631–645, 1998.

[62] Rodriguez, A., Rodriguez, P., System to calculate chambers and feeds to obtain a minimum single bearing, *Proceedings of the Fifth International Aluminium Extrusion Technology*, 1, 283–290, 1992.

[63] Rodriguez, A., Rodriguez, P., Process and system of calculation for construction of dies for extrusion of solid aluminium profiles, *United States Patent 5870922*, 1999.

[64] Saha P. K., Thermodynamics and tribology in aluminum extrusion, *Wear*, 218(2), 179–190, 1998.

[65] Saha P. K., Aluminum Extrusion Technology, *ASM publications*, 2000.

[66] Sheppard T., Prediction of structure during shaped extrusion and subsequent static recrystallization during the solution soaking operation, *Journal of material processing technology*, 177, 26–36, 2006.

[67] Shivpuri R., Advances in numerical modelling of manufacturing process, *TransIndian Inst Metals*, 57(4), 345–366, 2004.

[68] Sliwa R., and Zasadzii H. J., Surface cracking of bars in the metal extrusion process: part 1, *Journal of Mechanical Working Technology*, 14, 325–341.

[69] Sofuoglu H., and Gedikli H., Physical and numerical analysis of three dimensional extrusion process, *Computational Materials Science*, 31(1-2), 113-124.

[70] Storen S., The theory of extrusion–Advances and challenges, *International Journal of Mechanical Sciences*, 35(12), 1007-1020.

[71] Sun Y., Gupta M., Optimization of flat die geometry, *ANTEC*, 50, 3307–3311, 2004.

[72] Tiernan P., and Hillery M. T., Modelling of cold extrusion with experimental verification, *Journal of Materials Processing Technology*, 168(2), 360–366, 2005.

[73] Ulrich Aluminium, Hamilton, New Zealand, *www.ulrich-aluminium.co.nz-August 2008*.

[74] Ulysse P., Optimal extrusion die design to achieve flow balance, *International Journal of Machine Tools and Manufacture*, 39(7), 1047–1064, 1999.

[75] Valberg H., Applied Metal Forming: including FEM analysis, *Cambridge University Press*, 2010.

[76] Venugopal S., Medina E. A., Malas I., Medeiros S., and Frazier W. G., Optimization of microstructure during deformation processing using control theory principles, *Scripta materialia*, 36, 347–353, 1997.

[77] Venugopal S., and Rodriguez P., Strategy for the design of thermomechanical processes for AISI type 304L stainless steel using dynamic materials model stability criteria and model for the evolution of microstructure, *Journal of Materials Science*, 39, 5557–5560, 2004.

[78] Wifi A. S., Shatla M. N., and Abdel-Hamid., An optimum-curved die profile for the hot forward rod extrusion process, *Journal of Materials Processing Technology*, 73, 97–107, 1998.

[79] Wang L., Yang H., Frictioninal miniumextrusion-part 2: A review of friction models for aluminium extrusion, *Tribology International* 56, 99–106, 2012.

[80] Williams A. J., Computational modelling of metal extrusion and forging process, *Journal of Materials Processing Technology*, 125-126, 573–582, 2002.

[81] Yuan Z., Li F., and He Z., Effects of guiding angle on plastic metal flow and defects in extrusion of aluminium alloy, *Journal of Materials Science and Technology*, 24, 256–260, 2005.

[82] Zheng P. F., and Chan L. C., Numerical analysis of the sheet metal extrusion process, *Finite Elements in Analysis and Design*, 42(3), 189–207, 2005.

[83] Yan H., and Xia J., An approach to the optimal design of technological parameters in the profile extrusion process, *Science and Technology of Advanced Materials*, 7, 127–131, 2006.

[84] Zhou J., and Li L., Computer simulated and experimentally verified isothermal extrusion of 7075 aluminium through continuous ram speed variation, *Journal of Materials Processing Technology*, 146(2), 203–212, 2004.

[85] Zhou J., and Li L., 3D FEM simulation of the whole cycle of aluminium extrusion throughout the transient state and the steady state using the updated Lagrangian approach, *Journal of Materials Processing Technology*, 134(3), 383–397, 2003.

[86] Zhou L., Li. J., and Duszczyk J., A 3D FEM simulation study on the isothermal extrusion of a 7075 aluminium billet with a predetermined non-linear temperature distribution, *Modelling and Simulation in Materials Science and Engineering*, 11, 401–416, 2003.